Hurricane Motion On A Beta Plane In An Asymmetric Balance Model

Christopher T. Nicklas and Michael T. Montgomery

Research Supported by the Office of Naval Research
Grant # ONR N00014-93-1-0456

Colorado State University

DEPARTMENT OF ATMOSPHERIC SCIENCE

PAPER NO. 610

ABSTRACT

This work extends asymmetric balance theory (AB) to the shallow water beta plane (β-AB). The physical problem studied is that of vortex motion on a beta plane in the absence of environmental steering flow. To reduce the problem to its essential physics, the mathematical formulation developed is restricted to purely linear dynamics. The linear dynamics precludes wave-wave and wave-mean-flow interactions.

Vortices placed in the β-AB model correctly develop the wavenumber one asymmetries (the "beta" gyres) necessary for vortex self-advection. The vortices move in a northwest direction consistent with their relative strengths. Finite drift speeds are reached in all cases.

Both the β-AB model and a linear barotropic nondivergent model are used to investigate the existence of a translating normal mode of zero frequency. If such a mode exists, the beta gyres would be expected to remain unchanged in the absence of beta forcing. When the beta forcing is discontinued, the beta gyres axisymmetrize in both models, refuting the normal mode hypothesis.

ACKNOWLEDGEMENTS

This work was sponsored by the Office of Naval Research ONR-N00014-93-1-0456. Mr. Nicklas was supported through the Air Force Institute of Technology program. Numerical computations were performed using Hewlett Packard (HP) Apollo series computers belonging to the Montgomery Research Project. Programs were written in HP FORTRAN 9000 and in the Interactive Data Language (IDL) of Research Systems, Inc.

CONTENTS

Chapter 1

INTRODUCTION

The success of barotropic models in tropical cyclone track forecasting has been established and well documented (Aberson and DeMaria 1994; among others). Their success is likely due to the fact that in the deep tropics there is weak vertical shear of the horizontal winds and baroclinic processes appear secondary to what controls the motion of the vortex. Although George and Gray (1976) and Chan and Gray (1982) established the dominance of the environmental steering flow in tropical cyclone motion, deviations from the environmental steering flow can nevertheless be significant. The difference between the actual cyclone motion and the steering flow is called the propagation vector (Elsberry and Abbey 1990, Elsberry et al. 1993). The self-advection mechanism arising when a circular vortex is placed in the Earth's vorticity gradient, "beta drift," is one of several factors (e.g., vertical and horizontal shear, upper level anticyclone influences, cyclone intensity, asymmetric convection, vortex tilting, etc.) believed responsible for track deviations from a given steering flow.

Modeling studies suggest it is not the planetary vorticity gradient alone but the gradient of absolute environmental vorticity - an "effective beta" - which is partly responsible for a storm's propagation vector (DeMaria 1985, Evans et al. 1991). Other modeling studies showing a more tenuous relationship between the gradient of absolute environmental vorticity and the storm's propagation vector (Shapiro and Ooyama 1990) have gone as far to suggest that no practical relationship exists for tropical cyclones (Smith and Ulrich 1993). Observational studies, however, such as Carr and Elsberry (1990), Elsberry et al. (1993), and Franklin et al. (1996) suggest that effective beta contributes significantly to tropical cyclone track deviations from the environmental steering flow. Specifically, in an analysis

of 16 environmental datasets for 10 Atlantic tropical cyclones, Franklin et al. attribute 25% of the variance in the magnitude of the propagation vector to the effective-beta drift. Thus in order to correctly interpret results from complex three-dimensional primitive equation (PE) models we must thoroughly understand the dynamics of the beta drift problem.

Recently, Shapiro and Montgomery (1993; hereafter SM) developed a three dimensional theory for rapidly rotating vortices. The theory is called asymmetric balance (AB) and represents a new framework for investigating the slow evolution of rapidly rotating vortices. SM made use of the highly symmetric nature of strong atmospheric vortices to linearize about a symmetric balanced vortex and took advantage of the dominance but relative weakness of the low-wavenumber asymmetries. AB includes the full inertial dynamics of the vortex core, allows for order one asymmetric divergence, is valid for large Rossby numbers, and has a uniformly valid continuation to three-dimensional quasi-geostrophic theory in the environment, all while filtering gravity-inertia waves (SM).

To simplify the mathematics, Kallenbach and Montgomery (1995; hereafter KM) applied the theory to a shallow water model. In KM the AB formulation was validated on an f-plane through extensive axisymmetrization experiments. This thesis will extend AB theory to the shallow water beta plane. The physical problem studied is that of vortex motion on a beta plane in the absence of environmental steering flow. To reduce the problem to its essential physics, the mathematical formulation developed is restricted to purely linear dynamics. An investigation of the role of nonlinearities is a topic reserved for future work.

In addition to the "practical" side of this problem, there is also a geophysical fluid dynamical (GFD) interest in the purley linear formulation. The linear formulation allows us to examine the hypothesis of constantly accelerating vortices on the β-plane (Willoughby 1990b), a hypothesis which appears at odds with the analytical theory of Sutyrin and Flierl (1994) for quasi-geostrophic shallow water vortices. The linear formulation also enables us to determine if a near-zero frequency translating normal mode exists in the absence of beta forcing (Willoughby 1988, 1990b, 1992, 1995).

Chapter 2

AB THEORY ON A SHALLOW WATER BETA PLANE

2.1 Introduction

Previous work demonstrated the consistency and accuracy of the linear f-plane AB formulation by carrying out extensive symmetrization experiments on a stable hurricane-like vortex in gradient balance (KM). This thesis extends the AB formulation to the beta plane. A beta plane formulation of AB theory is desirable since it should prove useful in attaining a deeper understanding of vortex motion in barotropic and baroclinic vortex flows where large Rossby numbers and $O(1)$ asymmetric divergence is the rule rather than the exception. Other problems for which an asymmetric balance analysis should prove useful include horizontally and vertically sheared steering flows and upper-level anticyclonic outflows. Here we focus on the simplest motion problem, beta drift.

Complications associated with a moving coordinate system are circumvented by adopting a stationary coordinate system. When the vortex has moved more than a prescribed distance from the grid center, defined as a best circle fit around some closed height contour, the coordinate system is relocated to the center of the vortex and the total potential vorticity field is interpolated onto the new coordinate system. Future work will explore the potential advantages of a storm-relative coordinate system in the AB formulation.

2.2 Governing Equations

We begin with the shallow water equations in cylindrical coordinates on a β-plane. A stationary coordinate system positioned initially at the vortex center is adopted. The radial momentum, tangential momentum, and continuity equations are, respectively:

$$\frac{\partial u}{\partial t} + u\frac{\partial u}{\partial r} + \frac{v}{r}\frac{\partial u}{\partial \lambda} - fv - \frac{v^2}{r} = -\frac{\partial \phi}{\partial r}, \tag{2.1}$$

$$\frac{\partial v}{\partial t} + u\frac{\partial v}{\partial r} + \frac{v}{r}\frac{\partial v}{\partial \lambda} + fu + \frac{uv}{r} = -\frac{1}{r}\frac{\partial \phi}{\partial \lambda}, \tag{2.2}$$

$$\frac{\partial \phi}{\partial t} + u\frac{\partial \phi}{\partial r} + \frac{v}{r}\frac{\partial \phi}{\partial \lambda} + \phi\left(\frac{1}{r}\frac{\partial (ru)}{\partial r} + \frac{1}{r}\frac{\partial v}{\partial \lambda}\right) = 0. \tag{2.3}$$

In (2.1) – (2.3), r and λ denote radius and azimuthal angle, f denotes the Coriolis parameter, u and v denote ground-based radial and azimuthal winds, and ϕ denotes the geopotential. Consistent with the β-plane formulation, the Coriolis parameter is approximated by two terms in a Taylor series about a reference latitude. We therefore take $f = f_0 + \beta r \sin\lambda$, where f_0 denotes the planetary vorticity at the reference latitude and β denotes its meridional gradient there.

As shown by SM for Hurricane Gloria, within approximately 500 km from the storm center, hurricane vortices are dominated by their axisymmetric component. If the quadratic terms in the governing equations are small compared to their linear counterparts one may neglect them in a first approximation. Although this level of approximation precludes examination of nonlinear phenomena, previous work has demonstated that linearized dynamics captures much of the essential physics of the beta drift problem (Smith et al. 1990, Reznik and Dewar 1994). To this end let $u = u'$, $v = \bar{v}(r) + v'$, and $\phi = \bar{\Phi}(r) + \phi'$, where the overbar denotes an azimuthal mean basic state and a prime denotes non-axisymmetric departures from the basic state. In subsequent mathematical manipulations the material derivative following the basic state tangential wind will be designated as

$$\frac{D_{\mathrm{v}}}{Dt} = \frac{\partial}{\partial t} + \frac{\bar{v}}{r}\frac{\partial}{\partial \lambda}. \tag{2.4}$$

Upon neglecting products of primed quantities, the momentum and continuity equations become

$$\frac{D_{\mathrm{v}}}{Dt}u' - f_0\bar{v} - fv' - \frac{\bar{v}^2}{r} - \frac{2\bar{v}}{r}v' = -\frac{\partial}{\partial r}(\bar{\Phi} + \phi') + \beta\bar{v}r\sin\lambda, \tag{2.5}$$

$$\frac{D_{\mathrm{v}}}{Dt}v' + u'\frac{d\bar{v}}{dr} + fu' + \frac{\bar{v}}{r}u' = -\frac{1}{r}\frac{\partial}{\partial \lambda}(\bar{\Phi} + \phi'), \tag{2.6}$$

$$\frac{D_{\mathrm{v}}}{Dt}\phi' + u'\frac{d\bar{\Phi}}{dr} + \bar{\Phi}\left(\frac{1}{r}\frac{\partial (ru')}{\partial r} + \frac{1}{r}\frac{\partial v'}{\partial \lambda}\right) = 0. \tag{2.7}$$

The basic state vortex is assumed in gradient balance with f approximated by its reference value

$$f_0\bar{v} + \frac{\bar{v}^2}{r} = \frac{d\bar{\Phi}}{dr}. \tag{2.8}$$

A preponderance of observations support the gradient balance approximation. As one example, Willoughby (1990a) showed the mean tangential wind for a large sample of Atlantic storms was within 1.5 ms^{-1} of gradient balance.

Substituting (2.8) into (2.5) – (2.7) simplifies the linear PE to

$$\frac{D_v}{Dt}u' - \bar{\xi}v' = -\frac{\partial \phi'}{\partial r} + \beta \bar{v} r \sin\lambda, \tag{2.9}$$

$$\frac{D_v}{Dt}v' + \bar{\eta}u' = -\frac{1}{r}\frac{\partial \phi'}{\partial \lambda}, \tag{2.10}$$

and

$$\frac{D_v}{Dt}\phi' + \bar{\Phi}\left(\frac{1}{r}\frac{\partial (ru')}{\partial r} + \frac{1}{r}\frac{\partial v'}{\partial \lambda}\right) + u'\frac{d\bar{\Phi}}{dr} = 0. \tag{2.11}$$

In (2.9) – (2.11), $\bar{\zeta} = r^{-1}\, d(r\bar{v})/dr$ the basic state relative vorticity, $\bar{\eta} = f + \bar{\zeta}$ the basic state absolute vorticity, and $\bar{\xi} = f + 2\bar{v}/r$ the inertia parameter. The definitions for $\bar{\eta}$ and $\bar{\xi}$ include the azimuthally dependent Coriolis parameter on a beta plane and represent a departure from the customary practice of reserving a bar for an azimuthal mean. Unless otherwise stated all other barred quantities denote azimuthal averages.

Although the inviscid PE (2.1) – (2.3) possess well known conservation laws for vertical vorticity, energy, and potential vorticity, their linearized counterparts are summarized below as they help establish the formal consistency of the balance model to be proposed in the upcoming sections.

2.2.1 PE Vorticity

The linearized vorticity equation follows on taking the curl of (2.9, 2.10). The result is

$$\frac{D_v}{Dt}\zeta' + u'\frac{d\bar{\eta}}{dr} + (\bar{v} + v')\frac{1}{r}\frac{\partial f}{\partial \lambda} = -\bar{\eta}\left[\frac{1}{r}\frac{\partial (ru')}{\partial r} + \frac{1}{r}\frac{\partial v'}{\partial \lambda}\right], \tag{2.12}$$

where

$$\zeta' = \hat{\mathbf{k}} \cdot \nabla \times \mathbf{u}'. \tag{2.13}$$

2.2.2 PE Potential Vorticity

The linearized PV equation results upon eliminating the divergence term between the continuity equation (2.11) and the vorticity equation (2.12), and invoking the beta-plane approximation in the vorticity equation:

$$\frac{D_{\mathrm{v}}}{Dt}q' + u'\frac{d\bar{q}_0}{dr} + \frac{u'}{\bar{\Phi}}\frac{\partial f}{\partial r} + \frac{1}{\bar{\Phi}}\left(\bar{v}+v'\right)\frac{1}{r}\frac{\partial f}{\partial \lambda} = 0 \tag{2.14}$$

where

$$q' = \frac{\zeta'}{\bar{\Phi}} - \bar{q}_0\frac{\phi'}{\bar{\Phi}} \tag{2.15}$$

is the perturbation PV and

$$\bar{q}_0 = \frac{\bar{\eta}_0}{\bar{\Phi}} \tag{2.16}$$

is the basic state f-plane PV.

2.2.3 PE Energy

The disturbance energy equation results from the combination

$$\frac{\bar{\Phi}}{g}\left(u' \times (2.9) + v' \times (2.10)\right) + \frac{\phi'}{g} \times (2.11). \tag{2.17}$$

Some manipulation yields

$$\frac{D_{\mathrm{v}}}{Dt}\left[\frac{\bar{\Phi}}{2g}\left(u'^2+v'^2\right)+\frac{(\phi')^2}{2g}\right] + \nabla\cdot\left(\frac{\bar{\Phi}}{g}\phi'\mathbf{u}'\right) + \frac{\bar{\Phi}}{g}v'u'r\frac{d\bar{\Omega}}{dr} - \frac{\bar{\Phi}}{g}u'r\bar{v}\beta\sin\lambda = 0. \tag{2.18}$$

2.3 β-AB Formulation

The objective of this section is to develop a useful balance model for investigating vortex motion in divergent flows which contains full inertial effects in the near-vortex region yet blends smoothly onto linearized quasi-geostrophic (QG) β-plane dynamics in the environment where the Rossby number ($R = \bar{v}/f_0 r$) is small compared to unity and $\beta r/f_0 \sim O(R)$. Letting $\bar{\Phi}_\infty$ denote the environmental geopotential and $\bar{\phi} = \bar{\Phi}_\infty - \bar{\Phi}$, the pseudo-PV equation governing linearized QG β-plane vortex dynamics is

$$\frac{D_{\mathrm{v}}}{Dt}\left[\frac{1}{r}\frac{\partial}{\partial r}\left(r\frac{\partial\phi'}{\partial r}\right)+\frac{1}{r^2}\frac{\partial^2\phi'}{\partial\lambda^2}-\frac{f_0^2}{\bar{\Phi}_\infty}\phi'\right] - \frac{1}{r}\frac{\partial\phi'}{\partial\lambda}\frac{d\bar{q}_0}{dr} - \beta\sin\lambda\frac{1}{r}\frac{\partial\phi'}{\partial\lambda}$$
$$+\beta\cos\lambda\left(f_0\bar{v}+\frac{\partial\phi'}{\partial r}\right) = 0, \tag{2.19}$$

where

$$\bar{q}_0 = \frac{1}{f_0 r}\frac{\partial}{\partial r}\left(r\frac{\partial \bar{\phi}}{\partial r}\right) - \frac{f_0 \bar{\phi}}{\bar{\Phi}_\infty}$$

is the basic state pseudo-PV for the QG system. The asymptotic errors incurred in deriving (2.19) scale as $O(R^2, (\beta r/f_0)R)$. In the near vortex region, where $R > 1$, the QG β-plane formulation is no longer valid and a simple balance formulation incorporating gradient balance rather than geostrophic balance as a zeroth-order approximation is needed.

To include full inertial effects in the near-vortex region we follow SM and filter gravity-inertia waves at the momentum level. Differentiating (2.9) and (2.10) with respect to D_{V}/Dt and cross substituting yields an equivalent set of momentum equations in the radial and azimuthal directions, respectively:

$$\left(\frac{{D_{\mathrm{V}}}^2}{Dt^2} + \bar{\eta}\bar{\xi}\right) u' = -\frac{\bar{\xi}}{r}\frac{\partial \phi'}{\partial \lambda} - \frac{D_{\mathrm{V}}}{Dt}\left(\frac{\partial \phi'}{\partial r}\right) + v'\bar{v}\beta\cos\lambda + \bar{v}^2\beta\cos\lambda \tag{2.20}$$

$$\left(\frac{{D_{\mathrm{V}}}^2}{Dt^2} + \bar{\eta}\bar{\xi}\right) v' = \bar{\eta}\frac{\partial \phi'}{\partial r} - \frac{D_{\mathrm{V}}}{Dt}\left(\frac{1}{r}\frac{\partial \phi'}{\partial \lambda}\right) - u'\bar{v}\beta\cos\lambda - r\bar{\eta}\bar{v}\beta\sin\lambda. \tag{2.21}$$

Eqs. (2.20) and (2.21) resemble the forced harmonic oscillator equation. If the forcing is confined to "low frequencies", i.e., frequencies small compared to $\bar{\eta}\bar{\xi}$ (the intrinsic frequency of the vortex), the response should be confined to low frequencies also. For advective dynamics then the magnitude of ${D_{\mathrm{V}}}^2/Dt^2$ scales as

$$\frac{{D_{\mathrm{V}}}^2}{Dt^2} \sim n^2\frac{\bar{v}^2}{r^2}, \tag{2.22}$$

where n is the azimuthal wavenumber. It proves convenient to define

$$\mathcal{D}^2 = \frac{\frac{{D_{\mathrm{V}}}^2}{Dt^2}}{\bar{\eta}\bar{\xi}} \tag{2.23}$$

from which (2.22) implies

$$\mathcal{D}^2 \sim \frac{n^2\bar{v}^2/r^2}{\bar{\eta}\bar{\xi}} \equiv {R_n}^2, \tag{2.24}$$

the square of a local Rossby number for wavenumber n. The smallness of ${R_n}^2$ justifies neglecting the acceleration term in (2.20) and (2.21). SM provide an in-depth discussion of the conditions for which the neglect of terms scaling as ${R_n}^2$ can be considered

valid. For hurricane-like vortices only ${R_1}^2$ can be considered less than unity throughout the near-vortex region. For weaker vortices (i.e., vortices possessing order unity Rossby numbers) the approximation is also valid for $n = 2$ and becomes significantly more accurate for $n = 1$. For high azimuthal wavenumbers the quadratic dependence of ${R_n}^2$ with azimuthal wavenumber suggests that large errors may occur in the near-vortex region. In the strictly linear vortex motion problem, however, this issue is not a concern since the leading order dynamics is determined by the structure of wavenumber one asymmetries. Nevertheless, for weakly nonlinear dynamics including azimuthal wave-wave interactions this issue cannot be ignored. As a first step towards validating the consistency of the AB approximation in such flow regimes, KM showed that high wavenumber asymmetries on stable hurricane-like vortices quickly axisymmetrize in the linear AB formulation. Therefore, on the basis of previous work the wavenumber one restriction will be relaxed in the upcoming derivations.

Invoking the AB approximation ${R_n}^2 << 1$ allows (2.20) to be approximated by

$$\bar{\eta}\bar{\xi}u' = -\frac{\bar{\xi}}{r}\frac{\partial \phi'}{\partial \lambda} - \frac{D_{\mathrm{v}}}{Dt}\left(\frac{\partial \phi'}{\partial r}\right) + v'\bar{v}\beta\cos\lambda + \bar{v}^2\beta\cos\lambda. \tag{2.25}$$

Dividing (2.25) by $\bar{\xi}$ and using (2.9) to substitute for v' yields

$$\bar{\eta}u' = -\frac{1}{r}\frac{\partial \phi'}{\partial \lambda} - \frac{1}{\bar{\xi}}\frac{D_{\mathrm{v}}}{Dt}\left(\frac{\partial \phi'}{\partial r}\right) + \frac{\bar{v}^2\beta\cos\lambda}{\bar{\xi}} + \frac{\bar{v}\beta\cos\lambda}{\bar{\xi}^2}\left(\frac{D_{\mathrm{v}}}{Dt}u' + \frac{\partial \phi'}{\partial r} - \bar{v}r\beta\sin\lambda\right). \tag{2.26}$$

Now if throughout the flow

$$\frac{\bar{v}\beta\cos\lambda}{\bar{\xi}^2}\frac{D_{\mathrm{v}}}{Dt}u' << \bar{\eta}u', \tag{2.27}$$

then $(\bar{v}\beta\cos(\lambda)/\bar{\xi}^2)(D_{\mathrm{v}}\,u'/Dt)$ may be neglected. The quotient of these two terms scales as

$$\frac{\frac{\bar{v}\beta\cos\lambda}{\bar{\xi}^2}\frac{D_{\mathrm{v}}}{Dt}u'}{\bar{\eta}u'} \sim \frac{\beta\bar{v}\frac{n\bar{v}}{r}}{\bar{\eta}\bar{\xi}^2} = \frac{\beta r}{\bar{\xi}}\frac{1}{n}\frac{n^2\bar{v}^2}{r^2\bar{\eta}\bar{\xi}} = \frac{\beta r}{\bar{\xi}}\frac{{R_n}^2}{n}. \tag{2.28}$$

Figure 2.1 plots $(\beta r/\bar{\xi}_0){R_1}^2$ for the hurricane-like benchmark vortex of chapter 3 at 20° N and this term is clearly small throughout the vortex and its environment. Neglecting $(\bar{v}\beta\cos(\lambda)/\bar{\xi}^2)(D_{\mathrm{v}}\,u'/Dt)$ from (2.26) then yields

$$u' = -\frac{1}{\bar{\eta}r}\frac{\partial \phi'}{\partial \lambda} - \frac{1}{\bar{\eta}}\frac{D_{\mathrm{v}}}{Dt}\left(\frac{1}{\bar{\xi}}\frac{\partial \phi'}{\partial r}\right) + \frac{\bar{v}^2\beta\cos\lambda}{\bar{\eta}\bar{\xi}} - \frac{\beta^2\bar{v}^2 r\sin\lambda\cos\lambda}{\bar{\eta}\bar{\xi}^2}. \tag{2.29}$$

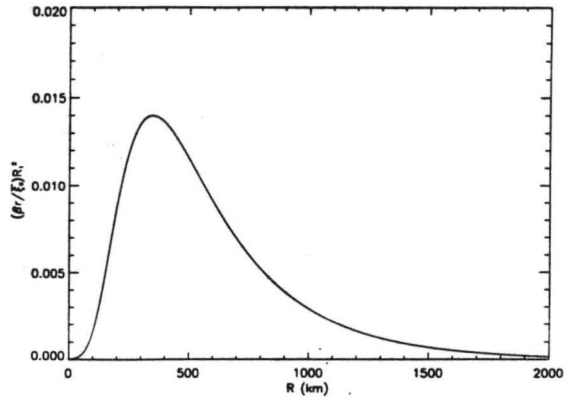

Figure 2.1: Plot of $(\beta r/\bar{\xi}_0){R_1}^2$ for the benchmark vortex.

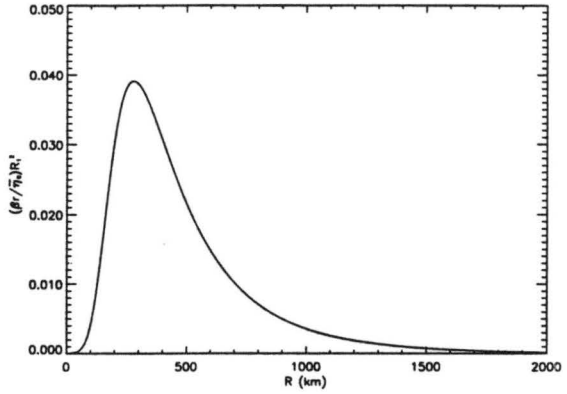

Figure 2.2: Plot of $(\beta r/\bar{\eta}_0){R_1}^2$ for the benchmark vortex.

Similar arguments applied to (2.21) give an equation for v' solely in terms of ϕ' provided

$$\frac{\bar{v}\beta\cos\lambda}{\bar{\eta}\bar{\xi}}\frac{D_{\mathrm{v}}}{Dt}v' << \bar{\eta}v'. \tag{2.30}$$

The corresponding quotient $(\bar{v}\beta\cos\lambda/\bar{\eta}^2\bar{\xi}v')(D_{\mathrm{v}}\,v'/Dt)$ scales as $(\beta r/\bar{\eta}n){R_n}^2$. A plot of $(\beta r/\bar{\eta}_0){R_1}^2$ for the benchmark vortex is shown in Fig. 2.2 and it is evident this term is also small throughout the vortex and its environment. Neglecting $(\bar{v}\beta\cos(\lambda)/\bar{\eta}\bar{\xi})\ (D_{\mathrm{v}}\,v'/Dt)$ then furnishes the equation for v':

$$v' = \frac{1}{\bar{\xi}}\frac{\partial\phi'}{\partial r} - \frac{1}{\bar{\xi}}\frac{D_{\mathrm{v}}}{Dt}\left(\frac{1}{\bar{\eta}r}\frac{\partial\phi'}{\partial\lambda}\right) - \frac{\bar{v}r\beta\sin\lambda}{\bar{\xi}}. \tag{2.31}$$

Together, (2.29) and (2.31) form approximate polarization equations for the balanced wind in the zeroth-order approximation:

$$u' = \underbrace{-\frac{1}{\bar{\eta} r}\frac{\partial \phi'}{\partial \lambda}}_{\text{"Geostrophic"}} \underbrace{-\frac{1}{\bar{\eta}}\frac{D_{\mathrm{v}}}{Dt}\left(\frac{1}{\bar{\xi}}\frac{\partial \phi'}{\partial r}\right)}_{\text{"Isallobaric"}} + \underbrace{\frac{\bar{v}^2 \beta \cos\lambda}{\bar{\eta}\bar{\xi}} - \frac{\beta^2 \bar{v}^2 r \sin\lambda \cos\lambda}{\bar{\eta}\bar{\xi}^2}}_{\text{"Beta terms"}}, \tag{2.32}$$

and

$$v' = \underbrace{\frac{1}{\bar{\xi}}\frac{\partial \phi'}{\partial r}}_{\text{"Geostrophic"}} \underbrace{+\frac{1}{\bar{\xi}}\frac{D_{\mathrm{v}}}{Dt}\left(-\frac{1}{\bar{\eta} r}\frac{\partial \phi'}{\partial \lambda}\right)}_{\text{"Isallobaric"}} - \underbrace{\frac{\bar{v} r \beta \sin\lambda}{\bar{\xi}}}_{\text{"Beta term"}}. \tag{2.33}$$

The "Geostrophic" and "Isallobaric" terms are gradient-wind generalizations of the geostrophic wind and isallobaric wind, respectively, from QG theory. Equations (2.32) and (2.33) are similar to those developed by Montgomery and Kallenbach (1996) except for the "beta" terms and the beta dependence implicit in $\bar{\eta}$ and $\bar{\xi}$.

Substituting (2.32) and (2.33) into the continuity equation (2.11) gives a first-order evolution equation for ϕ' that is a minimal truncation of the linear PE:

$$\frac{D_{\mathrm{v}}}{Dt}\phi' + \frac{1}{r}\frac{\partial}{\partial r}\left[r\bar{\Phi}\left\{-\frac{1}{r\bar{\eta}}\frac{\partial \phi'}{\partial \lambda} - \frac{1}{\bar{\eta}}\frac{D_{\mathrm{v}}}{Dt}\left(\frac{1}{\bar{\xi}}\frac{\partial \phi'}{\partial r}\right) + \frac{\bar{v}^2 \beta \cos\lambda}{\bar{\eta}\bar{\xi}} + \frac{\beta^2 \bar{v}^2 r \sin\lambda \cos\lambda}{\bar{\xi}^2}\right\}\right] + \frac{\bar{\Phi}}{r}\frac{\partial}{\partial \lambda}\left[\frac{1}{\bar{\xi}}\frac{\partial \phi'}{\partial r} - \frac{1}{\bar{\xi}}\frac{D_{\mathrm{v}}}{Dt}\left(\frac{1}{\bar{\eta} r}\frac{\partial \phi'}{\partial \lambda}\right) - \frac{\bar{v} r \beta \sin\lambda}{\bar{\xi}}\right] = 0 \tag{2.34}$$

The errors incurred to derive (2.34) scale as follows. In the near-vortex region the errors scale as $O\left({R_n}^2, (\beta r/\bar{\xi}){R_n}^2, (\beta r/\bar{\eta}){R_n}^2\right)$. In the vortex environment the Rossby number is small compared to unity and the errors scale as $O(R^2, (\beta r/f_0)R^2)$. Since $\beta r/f_0 = (\beta r^2/\bar{v})R$, then for horizontal scales such that $R << 1$ and $\beta r^2/\bar{v} \sim O(1)$ the neglected $(\beta r/f_0)R^2$ terms scale as $O(R^3)$. In practice, the ratio $\beta r^2/\bar{v}$ becomes large in the vortex environment ($r > 1000$ km) and the β-plane approximation begins to break down. Since the beta gyres typically form within this region the inaccuracy of the beta-plane approximation at a large radius is not a serious concern for vortex motion studies.

Although (2.34) is a minimal truncation of the PE it can be nonetheless simplified by making additional approximations which are formally no worse than the approximations already made. In addition, terms containing beta can be approximated by their f-plane counterparts unless these terms are explicitly differentiated (β-plane approximation). The

further simplified balance system incurs errors that scale with (2.34) and (2.19) in the near-vortex region and environment, respectively. Details of the additional approximations are summarized in Appendix A. Adopting subscript notation for partial derivatives, the final geopotential evolution equation is given by:

$$\frac{D_{\mathrm{V}}}{Dt}\left[\frac{\bar{\gamma}_0^2}{r}\frac{\partial}{\partial r}\left(\frac{r\phi'_r}{\bar{\gamma}_0^2}\right)+\frac{\phi'_{\lambda\lambda}}{r^2}-\bar{\gamma}_0^2\phi'\right]-\frac{\bar{\xi}_0}{\bar{q}_0}\frac{d\bar{q}_0}{dr}\frac{\phi'_\lambda}{r}-\beta\sin\lambda\frac{\bar{\xi}_0}{\bar{\eta}_0}\bar{\Phi}\frac{\partial}{\partial r}\left(\frac{r}{\bar{\Phi}}\right)\frac{\phi'_\lambda}{r}$$
$$+\bar{\eta}_0\left(\bar{v}+\frac{\phi'_r}{\bar{\xi}_0}\right)\beta\cos\lambda=0, \qquad (2.35)$$

where $\bar{\eta}_0$, $\bar{\xi}_0$,and $\bar{\gamma}_0^2$ denote the f-plane counterparts of $\bar{\eta}$, $\bar{\xi}$ and $\bar{\gamma}^2$, where $\bar{\gamma}^2=\bar{\eta}\bar{\xi}/\bar{\Phi}$. Denoting the AB-Laplacian operator as

$$\nabla^2_{\mathrm{AB}}=\frac{\bar{\gamma}_0^2}{r}\frac{\partial}{\partial r}\left(\frac{r}{\bar{\gamma}_0^2}\frac{\partial}{\partial r}\right)+\frac{1}{r^2}\frac{\partial^2}{\partial\lambda^2} \qquad (2.36)$$

and inverting (2.35) for $\partial\phi'/\partial t$ gives the geopotential tendency

$$\frac{\partial\phi'}{\partial t}=\left(\nabla^2_{\mathrm{AB}}-\bar{\gamma}_0^2\right)^{-1}\left[\frac{\bar{\xi}_0}{\bar{q}_0}\frac{d\bar{q}_0}{dr}\frac{\phi'_\lambda}{r}-\frac{\bar{v}}{r}\left(\nabla^2_{\mathrm{AB}}-\bar{\gamma}_0^2\right)\phi'_\lambda+\beta\sin\lambda\frac{\bar{\xi}_0}{\bar{\eta}_0}\bar{\Phi}\frac{\partial}{\partial r}\left(\frac{r}{\bar{\Phi}}\right)\frac{\phi'_\lambda}{r}\right.$$
$$\left.-\beta\cos\lambda\bar{\eta}_0\left(\bar{v}+\frac{\phi'_r}{\bar{\xi}_0}\right)\right]. \qquad (2.37)$$

The β-plane model encapsulated by (2.35) is hereafter designated β-AB. The β-AB model has two noteworthy and desirable properties:

(i) When $\bar{v}=0$ it reduces to the linearized QG β-plane PV equation (eq. 2.19 with $\bar{v}=0$).

(ii) When $\beta=0$ it reduces to the f-plane AB evolution equation of Montgomery and Kallenbach (1996) bridging quasi-gradient and quasi-geostrophic balance dynamics in flow regimes of order one asymmetric divergence.

The β-AB model thus qualifies as a valid intermediate balance model which should prove useful in examining intense vortex motion in divergent flows retaining full inertial effects.

For Rossby numbers of order unity the β-AB model is expected to furnish accurate forecasts since in such flows ${R_1}^2$ is typically very small compared to unity (SM). Because the balance approximation places no restriction on the magnitude of asymmetric

divergence it remains valid for relatively shallow flows where the squared Froude number is subcritical (i.e., $\bar{v}^2/g\bar{h} < 1$) but near unity. The β-AB model therefore complements the nonlinear balance model proposed by McWilliams et al. (1986) and McWilliams and Gent (1986) for examining the motion of mesoscale and sub-mesoscale oceanic vortices possessing order unity Rossby numbers and small Froude numbers.

2.4 Analogous Conservation Laws

As verification of formal consistency, several conservation laws for (2.35) analogous to those of the linearized PE may be derived.

2.4.1 Momentum

Consistent with the approximations made to obtain (2.37), equations (2.32) and (2.33) may be rewritten as

$$u' = -\frac{1}{\bar{\eta} r}\frac{\partial \phi'}{\partial \lambda} - \frac{1}{\bar{\eta}_0 \bar{\xi}_0}\frac{D_{\mathrm{v}}}{Dt}\left(\frac{\partial \phi'}{\partial r}\right), \tag{2.38}$$

$$v' = \frac{1}{\bar{\xi}}\frac{\partial \phi'}{\partial r} - \frac{1}{\bar{\eta}_0 \bar{\xi}_0}\frac{D_{\mathrm{v}}}{Dt}\left(\frac{1}{r}\frac{\partial \phi'}{\partial \lambda}\right) - \frac{\bar{v} r \beta \sin\lambda}{\bar{\xi}_0}. \tag{2.39}$$

Upon defining

$$u'_{\eta_0} = -\frac{1}{r\bar{\eta}_0}\frac{\partial \phi'}{\partial \lambda},$$
$$v'_{\xi_0} = \frac{1}{\bar{\xi}_0}\frac{\partial \phi'}{\partial r},$$

and multiplying (2.38) by η_0 and (2.39) by ξ_0 yields the following the radial and azimuthal pseudo-momentum equations:

$$\frac{D_{\mathrm{v}}}{Dt}u'_{\eta_0} - \bar{\xi}_0 v' = -\frac{\bar{\xi}_0}{\bar{\xi}}\frac{\partial \phi'}{\partial r} + \bar{v} r \beta \sin\lambda, \tag{2.40}$$

$$\frac{D_{\mathrm{v}}}{Dt}v'_{\xi_0} + \bar{\eta}_0 u' = -\frac{\bar{\eta}_0}{\bar{\eta}}\frac{1}{r}\frac{\partial \phi'}{\partial \lambda}. \tag{2.41}$$

On an f-plane the multiplicative factors in front of the pressure gradient terms are equal to one. On a β-plane these terms are necessary to correctly represent Rossby wave dispersion in a resting fluid layer ($\bar{v} = 0$).

2.4.2 *Vorticity*

A pseudo-vorticity equation results upon curling the pseudo-momentum equations and making approximations consistent with (2.35). The result is

$$\frac{D_{\mathrm{V}}}{Dt}\zeta'_{\xi_0} + u'\frac{d\bar{\eta}_0}{dr} + u'_{\eta_0}\frac{\partial f}{\partial r} + \frac{\bar{\eta}_0}{\bar{\xi}_0}(\bar{v} + v'_{\xi_0})\frac{1}{r}\frac{\partial f}{\partial \lambda} = -\bar{\eta}_0\left[\frac{1}{r}\frac{\partial (ru')}{\partial r} + \frac{1}{r}\frac{\partial v'}{\partial \lambda}\right]. \tag{2.42}$$

The pseudo-vorticity $\zeta'_{\xi_0} = \hat{\mathbf{k}} \cdot \nabla \times \mathbf{u}'_{\xi_0}$ is derived from the pseudo-momentum based on the inertia parameter $\bar{\xi}_0$:

$$\mathbf{u}'_{\xi_0} = \left(\frac{-1}{r\bar{\xi}_0}\frac{\partial \phi'}{\partial \lambda}, \frac{1}{\bar{\xi}_0}\frac{\partial \phi'}{\partial r}\right). \tag{2.43}$$

The pseudo-vorticity equation (2.42) and the corresponding PE vorticity equation (2.12) are quite similar. Both include advection of f-plane absolute vorticity by a perturbation radial wind. Both also include the convergence of basic state vorticity. The PE, however, converges β-plane basic state vorticity while β-AB converges the f-plane counterpart. They also differ slightly in the advection of the planetary vorticity by the total tangential wind. The AB version carries the distortion term $\bar{\eta}_0/\bar{\xi}_0$ in front of the "total" azimuthal wind, $\bar{v} + v'_{\xi_0}$. Since $\bar{\eta}_0/\bar{\xi}_0$ approaches one in the environment, where the beta gyres typically attain their maximum amplitude, it is anticipated that the $\bar{\eta}_0/\bar{\xi}_0$ term should only introduce quantitative but not qualitative differences between the PE and the β-AB solutions when the β-AB approximation is valid.

2.4.3 *Potential Vorticity*

The PV conservation principle for the β-AB model results by eliminating the divergence term between the continuity and pseudo-vorticity equations:

$$\frac{D_{\mathrm{V}}}{Dt}q'_{\xi_0} + u'\frac{d\bar{q}_0}{dr} + \frac{u'_{\eta_0}}{\bar{\Phi}}\frac{\partial f}{\partial r} + \frac{1}{\bar{\Phi}}\frac{\bar{\eta}_0}{\bar{\xi}_0}\left(\bar{v} + v'_{\xi_0}\right)\frac{1}{r}\frac{\partial f}{\partial \lambda} = 0, \tag{2.44}$$

where

$$q'_{\xi_0} = \frac{\zeta'_{\xi_0}}{\bar{\Phi}} - \bar{q}_0\frac{\phi'}{\bar{\Phi}} \tag{2.45}$$

is the perturbation pseudo-PV. Except for the distortion term multiplying the tangential wind (2.44) is similar to its PE counterpart (2.14).

2.4.4 *Energy*

A disturbance energy equation results upon forming,

$$\frac{\bar{\Phi}}{g}\left(u'_{\xi_0}\times(2.40)+v'_{\eta_0}\times(2.41)\right)+\frac{\phi'}{g}\times(2.11), \tag{2.46}$$

and applying the β-plane approximation. The result is

$$\underbrace{\frac{D_{\mathrm{V}}}{Dt}\left[\frac{\bar{\Phi}}{2g}\left(u'_{\xi_0}u'_{\eta_0}+v'_{\xi_0}v'_{\eta_0}\right)+\frac{(\phi')^2}{2g}\right]}_{\text{Term A}}+\underbrace{\frac{\phi'}{g}\left[\frac{1}{r}\frac{\partial}{\partial r}\left(r\bar{\Phi}u'\right)+\frac{1}{r}\frac{\partial\bar{\Phi}v'}{\partial\lambda}\right]}_{\text{Term B}}$$

$$\underbrace{+\frac{\bar{\Phi}}{g}\left[\bar{\eta}_0u'v'_{\eta_0}-\bar{\xi}_0v'u'_{\xi_0}\right]}_{\text{Term C}}\underbrace{+\frac{\bar{\Phi}}{g}\left[u'_{\xi_0}\frac{\partial\phi'}{\partial r}+\frac{v'_{\eta_0}}{r}\frac{\partial\phi'}{\partial\lambda}\right]}_{\text{Term D}}\underbrace{-\frac{\bar{\Phi}}{g}\left[u'_{\xi_0}\bar{v}r\beta\sin\lambda\right]}_{\beta\text{-plane term}}=0. \tag{2.47}$$

Term A represents the disturbance energy (kinetic plus potential) integrated over the fluid depth. Terms B and C combine to

$$\nabla\cdot\left(\frac{\bar{\Phi}}{g}\phi'\mathbf{u}'\right), \tag{2.48}$$

a depth integrated pressure work term. Term D simplifies to

$$\frac{\bar{\Phi}}{g}v'_{\xi_0}u'_{\eta_0}r\frac{d\bar{\Omega}}{dr}, \tag{2.49}$$

a depth integrated Reynolds stress. The last term in (2.47) arises due to the β-effect and represents a source of perturbation energy associated with the advection of planetary vorticity by the mean circular vortex. Inserting these substitutions into (2.47) yields an equation similar to the PE energy equation (2.18):

$$\frac{D_{\mathrm{V}}}{Dt}\left[\frac{\bar{\Phi}}{2g}\left(u'_{\xi_0}u'_{\eta_0}+v'_{\xi_0}v'_{\eta_0}\right)+\frac{(\phi')^2}{2g}\right]+\nabla\cdot\left(\frac{\bar{\Phi}}{g}\phi'\mathbf{u}'\right)$$
$$+\frac{\bar{\Phi}}{g}v'_{\xi_0}u'_{\eta_0}r\frac{d\bar{\Omega}}{dr}-\frac{\bar{\Phi}}{g}u'_{\xi_0}r\bar{v}\beta\sin\lambda=0, \tag{2.50}$$

Integrating (2.50) over the entire vortex gives a bulk measure of the amplitude of the asymmetries. Assuming $\phi'\mathbf{u}'\to 0$ as $r\to\infty$ and recalling $\phi'(r=0)=0$, the boundary terms vanish leaving

$$\frac{\partial}{\partial t}\int_0^{2\pi}\int_0^{\infty}\left[\frac{\bar{\Phi}}{2g}\left(u'_{\xi_0}u'_{\eta_0}+v'_{\xi_0}v'_{\eta_0}\right)+\frac{(\phi')^2}{2g}\right]r\,dr\,d\lambda=$$
$$-\int_0^{2\pi}\int_0^{\infty}\left[\frac{\bar{\Phi}}{g}v'_{\xi_0}u'_{\eta_0}r\frac{d\bar{\Omega}}{dr}\right]r\,dr\,d\lambda+\int_0^{2\pi}\int_0^{\infty}\left[\frac{\bar{\Phi}}{g}u'_{\xi_0}\bar{v}r\beta\sin\lambda\right]r\,dr\,d\lambda. \tag{2.51}$$

A useful model diagnostic is therefore the integrated disturbance energy

$$E(t) = \int_0^{2\pi}\int_0^{\infty}\left[\frac{\bar{\Phi}}{2g}\left(u'_{\xi_0}u'_{\eta_0} + v'_{\xi_0}v'_{\eta_0}\right) + \frac{(\phi')^2}{2g}\right] r\,dr\,d\lambda. \tag{2.52}$$

2.5 Summary

The β-AB shallow water model is both a simplification and an extension of the SM balance model originally developed for studying continuously stratified baroclinic hurricane vortices on an f-plane. The theory has been simplified to shallow water dynamics, yet retains the Earth's planetary vorticity gradient. Unlike the linear f-plane formulation employing a binomial expansion in the square of the local Rossby number and a truncation of the asymptotic series at zeroth order, the β-plane formulation requires not only the smallness of the local Rossby number squared but also the smallness of certain beta terms that arise in the derivation of the traditional quasigeostrophic β-plane equations. Making further approximations consistent with the derivation of the minimally truncated system yields a natural extension of the f-plane geopotential tendency equation derived by Montgomery and Kallenbach (1996). The simplified forecast equation has an associated pseudo-momentum principle, a vertical vorticity equation, a PV equation, and an energy equation that are all analogous to the linearized PE.

We next examine the usefulness of the β-AB model by investigating by the canonical problem of vortex motion on a beta plane.

Chapter 3

THE LINEAR BETA DRIFT PROBLEM

3.1 Introduction

For the most part the physics of the beta drift problem is reasonably well understood. When an intense cyclonic circular vortex is placed on a beta plane in the Northern Hemisphere the vortex advects higher planetary vorticity to the south on the west side of the storm, while lower planetary vorticity is advected to the north on the east side. The advection of planetary vorticity distorts the vortex, its asymmetric part dominated by a wavenumber one asymmetry. The resulting vorticity dipole (the "beta gyres") is initially oriented east-west and the flow between these gyres advects the vortex to the north. The basic state vortex then advects these gyres so as to orient the flow between them to the northwest. Fiorino and Elsberry (1989) describe this as a balance between the beta forcing and the advection of the gyres. The advection of the beta gyres is in equilibrium against the forcing of the gyres and is responsible for the westward component of the drift.

A vortex on a beta plane in the absence of environmental flow has been investigated by many researchers in a variety of different ways. Much work has been done using the barotropic nondivergent vorticity equation, as in DeMaria (1985), Smith et al. (1990), Chan and Williams (1987), and Fiorino and Elsberry (1989; hereafter FE) among others. Shapiro and Ooyama (1990), Sutyrin and Flierl (1994), Willoughby (1988, 1990b, 1992, 1994, 1995) and others have investigated this problem in a shallow water setting to allow for the effect of divergence. Shapiro and Ooyama (1990) attribute little difference in vortex track to divergent effects, while Willoughby (1990) predicts up to a factor of ten in the asymptotic drift speed of the vortex due to divergence. The shallow water AB formulation naturally lends itself to examining such potential effects.

The "linear" aspect of this presentation follows that of Willoughby (1988). Here, as in Willoughby's work, linearity means axisymmetric mean PV is advected by the perturbation flow, and axisymmetric mean flow advects both planetary and perturbation PV. Explicitly left out is the perturbation advection of planetary vorticity. Smith et al. (1990; hereafter SUD) and Reznik and Dewar (1994) give scaling arguments for discarding this term.

For the AB model to capture the essential physics of the beta drift problem, the desired results are clear. The vortex should initially force east-west oriented gyres, then advect them so that the flow between them is towards the northwest. The vortex should then asymptote to a steady state speed of a few meters a second.

3.2 Governing Equations

As discussed above, we consider the canonical beta drift problem. Because the ensuing asymmeteries are proportional to the forcing, they scale as $O(\beta)$. The solution can then be expanded in an asymptotic series (Reznik and Dewar 1994) involving the dimensionless parameter $\alpha = \beta(RMW)^2/V_{max} << 1$. To first order in α the asymmetries are determined by neglecting the perturbation advection of planetary vorticity. Planetary Rossby wave radiation is therefore precluded at this level of approximation. The simplified forecast equation is equivalent to ignoring the beta dependence in the dimensionless distortion factors multiplying the perturbation pressure gradient terms in the radial and tangential pseudo-momentum equations (2.40 and 2.41).

3.2.1 Momentum

The simplified pseudo-momentum equations are

$$\frac{D_v}{Dt}u'_{\eta_0} - \bar{\xi}_0 v' = -\frac{\partial \phi'}{\partial r} + \bar{v} r \beta \sin\lambda \tag{3.1}$$

$$\frac{D_v}{Dt}v'_{\xi_0} + \bar{\eta}_0 u' = -\frac{1}{r}\frac{\partial \phi'}{\partial \lambda}. \tag{3.2}$$

3.2.2 Vorticity

The simplified vorticity equation is

$$\frac{D_v}{Dt}\zeta'_{\xi_0} + u'\frac{d\bar{\eta}_0}{dr} = -\bar{\eta}_0\left[\frac{1}{r}\frac{\partial(ru')}{\partial r} + \frac{1}{r}\frac{\partial v'}{\partial \lambda}\right] - \frac{\bar{\eta}_0}{\bar{\xi}_0}\bar{v}\beta\cos\lambda. \tag{3.3}$$

3.2.3 Potential Vorticity

The simplified PV equation is

$$\frac{D_v}{Dt} q'_{\xi_0} + u' \frac{d\bar{q}_0}{dr} + \frac{1}{\bar{\Phi}} \frac{\bar{\eta}_0}{\bar{\xi}_0} \bar{v} \beta \cos\lambda = 0. \tag{3.4}$$

3.2.4 Forecast Equation

The simplified forecast equation is

$$\frac{\partial \phi'}{\partial t} = \left(\nabla^2_{AB} - \bar{\gamma}_0^2 \right)^{-1} \left[\frac{\bar{\xi}_0}{\bar{q}_0} \frac{d\bar{q}_0}{dr} \frac{\phi'_\lambda}{r} - \frac{\bar{v}}{r} \left(\nabla^2_{AB} - \bar{\gamma}_0^2 \right) \phi'_\lambda - \bar{\eta}_0 \bar{v} \beta \cos\lambda \right]. \tag{3.5}$$

3.3 Setting Up The Model

The benchmark vortex is identical to the one used in KM (1995), see Fig. 3.1. It possesses a large Rossby number in the inner core region ($R \simeq 18$) and is assumed in gradient balance with $f_0 = 5 \times 10^{-5} s^{-1}$. As shown in KM (1995), the vortex scales as a minimal hurricane while ensuring that ${R_1}^2 < 1$ throughout. By choosing the basic state PV to be smooth, monotonic and everywhere positive the profile is guaranteed to be both inertially (centrifugally) stable and shear stable in the AB formulation.

The numerical model is semi-spectral, using Fourier modes azimuthally and grid points radially. Because of the pure linearity of the problem, all wavenumbers higher than one are forced to zero throughout the model runs. Thus in the linear beta drift problem the basic state vortex is modeled as a time invariant swirl in gradient balance and all wave-mean-flow interactions are neglected. The model is time-stepped with a fourth-order Runge Kutta scheme and typical time steps are on the order of five minutes. With a radial grid spacing of 2.5 km, the chosen timestep falls sufficiently below the empirically determined CFL stability threshold. In the case of the Willoughby vortex a 2 km gridspacing is employed. All model runs use 1200 radial gridpoints and employ energetically consistent $\nu\nabla^2$ diffusion with $\nu \simeq 200$ m^{2}s^{-1} in the near-core region in order to remove fine-scale PV associated with the potential enstrophy cascade.

The model is a stationary grid model whose center is located at the center of the vortex. A stationary grid model is adequate for the physics examined since the difference

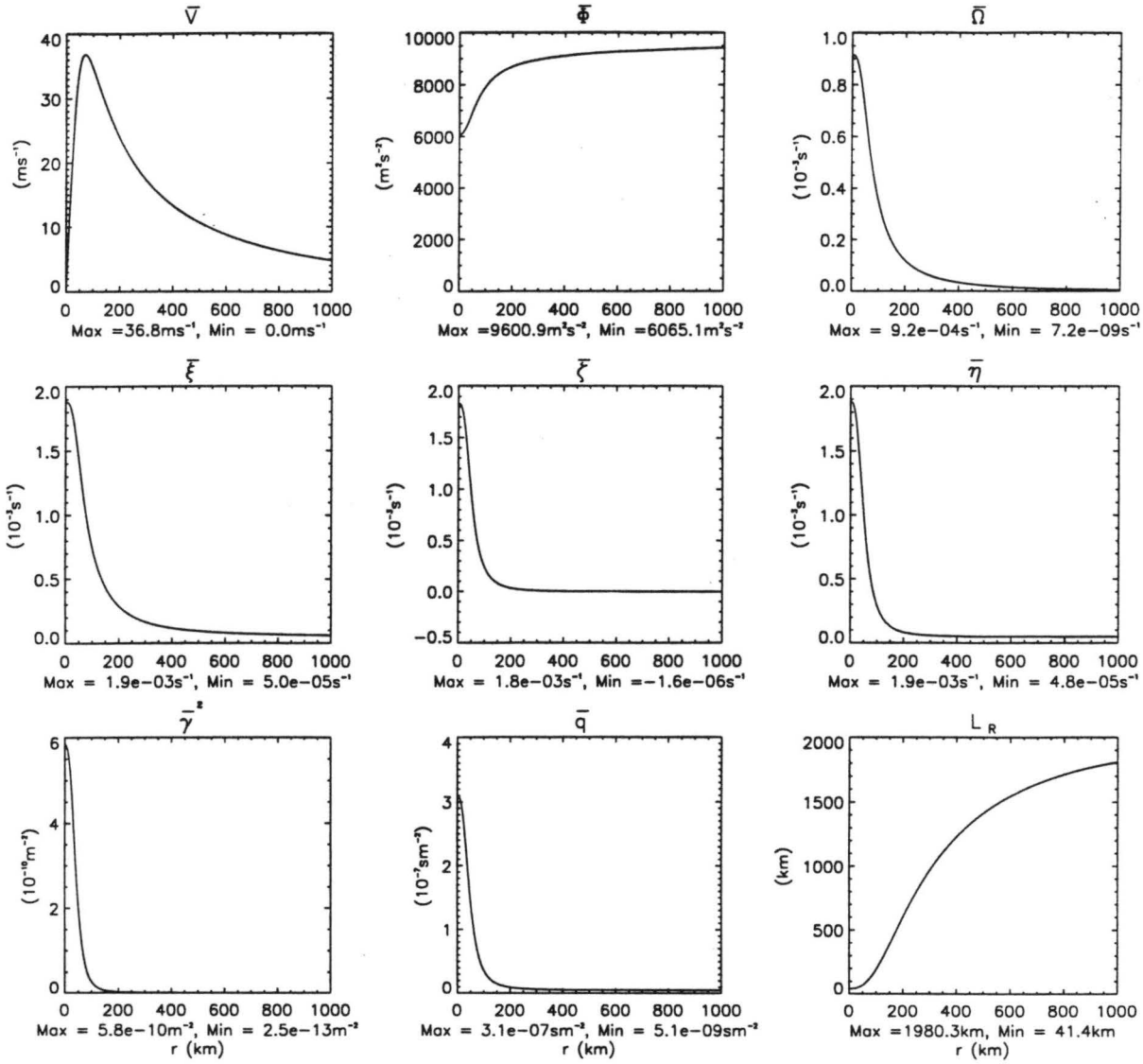

Figure 3.1: The benchmark vortex: $\bar{v}$ the tangential wind; $\bar{\Phi}$ the geopotential for a fluid with a resting depth of 1 km; $\bar{\Omega}$ the storm rotation rate; $\bar{\xi}$ the f-plane inertia parameter; $\bar{\zeta}$ the f-plane relative vorticity; $\bar{\eta}$ the f-plane absolute vorticity for $f_0 = 5 \times 10^{-5} s^{-1}$; $\bar{\gamma}^2$ the inverse deformation radius squared on the f-plane; $\bar{q}$ the f-plane potential vorticity $= \bar{\eta}/\bar{\Phi}$; and L_R the deformation radius. Only the inner 1000 km of the 3000 km domain are shown.

between the tracks in a stationary vs. moving coordinate system has been found to be less than one percent in (FE). The center of the vortex is identified using a best circle fit to the height field inside the radius of maximum winds. The method parallels that of Flatau (1992). The center of the vortex is checked after a prescribed time, and if it has moved more than a desired distance, the grid center is moved and the total potential vorticity is reinterpolated to the new grid. "High-wavenumber noise" associated with multiple grid moves and interpolations is avoided by the zeroing of higher azimuthal wavenumber coefficients.

The linear β-AB formulation was found to be somewhat sensitive to the initial profile used in these runs. A popular vortex profile used by many researchers is the Chan and Williams profile (1987). Presented in Fig. 3.26 is their "benchmark" profile, given by the formula

$$V(r) = V_{max}\left(\frac{r}{r_{max}}\right)\exp\left\{\frac{1}{b}\left[1-\left(\frac{r}{r_{max}}\right)^{b}\right]\right\}, \tag{3.6}$$

where $b = 1$, $V_{max} = 40$ ms^{-1}, and $r_{max} = 100$ km. Figure 3.26 elucidates the problem with this vortex when using it in the linear β-AB model. Most striking are the spikes in local Rossby number for wavenumber one between 200 km and 400 km. These are caused by a sign change in the absolute vorticity in these regions. The AB formulation is not valid for inertially unstable vortices.

SUD slightly modified the Chan and Williams profile to avoid the nonzero derivative in relative vorticity at $r = 0$. Their remedied profile is presented in Fig. 3.27. The SUD profile is essentially the same as Chan and Williams, except the nonzero value of dq_0/dr at $r = 0$ and the sign change in absolute vorticity has been eliminated. The SUD vortex still has the undesirable property that the local Rossby number for wavenumber one is not small, approaching three near $r = 250$ km (see Fig. 3.27).

Also presented are Willoughby's completely cyclonic vortex (Fig. 3.28) and DeMaria's (Fig. 3.29) vortex. As is evident from Fig. 3.28, Willoughby's profile possesses a discontinuity in $d\bar{\zeta}_0/dr$, reflected by the kink in the plot of local Rossby number. DeMaria's profile, on the other hand, is well behaved throughout the near-vortex region and the environment.

Another vortex considered here is the Schloemer vortex (Myers 1957) shown in Fig. 3.30. It most resembles the benchmark vortex in that the tangential wind decays relatively slowly with radius and exponentially approaches but never reaches zero in the model domain. Track results with the Schloemer vortex have been included here to facilitate a direct comparison with recent work by Willoughby (1995).

By observing the behavior of vortices with $O(1)$ Rossby numbers the robustness of the AB approximation may be elucidated. When ${R_1}^2$ is not much less than unity we are pushing the limit of the AB approximation. Although AB was shown to correctly represent the symmetrization process for freely evolving asymmetries on an f-plane (KM 1995), it proves constructive to consider two vortices that have truly small *local* Rossby numbers in the forced beta drift problem. These are presented in Figs. 3.32 and 3.33. Both vortices have positive, monotonically decreasing, and infinitely differentiable PV profiles but because of the reduced tangential winds have small *local* Rossby numbers for azimuthal wavenumber one.

3.4 Cyclone Track Results for the Benchmark Vortex

3.4.1 Geopotential and Potential Vorticity Fields

When a circular vortex is placed on a beta plane an initial vorticity dipole forms which is oriented east-west possessing maxima and minima near the vortex core. At subsequent times the distance between these extrema gradually increases and the dipole axis rotates counterclockwise (SUD). From Figs. 3.2 – 3.5 we see that the AB model evolves the beta gyres as described. The gyres are qualitatively similiar to the gyres presented in SUD, Willoughby (1995), and Shapiro and Ooyama (1990). At long times the ϕ' and q'_{ξ_0} fields possess extrema at approximately 1500 km. The time series clearly shows the extrema working their way outwards and approaching a steady state limit. Both the ϕ' and q'_{ξ_0} fields even show the trailing spiral pattern mentioned in Willoughby (1995) as a byproduct of having a vortex where tangential winds do not vanish within the model boundary.

While the gross features of the AB beta gyres are qualitatively similar to previous works, a quantitative difference in the near-core asymmetric structure is noteworthy and

deserves mention. Close inspection of the ϕ' fields shows a slight "pinching" in the inner part of the beta gyres. This pinching shows up as a secondary wave peak in Figs. 3.2 and 3.3. At this time it is unclear whether the pinching is an artifact of a misplaced center and numerous interpolations or the manifestation of the distortion factor $\bar{\eta}_0/\bar{\xi}_0$ in equations (3.3) and (3.4) which deviates significantly from unity for intense vortices where ${R_1}^2$ is less than but not much less than unity. The pinched geopotential field is thus slightly different from those presented in previous work showing a "near uniform" flow between the gyres (Elsberry and Abbey 1991). Further discussion of this issue is reserved for section 3.6.2.

3.4.2 Speed, Direction, and Track for the Benchmark Vortex

The speed of the benchmark vortex has been correlated with the vortex's outer wind-strength (FE). The slow decay of $\bar{v}$ with radius of the benchmark vortex prevents direct comparison to the majority of previous track studies using more confined vortices. Fortunately FE used several vortices which scale similarly to the ones presented here. FE define outer wind-strength as

$$V_s = \left[\frac{\int_{300km}^{1000km} r v^2 dr}{\int_{300km}^{1000km} r dr} \right]^{\frac{1}{2}} . \tag{3.7}$$

The relationship between asymptotic speeds in the FE runs and outer wind-strength are plotted in Fig. 3.6. The asymptotic speeds attained in the AB model for both the benchmark and the Schloemer vortex are also indicated in Fig. 3.6. For both vortices the asymptotic speeds slightly exceed those calculated by FE. This is consistent with the findings of Willoughby (1994) where nonlinear interactions were shown to reduce the drift speed relative to its purely linear model run. FE's numerical simulations include these nonlinear interactions. As Fig. 3.6 is for the initial strength, nonlinear interactions tend to reduce the basic state vortex tangential wind (FE) and should reduce the asymptotic limit. Since the basic state was not allowed to vary in the β-AB calculations the vortex strength does not change and a higher asymptotic speed should be expected.

Figure 3.7 plots the speed of the benchmark vortex with time. After 240 hours the

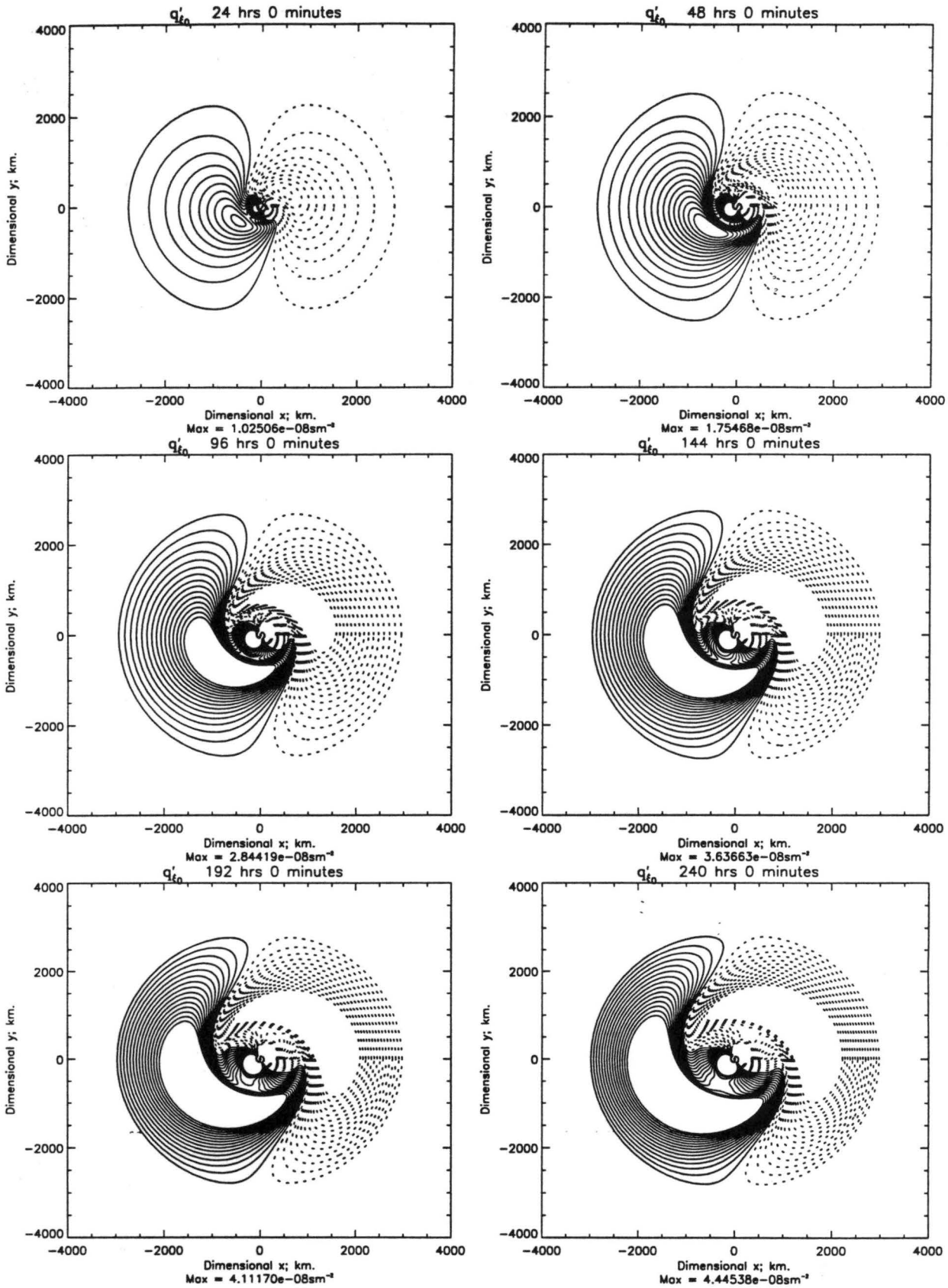

Figure 3.2: Wavenumber one q'_{ξ_0} evolution of the benchmark vortex, contour interval 1×10^{-10} sm^{-2}. Values outside of $\pm 14.5 \times 10^{-10}$ sm^{-2} have not been contoured.

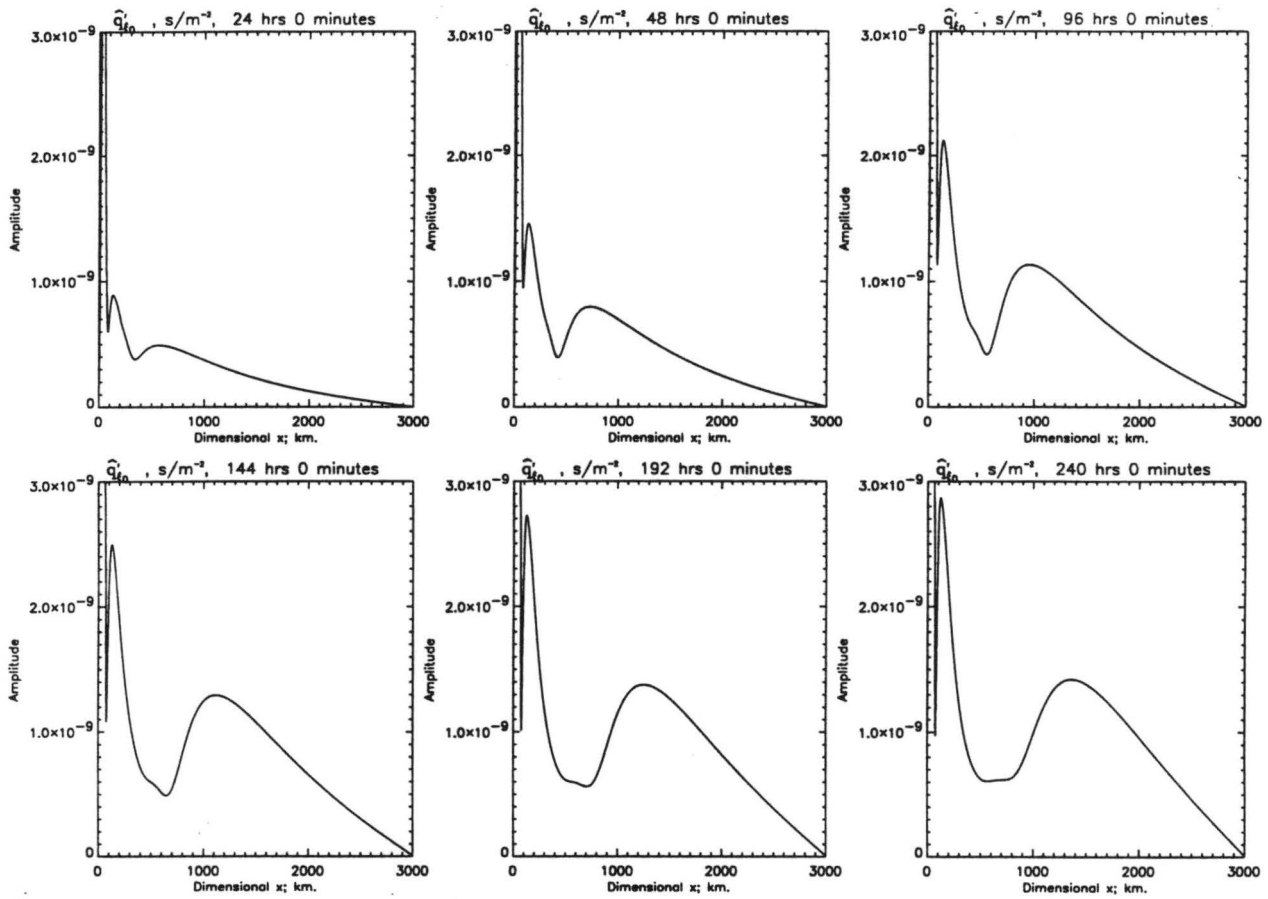

Figure 3.3: Radial representation of $|\hat{q}_{\xi_0}|$ for wavenumber one for the benchmark vortex, where $|\hat{q}_{\xi_0}|$ is the Fourier azimuthal amplitude of q'_{ξ_0}. Note the outward migration of the beta gyre peak (near 1500 km) and its attaining a fairly constant amplitude.

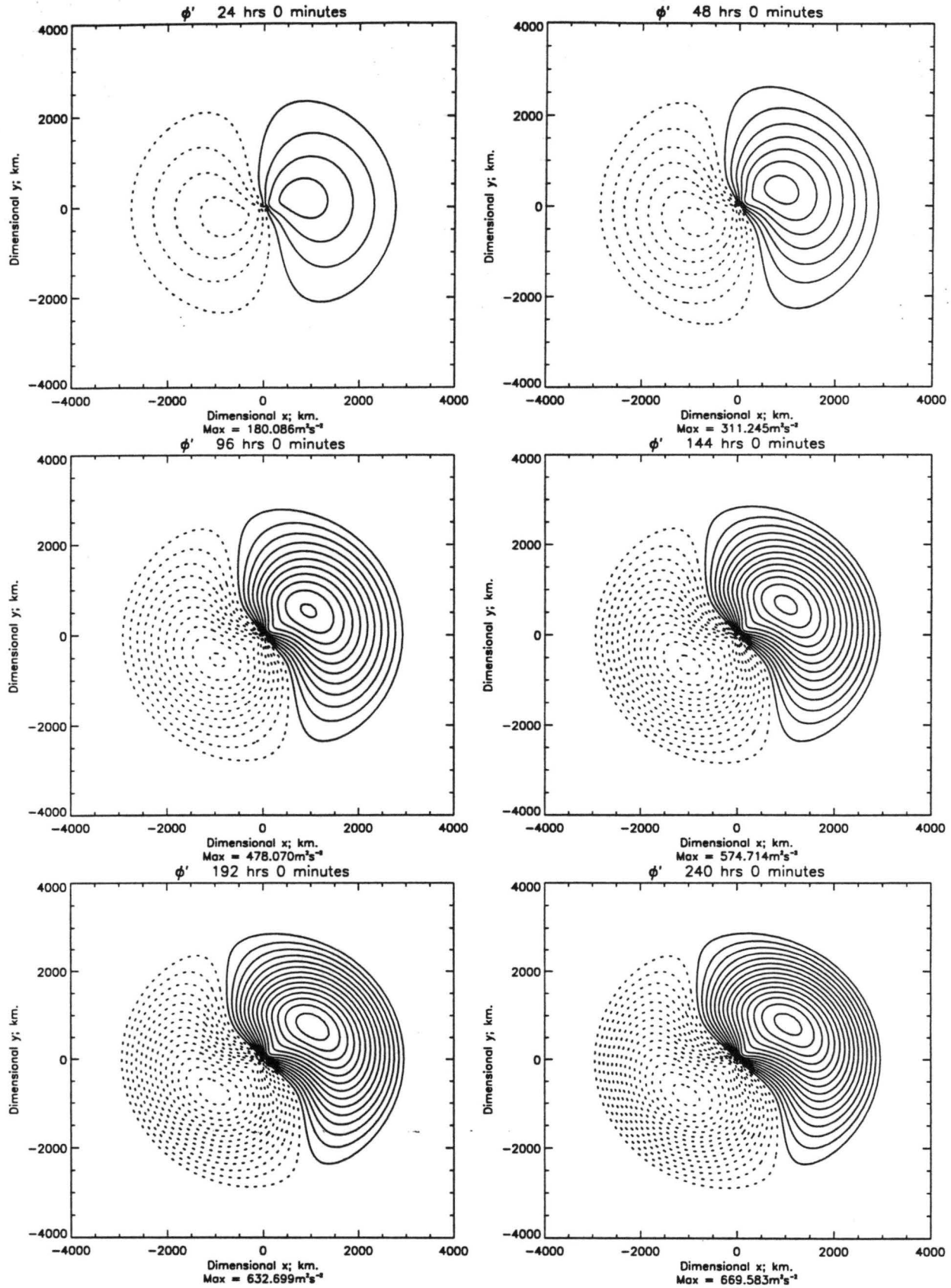

Figure 3.4: The wavenumber one ϕ' evolution of the benchmark vortex, contour interval 45 m^2s^{-2}.

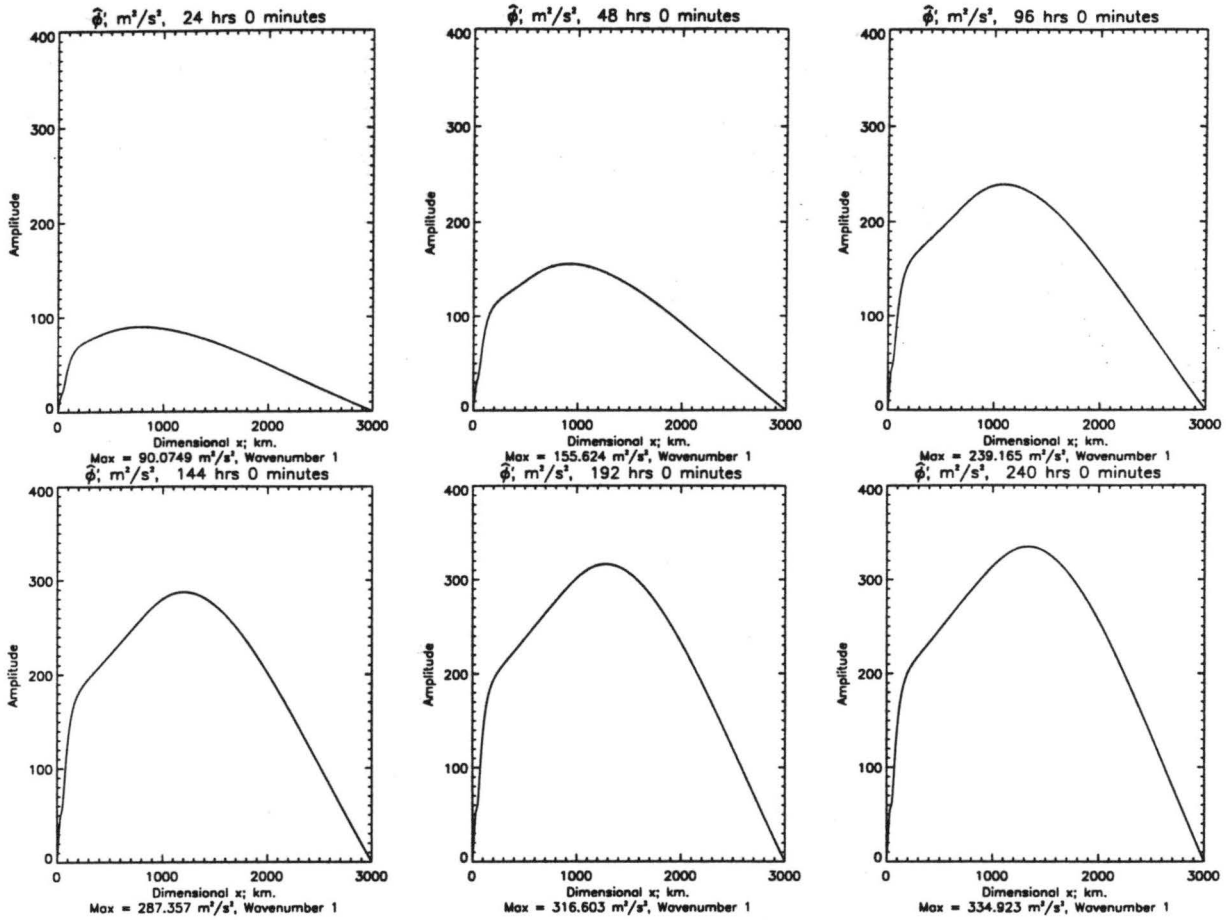

Figure 3.5: Radial representation of $|\hat{\phi}|$ for wavenumber one for the benchmark vortex, where $|\hat{\phi}|$ is the Fourier azimuthal amplitude of ϕ'. Note the outward migration of the beta gyre peak and its attaining a fairly constant amplitude (near 1500 km).

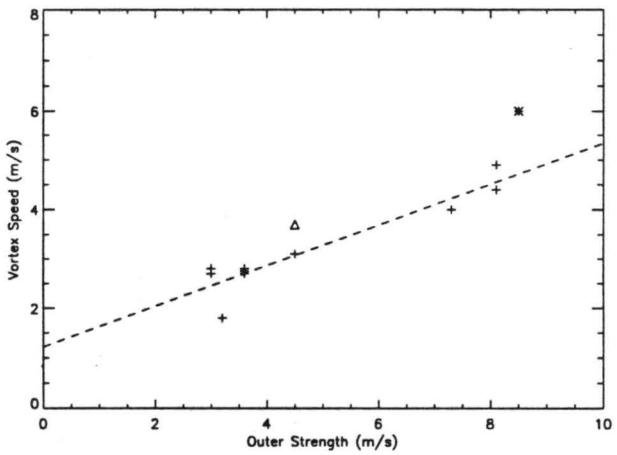

Figure 3.6: Adapted from FE. The crosses represent FE runs for vortices of varying initial strengths. The asterisk represents the benchmark vortex and the triangle the Schloemer profile. The dotted line represents a simple least squares fit of the FE runs.

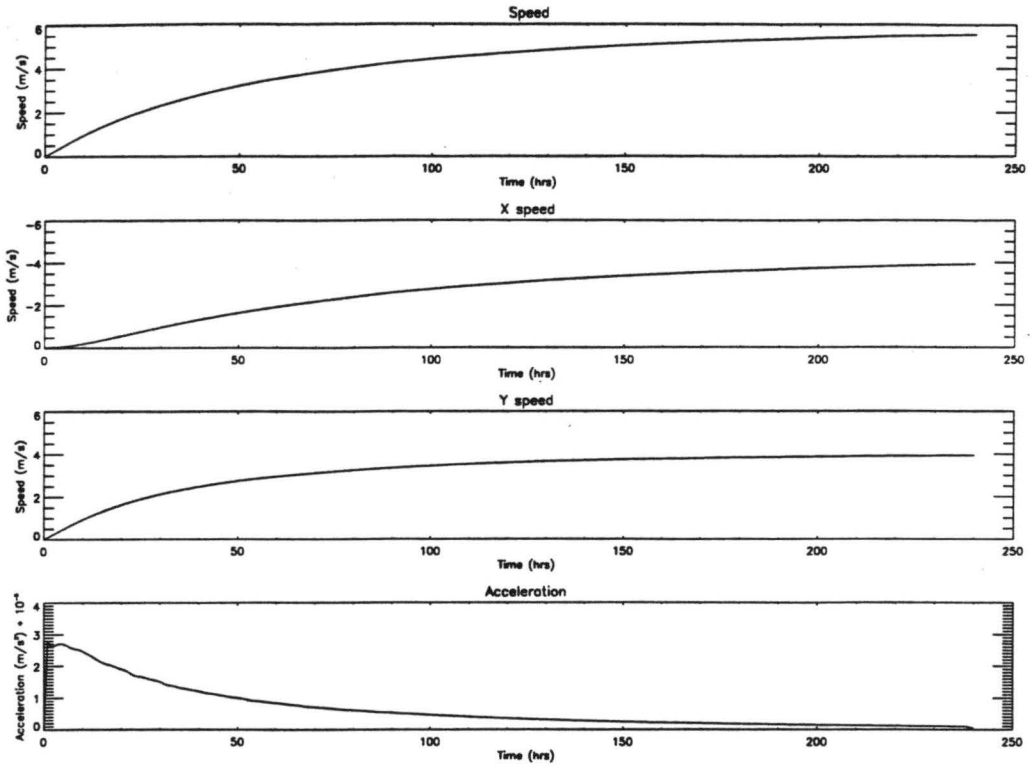

Figure 3.7: 240 hour plot of total speed, northward speed, westward speed and total acceleration of the benchmark vortex.

vortex is close to obtaining its asymptotic limit of approximately 6 ms^{-1}. By this time the vortex has reached its asymptotic northward drift speed, but has not yet attained its westward speed. These properties are also reflected in Fig. 3.8 showing vortex direction (clockwise from north) with time. The qualitative behavior of the linear β-AB model with respect to storm speed and direction is similiar to previous motion studies on the β-plane. As evidenced by the track plot in Fig. 3.9 the vortex undergoes an initial northward drift, followed by an increasing westward component as the beta gyres get cyclonically advected. In the linear β-AB model the drift speed asymptotes to a finite value as a balance is obtained between the forcing of the beta gyres, advection of perturbation PV by the basic state, and perturbation advection of basic state PV [1]. This balance is obtained by setting $\partial/\partial t = 0$ in either (3.4) or (3.5). In contrast to other investigations employing

[1]The speed and track results presented here are not sensitively dependent on the frequency with which the grid is moved. For example, doubling or halving the grid-move frequency produces virtually identical tracks.

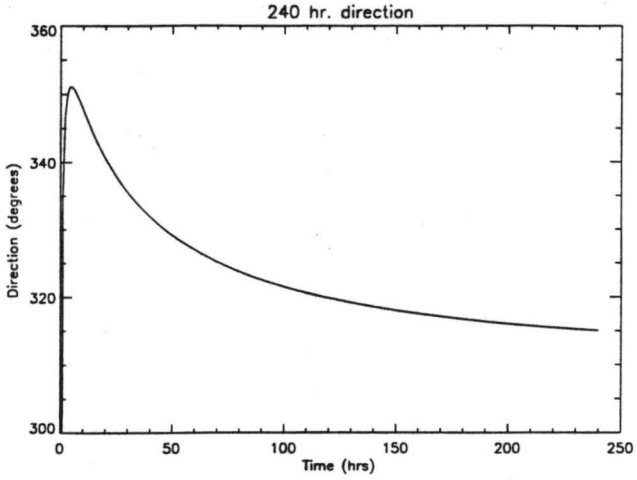

Figure 3.8: 240 hr. direction plot clockwise from north (360°) of the benchmark vortex.

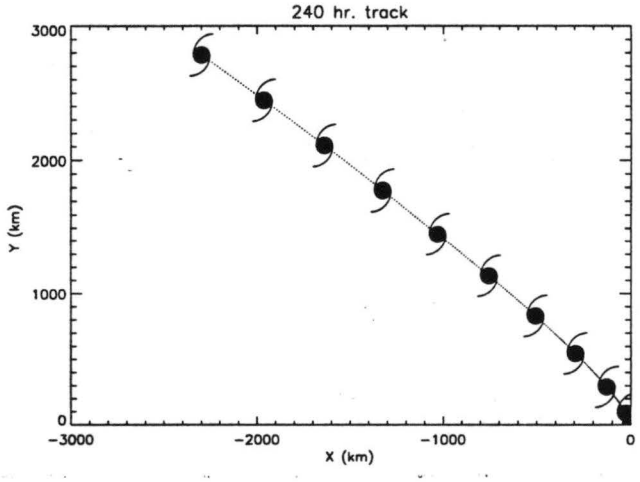

Figure 3.9: 240 hr. track of the benchmark vortex. Cyclone symbols denote vortex location every 24 hours.

fully nonlinear nondivergent models on the β-plane (DeMaria 1985, FE, and many others) vortices in the linear β-AB model take a relatively long time to attain their asymptotic drift speed. This is most likely an artifact of the linear formulation. These results are in contrast to Willoughby's purely linear PE formulation where the vortex continues to accelerate, never reaching a constant speed. The β-AB track forecast is a compromise between the nonlinear nondivergent model and Willoughby's linear work: The vortex speed ultimately asymptotes to a constant value but only after a relatively long time.

3.5 Cyclone Track Results for the Schloemer Vortex

As a consistency test it is important that the linear β-AB formulation of the AB model give qualitatively similar results for other vortex profiles. An alternate profile presented in Figs. 3.30 – 3.31 is based on the empirically deduced pressure profile of Myers (1957).

3.5.1 Geopotential and Potential Vorticity Fields

Inspection of Figs. 3.10 – 3.13 shows that both the wavenumber one q'_{ξ_0} and ϕ' fields are similiar to the fields presented for the benchmark vortex. On comparing the evolution of wavenumber one perturbation PV and ϕ' fields for the two vortices some subtle differences are apparent. The beta gyres have less magnitude in the Schloemer vortex and are located closer to the center.

3.5.2 Speed, Direction, and Track for the Schloemer Vortex

The Schloemer vortex exhibits qualitatively similar characteristics as the benchmark vortex. It eventually asymptotes to a steady-state speed of approximately 3.7 ms^{-1}, see Fig. 3.14. The asymptotic drift speed compares favorably to the outer-wind strength dependence demonstrated by FE (1989). Like the benchmark vortex, the vortex speed lies above the least squares fit to the FE data.

The direction and track (Figs. 3.15 and 3.16) are in agreement with previously published results and with the benchmark vortex runs. The vortex takes an initially northward track, gradually turning more to the west as the beta gyres are advected by the basic state flow. The Schloemer vortex reaches a drift angle of about 315°, close to the 310° drift

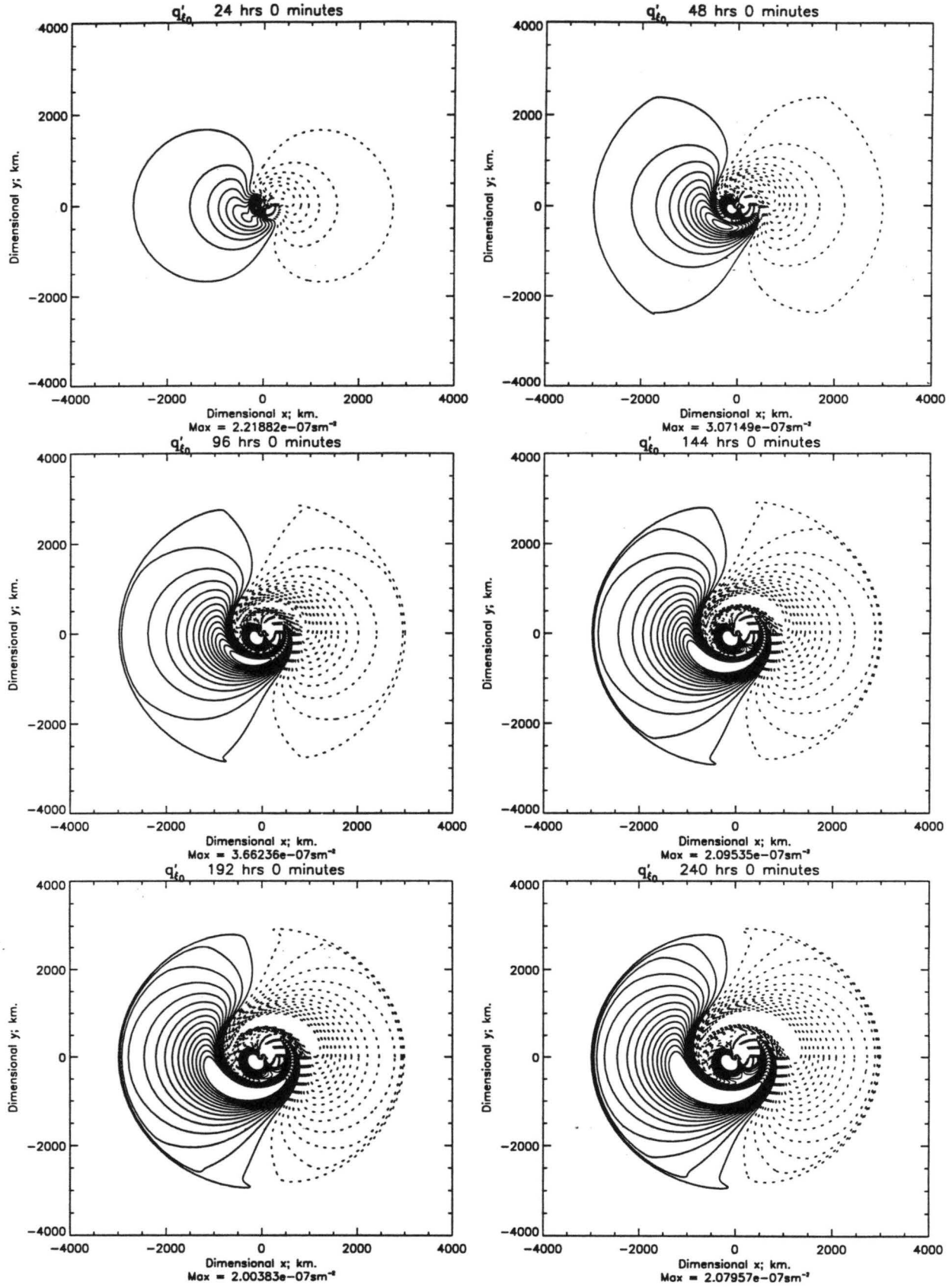

Figure 3.10: Wavenumber one q'_{ξ_0} evolution of the Schloemer vortex, contour interval 1×10^{-10} sm^{-2}. Values outside of $\pm 14.5 \times 10^{-10}$ sm^{-2} have not been contoured.

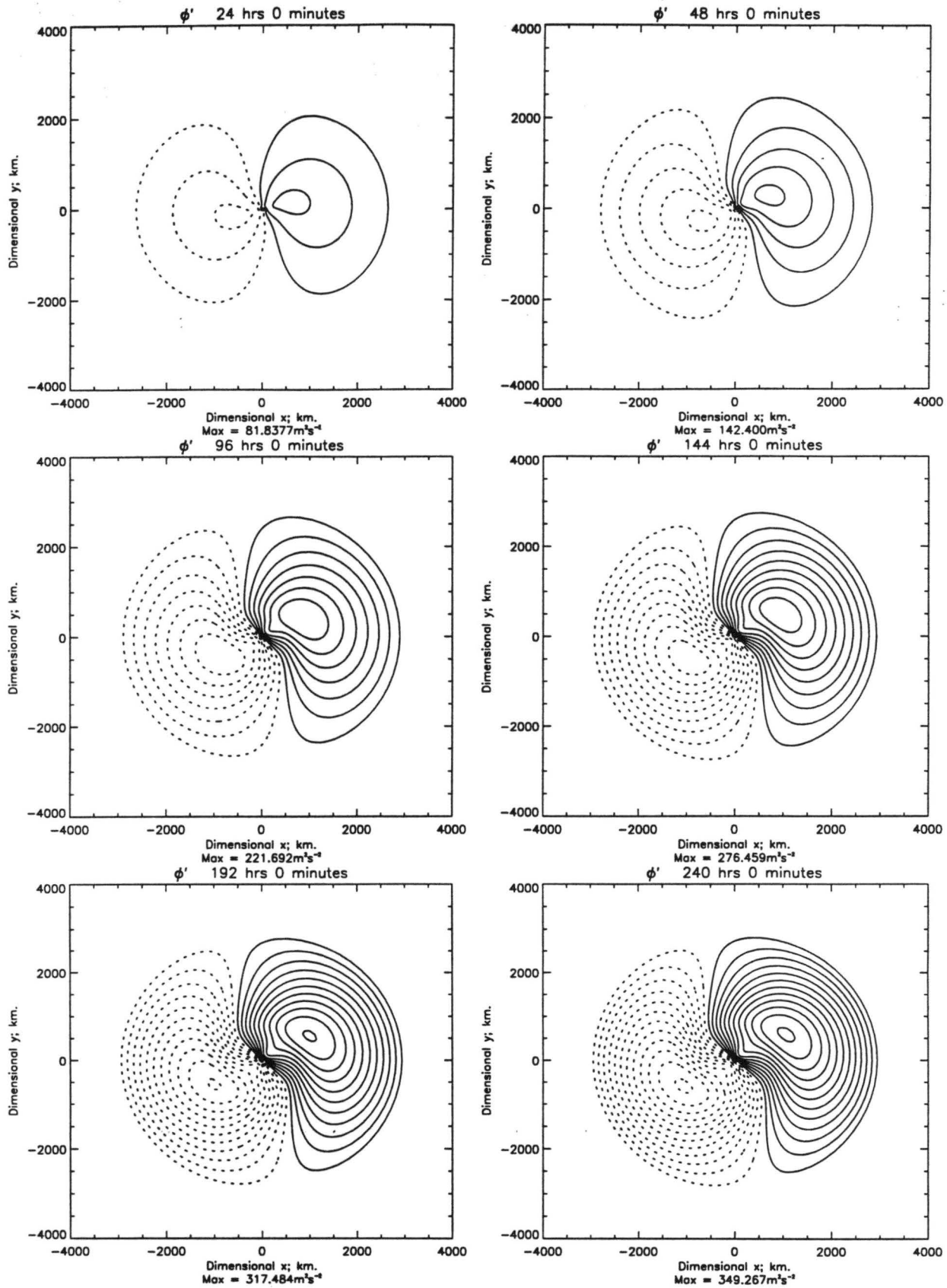

Figure 3.11: The wavenumber one ϕ' evolution of the Schloemer vortex, contour interval 30 m^2s^{-2}.

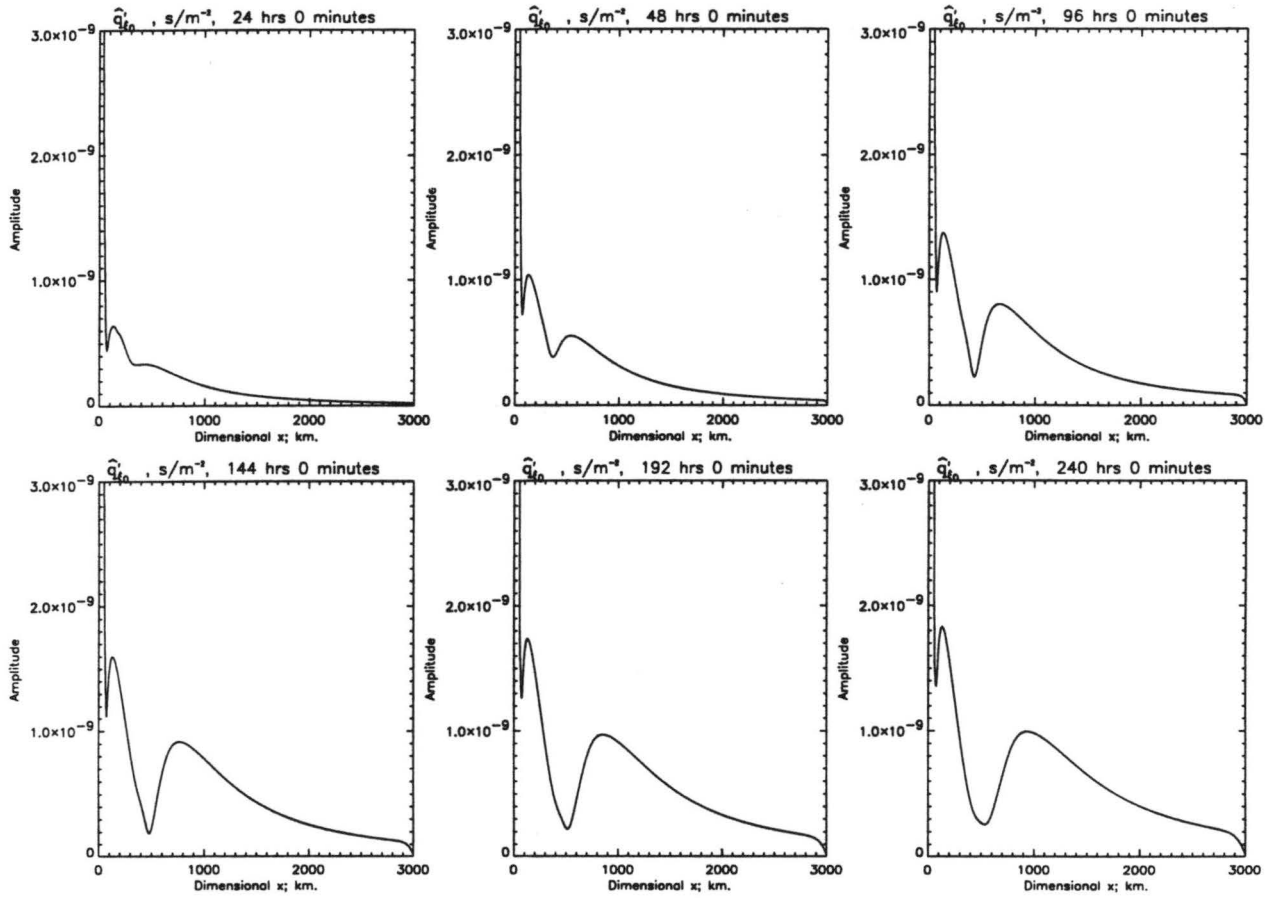

Figure 3.12: Wavenumber one $|\hat{q}_{\xi_0}|$ evolution for the Schloemer vortex.

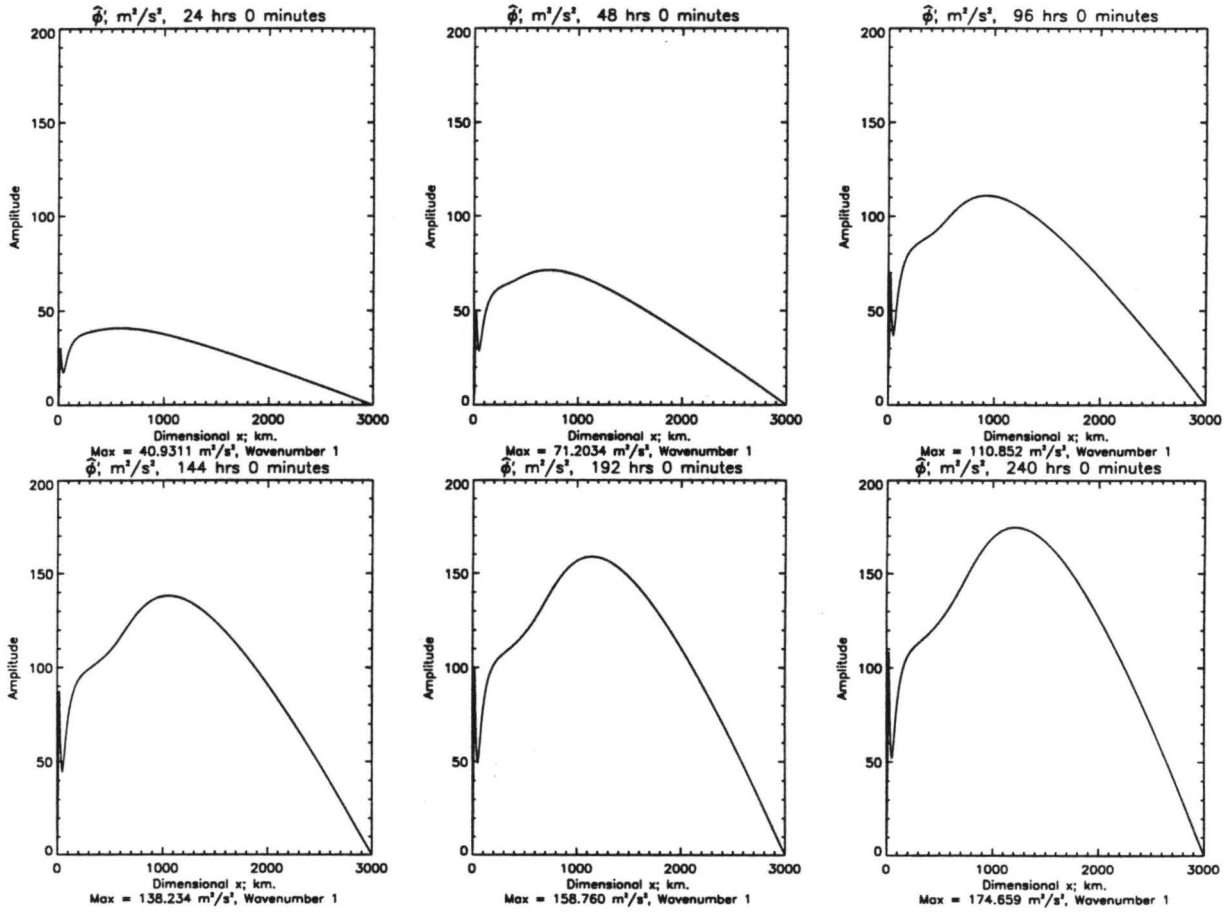

Figure 3.13: The wavenumber one $|\hat{\phi}|$ evolution of the Schloemer vortex.

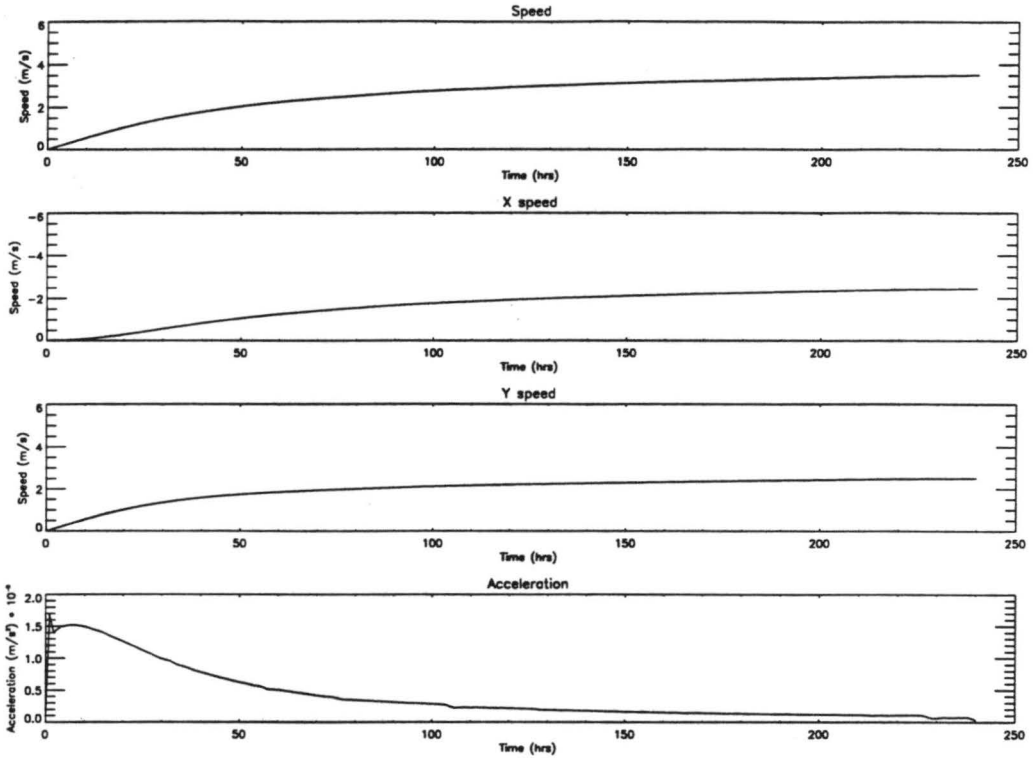

Figure 3.14: 240 hr. plot of total speed, northward speed, westward speed and total acceleration of the Schloemer vortex.

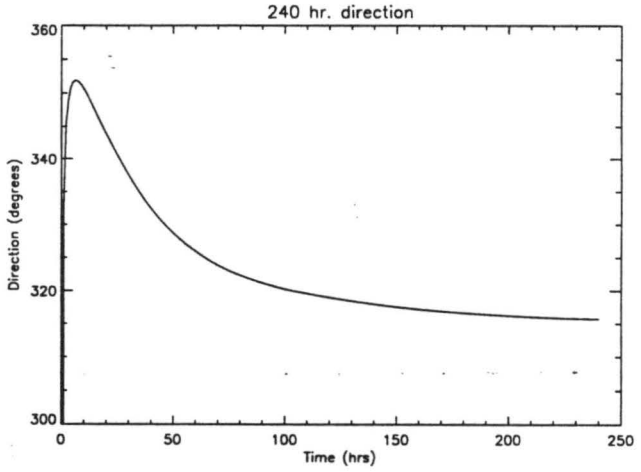

Figure 3.15: 240 hr. direction plots of the Schloemer vortex.

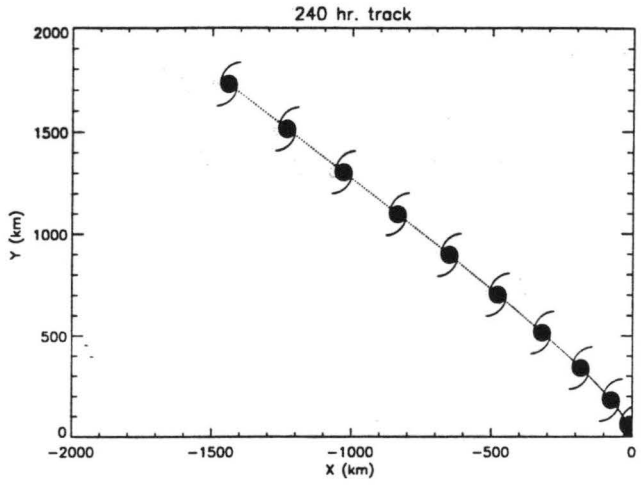

Figure 3.16: 240 hr. track of the Schloemer vortex. Cyclone symbols denote vortex location every 24 hours.

angle found by Willoughby (1995) when his model was run 240 hrs. with the same vortex. The β-AB model contains an option for including a sponge layer near the outer boundary as described by Willoughby. However, a sponge layer was not found to be necessary in any of these calculations. Depending on the strength of the imposed sponge layer, seperate numerical experiments (not shown) showed that the Schloemer vortex could be made to asymptote to a direction more westward than 315°. The sponge ring acted to inhibit the very outermost part of the gyres. Because of the weak basic state flow near the edge of the domain, these gyres are mainly oriented east-west. If these edges of the beta gyres are not allowed to exist due to the sponge layer, the vortex loses a slight northward component to its translation. This serves to turn the vortex more to the west. The Schloemer vortex also does not show the uniform acceleration to over 9 ms^{-1} as in Willoughby. Therefore, while the directions are similiar, the 240 hour tracks are not. In Willoughby's PE model (1995) the vortex travels nearly 5000 km in 240 hours, compared to a traverse about of 2200 km in the linear β-AB run.

3.6 Other Vortices

3.6.1 More Confined Hurricane-like Vortices

The track of the DeMaria vortex in the β-AB model is shown in Fig. 3.17. Up to 72 hours, the track looks quite reasonable. The vortex has obtained a speed of about 2 ms^{-1} and a direction of 325°, comparable to DeMaria's nondivergent work with the same profile (2.5 ms^{-1} and 320°). After 72 hours, however, the vortex starts a westward turn, heading due west by about 240 hours. This behavior was also observed when the Willoughby vortex was run in β-AB, except the Willoughby vortex made its westward turn at an earlier time. Whether the secondary gyre inside the beta gyres is responsible for this behavior is unclear. The distortion in the basic state advection of planetary vorticity associated with $\bar{\eta}_0/\bar{\xi}_0$ is certainly closer to the beta gyres in both the Willoughby or DeMaria case than in the benchmark or Schloemer cases. On the other hand, this behavior seems most accute at later times for vortices with sharper gradients in the basic state variables than the benchmark – possibly causing truncation errors in the interpolation scheme to accumulate and force spurious asymmetries in the near-core region. The large distance between the near-core beta distortion and the beta gyres in the larger intense vortices may be the factor enabling the β-AB formulation to correctly capture the physics of the beta gyres for high Rossby number ($R >> 1$) vortices. These issues require further exploration.

3.6.2 Reducing the Rossby Number

For truly hurricane-like vortices the AB approximation is not expected to be highly accurate as ${R_1}^2$ is often less than but not much less than one. Perhaps it is this stretching of the theory that manifests itself in such a way as to pinch the ϕ' fields in the benchmark vortex and give rise to an inner peak in q'_{ξ_0}. This section presents work done with vortices with order unity Rossby numbers but small *local* Rossby numbers, representative of a sub-mesoscale oceanic ring vortex (McWilliams et al. 1986) or a weak tropical storm or depression.

The first case shown in Fig. 3.32 is the monopolar vortex scaled as a tropical depression. It is evident that the local Rossby number squared is never much above 0.1, making

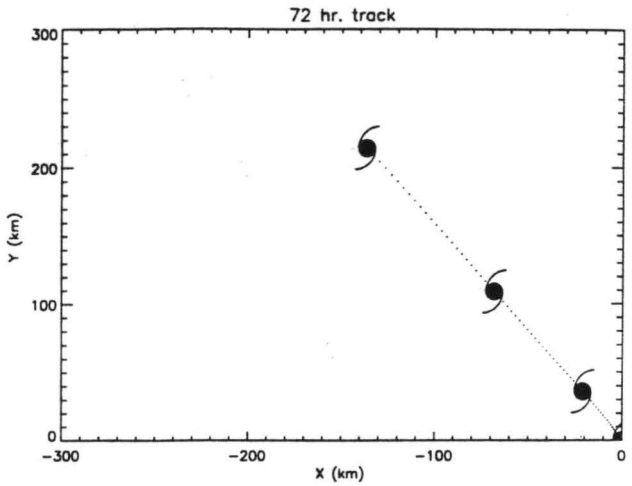

Figure 3.17: The track of the DeMaria vortex. The hurricane symbols denote the vortex position every 24 hours.

the AB approximation (${R_1}^2 << 1$) a very good one. The evolution of the fields (Fig. 3.18 and 3.19) is evidence of the validity of such an approximation. The β-AB model develops clean q'_{ξ_0} gyres, and shows no hint of a maximum inside the main beta gyres (except for a pseudomode). The ϕ' field has uniform flow between the gyres and exhibits none of the pinching of the previous examples.

The second case is a vortex that scales as a tropical storm. It possesses a local Rossby number between that of the benchmark vortex and the depression (Fig. 3.33). This intermediate vortex shows properties of both the tropical depression and the minimal hurricane. Unlike the benchmark vortex, the tropical storm vortex develops an inner peak in q'_{ξ_0} (Fig. 3.20) whose amplitude is smaller than the beta gyres. The ϕ' fields exhibit only a slight pinching near the center (Fig. 3.21).

The distortion in the wavenumber one ϕ' and q'_{ξ_0} was already anticipated in the formulation of the vorticity equation. The AB vorticity equation differed from the PE vorticity equation in the distortion factor $\bar{\eta}_0/\bar{\xi}_0$ multiplying the advection of planetary vorticity, $\bar{v}\beta\cos\lambda$. A plot of $\bar{\eta}_0/\bar{\xi}_0$ is shown in Fig. 3.22 for the minimal hurricane, tropical storm, and the tropical depression vortices. A ratio of $\bar{\eta}_0/\bar{\xi}_0$ approaching unity corresponds to a small local Rossby number, so it is not possible to separate the two effects. The maximum local Rossby number and minimum $\bar{\eta}_0/\bar{\xi}_0$ nearly coincide with the secondary peak in q'_{ξ_0}.

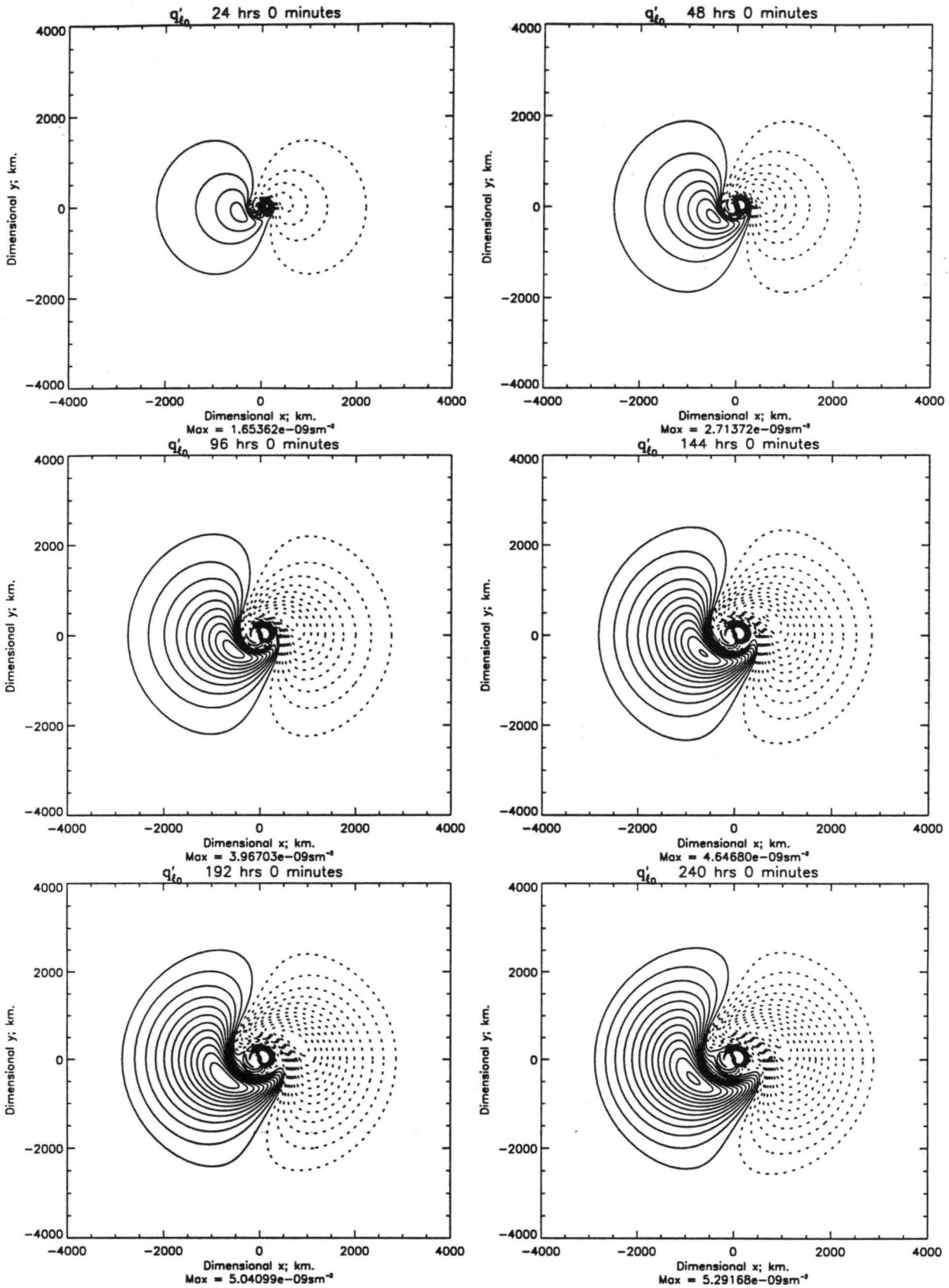

Figure 3.18: Tropical depression q'_{ξ_0} evolution for wavenumber one. Contour interval 1×10^{-10} sm^{-2}. Values outside of $\pm 14.5 \times 10^{-10}$ sm^{-2} have not been contoured.

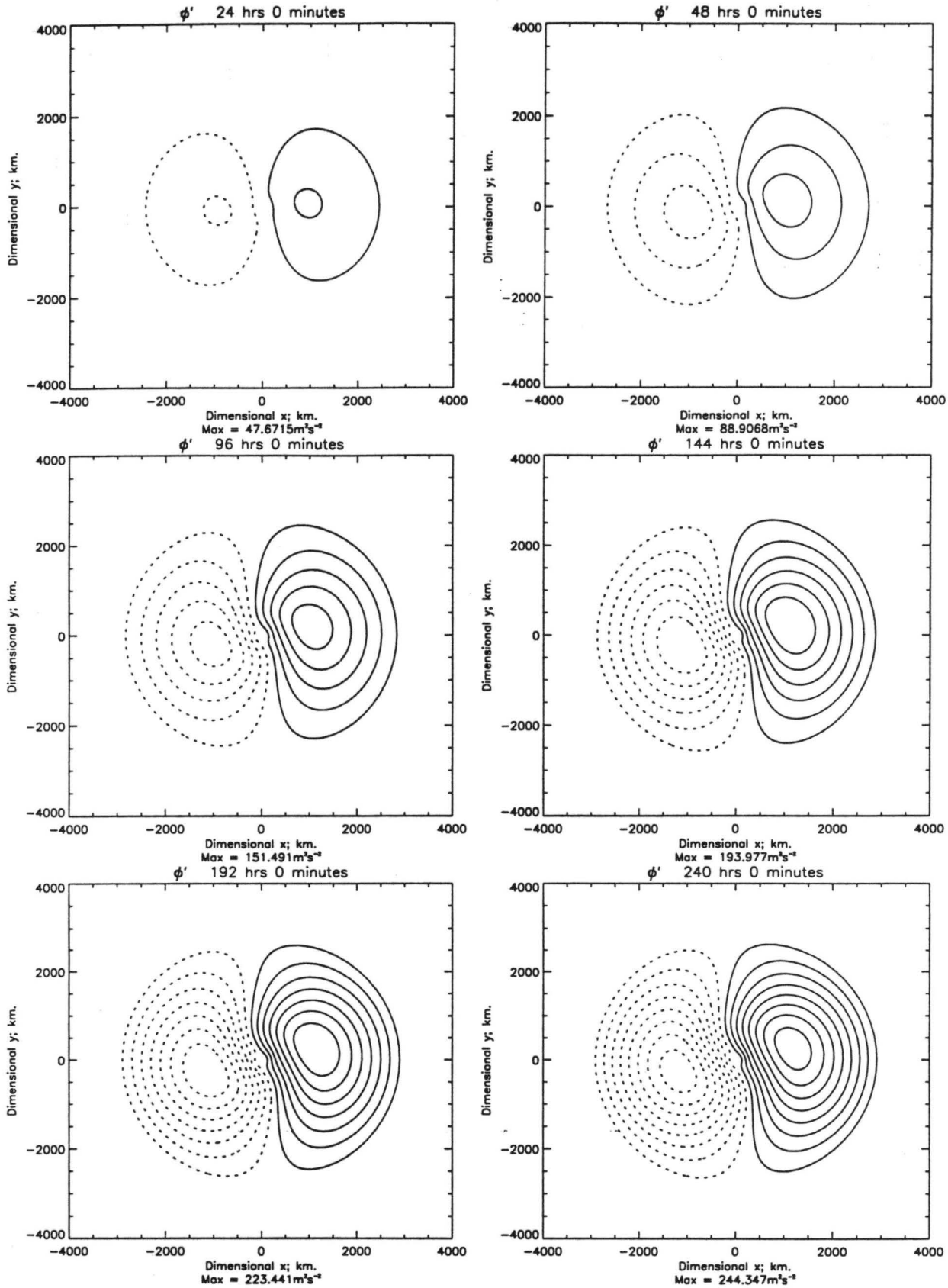

Figure 3.19: Tropical depression ϕ' evolution for wavenumber one. Contour interval 30 m^2s^2.

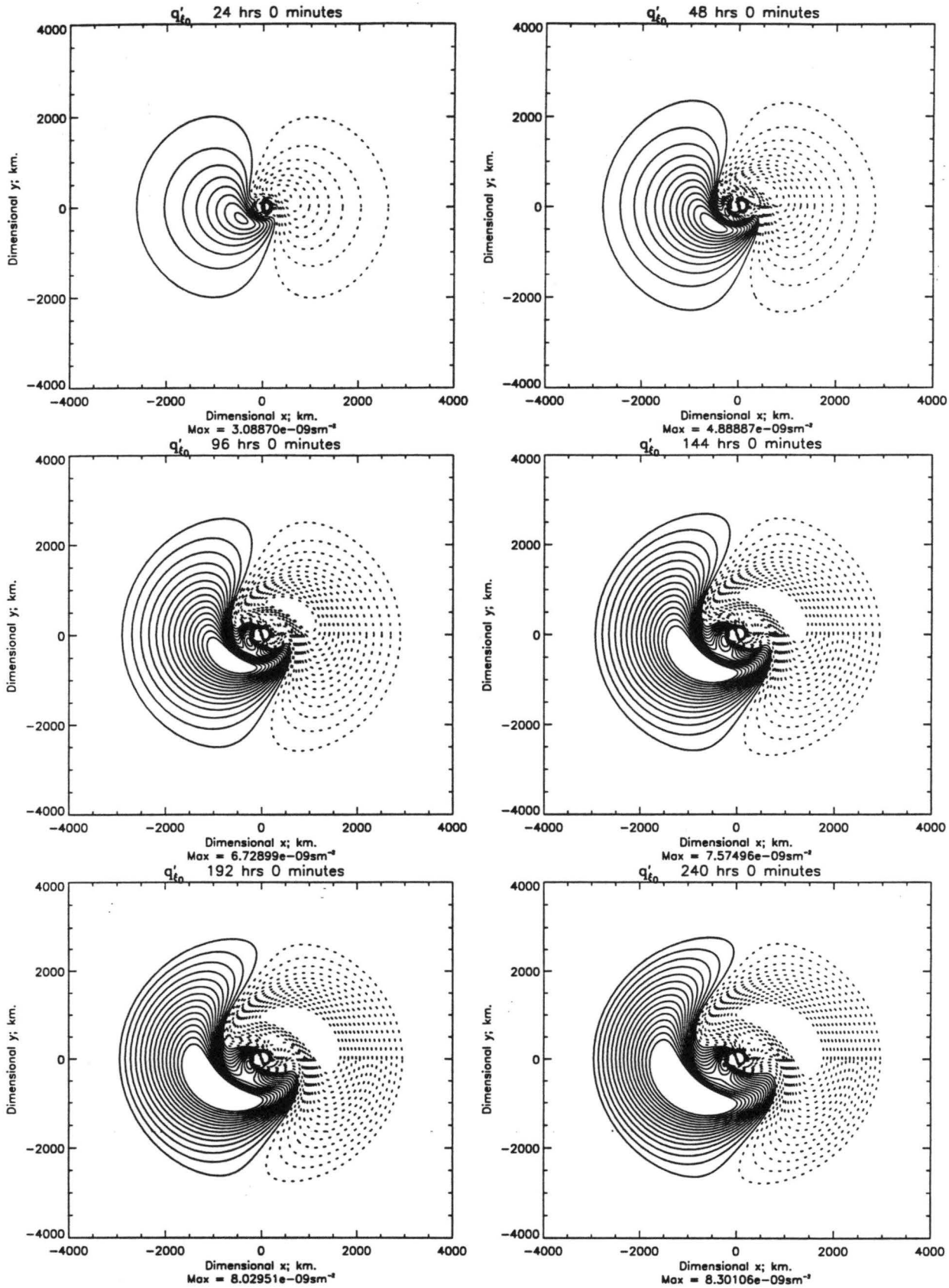

Figure 3.20: Tropical storm q'_{ξ_0} evolution for wavenumber one. Contour interval 1×10^{-10} sm^{-2}. Values outside of $\pm 14.5 \times 10^{-10}$ sm^{-2} have not been contoured.

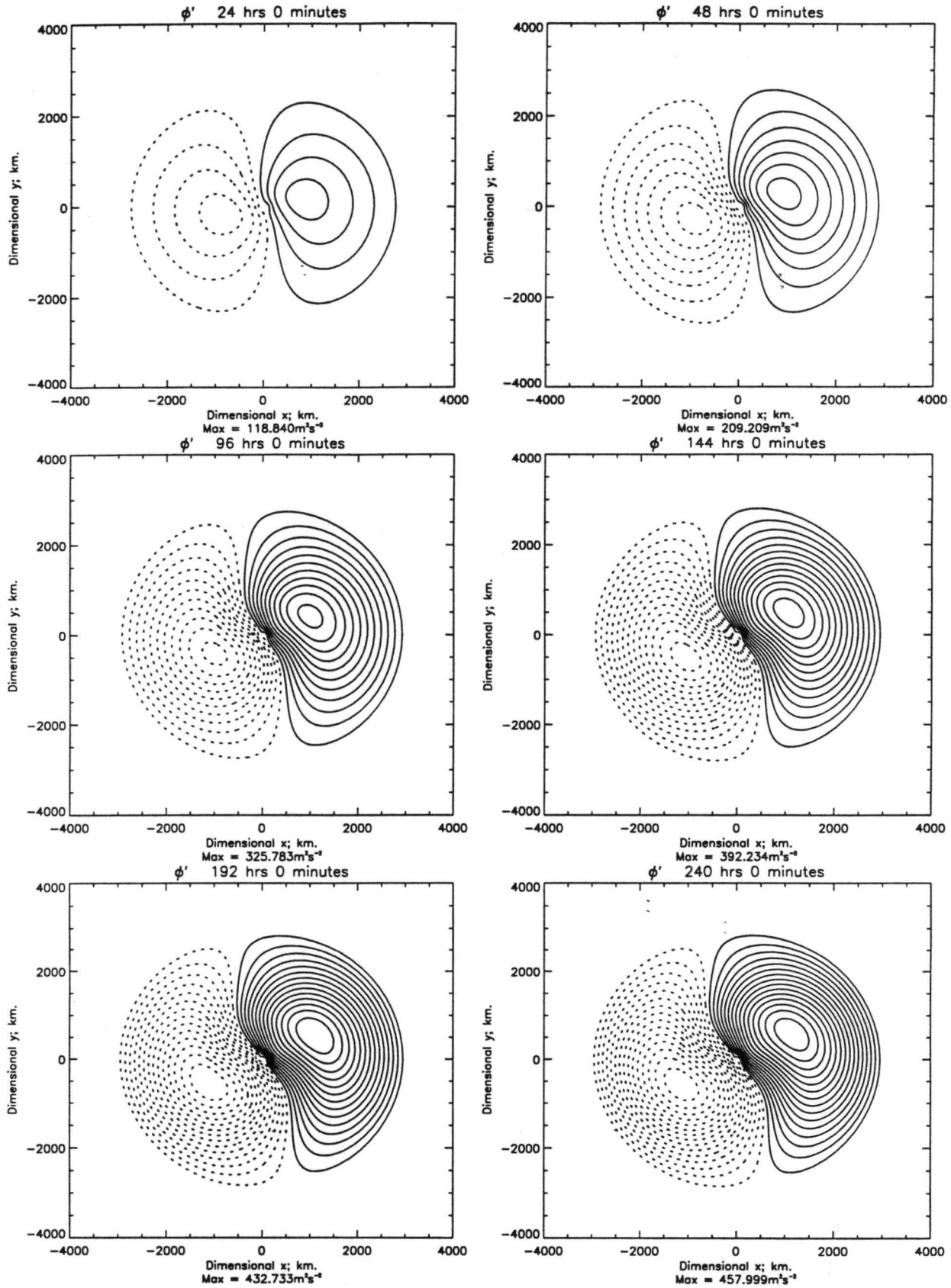

Figure 3.21: Tropical storm ϕ' evolution for wavenumber one. Contour interval 30 m^2s^2.

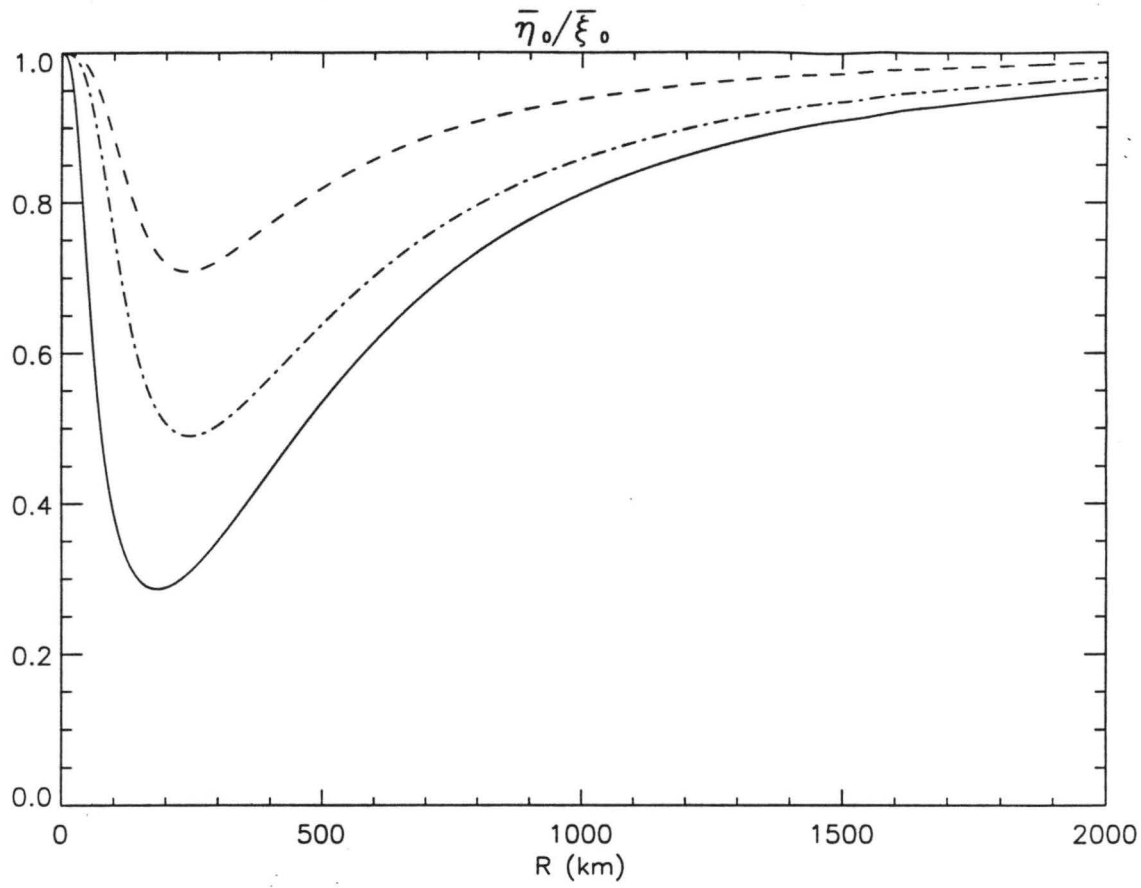

Figure 3.22: $\bar{\eta}_0/\bar{\xi}_0$ for the benchmark vortex (solid), the tropical storm (solid, dot), and the tropical depression (dashed).

The final family of vortices considered briefly are spatially confined but are of small amplitude. Consider a profile analogous to the DeMaria profile in every way except all velocities have been divided by nine. Such a profile possesses the property that $\bar{v} = 0$ near 1000 km, but it also possesses very small local Rossby number and a ratio of $\bar{\eta}_0/\bar{\xi}_0$ close to unity. The β-AB model produced fields and tracks consistent with those produced in the barotropic nondivergent model, where such "problems" associated with the local Rossby number and $\bar{\eta}_0/\bar{\xi}_0$ are not a consideration.

3.7 The Linear Barotropic Nondivergent Model

As an investigative tool into both the previously mentioned distortion effects and Willoughby's translating normal mode (Ch. 4), a barotropic nondivergent model linearized on a circular vortex in gradient balance has also been developed. The forecast equation for this model is

$$\frac{\partial \psi'}{\partial t} = \left(\nabla^2\right)^{-1} \left[\frac{d\bar{\eta}_0}{dr}\frac{\psi'_\lambda}{r} - \frac{\bar{v}}{r}\nabla^2(\psi'_\lambda) - \bar{v}\beta\cos\lambda\right], \tag{3.8}$$

where ψ' is the perturbation streamfunction.

3.7.1 Steamfunction and Vorticity Fields

For the benchmark vortex, the linear barotropic nondivergent model develops vorticity and streamfunction fields (Figs. 3.23 and 3.24) similar to the β-AB runs. Of note is the absence of the aforementioned secondary gyre and lack of pinching in the streamfunction fields. Between the wavenumber one dipole we find uniform flow as described by FE.

3.7.2 Vortex Tracks

As a further test of the robustness of the linear barotropic nondivergent formulation, a plot of two qualitatively different vortex tracks is presented in Fig. 3.25. The first track is for the standard benchmark vortex, which slowly accelerates in a straight line. The second track is for the DeMaria vortex, which takes a northward turn at long times. Both tracks are consistent with the theoretical predictions for (3.8) in storm-moving coordinates by Reznik and Dewar (1994). In their analytical theory of distributed vortices on a β-plane, they predict that large distributed vortices (like the benchmark), will accelerate

along a straight line path. On the other hand, confined vortices (like DeMaria's vortex) will approach purely meridional motion at long times.

3.8 Summary

For a smooth hurricane-like vortex the linear β-AB formulation has been shown to correctly capture the formation of the beta gyres and produces vortex tracks consistent with previous research results using fully nonlinear, nondivergent vortex models. The gyres are initially oriented east-west, and get advected by the basic state swirl so the flow between the gyres is oriented towards the northwest. Storm track and direction were also shown to be consistent for another relatively large-sized vortex, the Schloemer vortex. Of note is the finite speed of the vortices obtained in the β-AB model.

Fully nonlinear divergent models have long demonstrated that intense vortices attain finite and steady drift speeds on time scales smaller than the Rossby radiation time scale (McWilliams et al. 1986, McWilliams and Gent 1986, Willoughby 1994). Sutyrin and Flierl (1994) have recently shown, however, that QG vortices attain finite drift speeds even in the limit of linear dynamics on a circular Rankine-like vortex possessing piecewise uniform PV. Their result suggesting nonlinearity is unessential for attaining finite drift speeds is limited to small Rossby number vortex flows. This work confirms and extends Sutyrin and Flierl's analytical prediction to order unity and higher Rossby number flows with distributed PV profiles.

McWilliams and Gent (1986) showed the asymptotic drift speed of oceanic mesoscale and sub-mesoscale vortices in the nonlinear formulation is a significant fraction ($\approx 70\%$) of $(R_{d_\infty})^2\beta$, where ${R_{d_\infty}}^2$ is the square of the environmental Rossby deformation radius. In this chapter the drift speed was found to be a smaller fraction ($\approx 7\%$) of $(R_{d_\infty})^2\beta$ for the benchmark vortex. These results indicate the drift speed in the linear problem should be described by $(R_d)^2\beta$, where R_d is the *local* Rossby radius. For this description to be useful, however, one needs to know the appropriate radius at which R_d is to be evaluated. For the benchmark vortex one obtains a radius $\approx$ 200 km. It would be of great interest to be able to predict this radius a priori since this would enable one to predict the asymptotic drift speed of an arbitrary vortex profile. This is reserved for future work.

A linear barotropic nondivergent model has also been developed and tested. As both linear models have been demonstrated to capture the fundamental physics of the beta drift problem, both can be used to investigate the performance of other linear models; specifically the search for a translating normal mode.

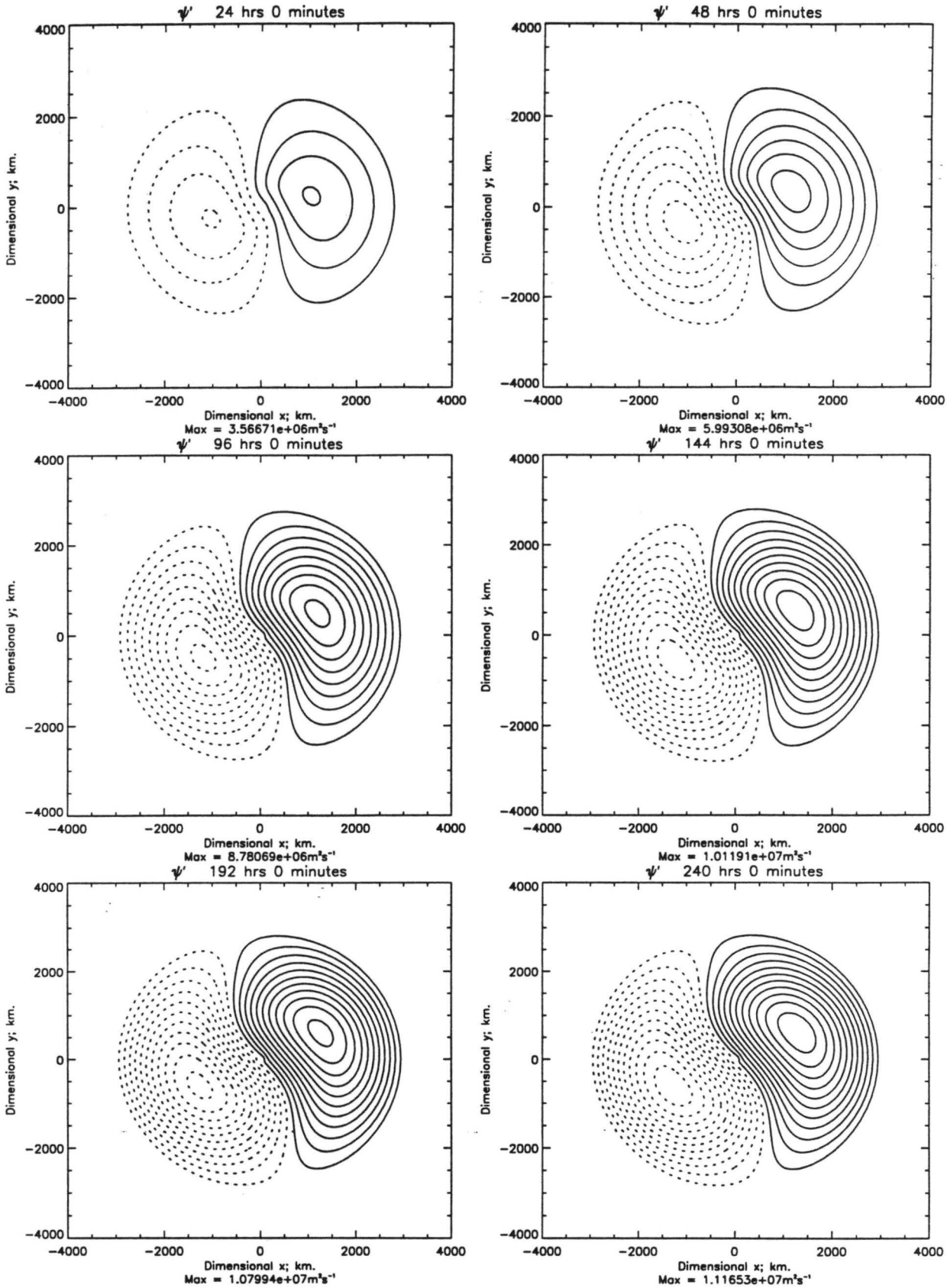

Figure 3.23: Wavenumber one ψ' evolution of the benchmark vortex in the linear barotropic nondivergent model, contour interval 1×10^6 m^{2}s^{-1}.

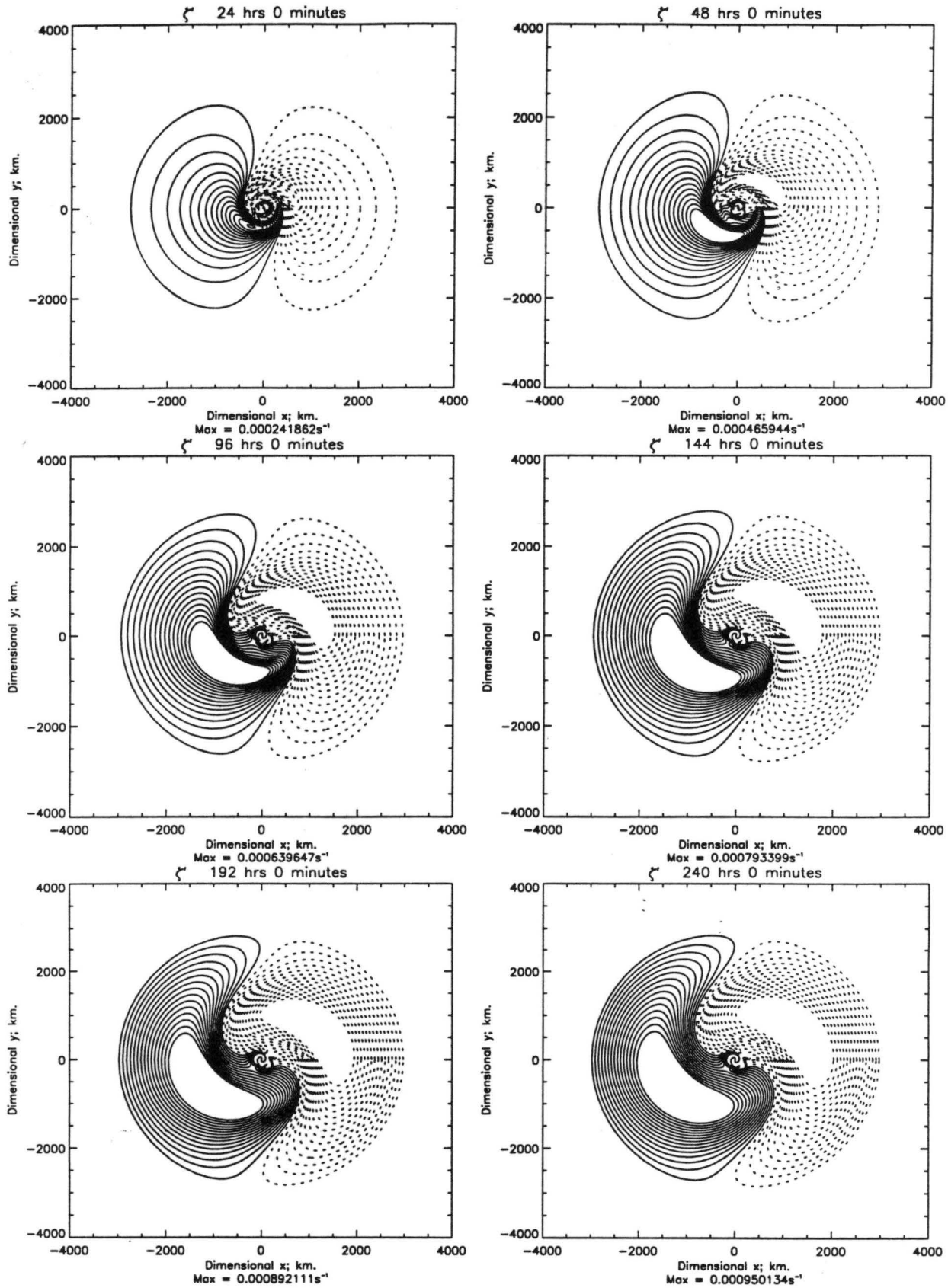

Figure 3.24: Wavenumber one ζ' evolution of the benchmark vortex in the linear barotropic nondivergent model, contour interval 1×10^{-6} s^{-1}. Values outside of $\pm 14.5 \times 10^{-6}$ s^{-1} have not been contoured.

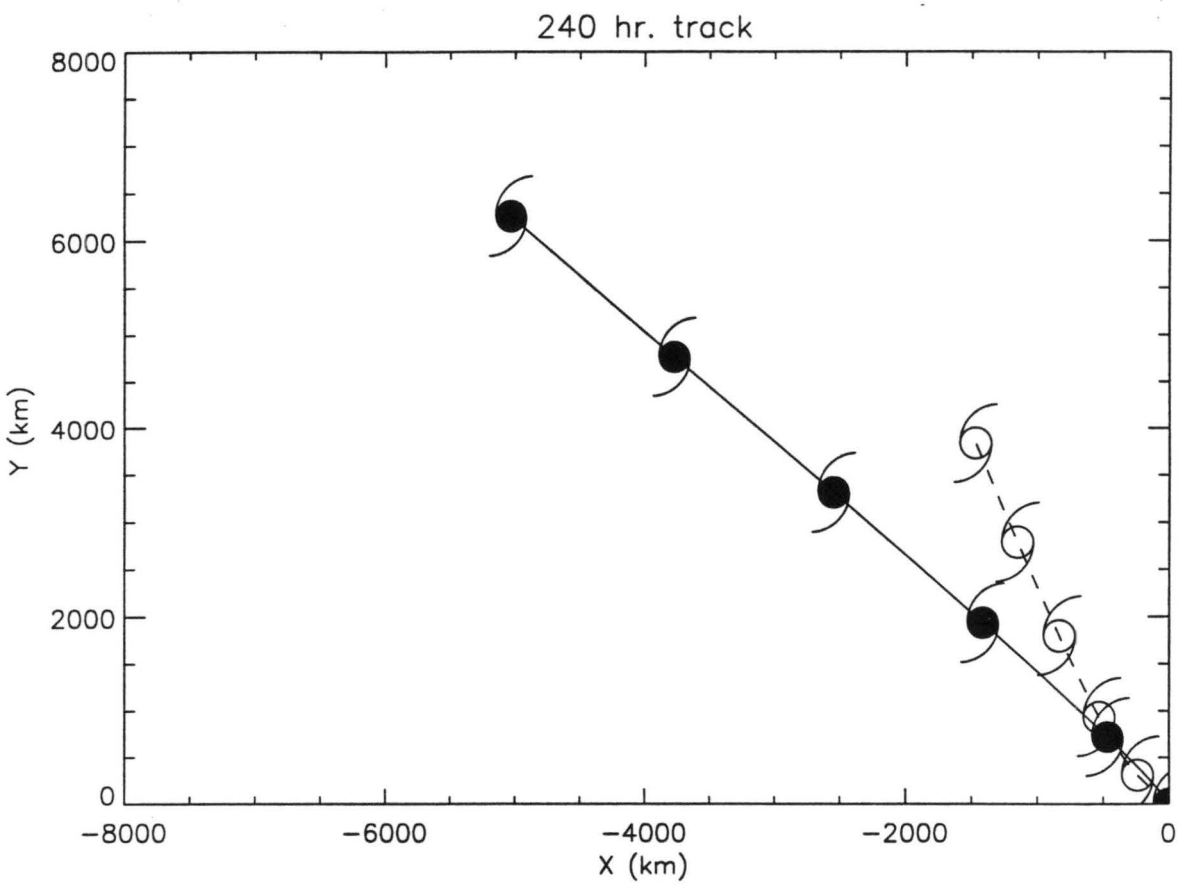

Figure 3.25: 240 hour tracks of the benchmark (hurricane symbols) and the DeMaria (tropical storm symbols) vortices. Each symbol denotes the vortex position every 48 hours.

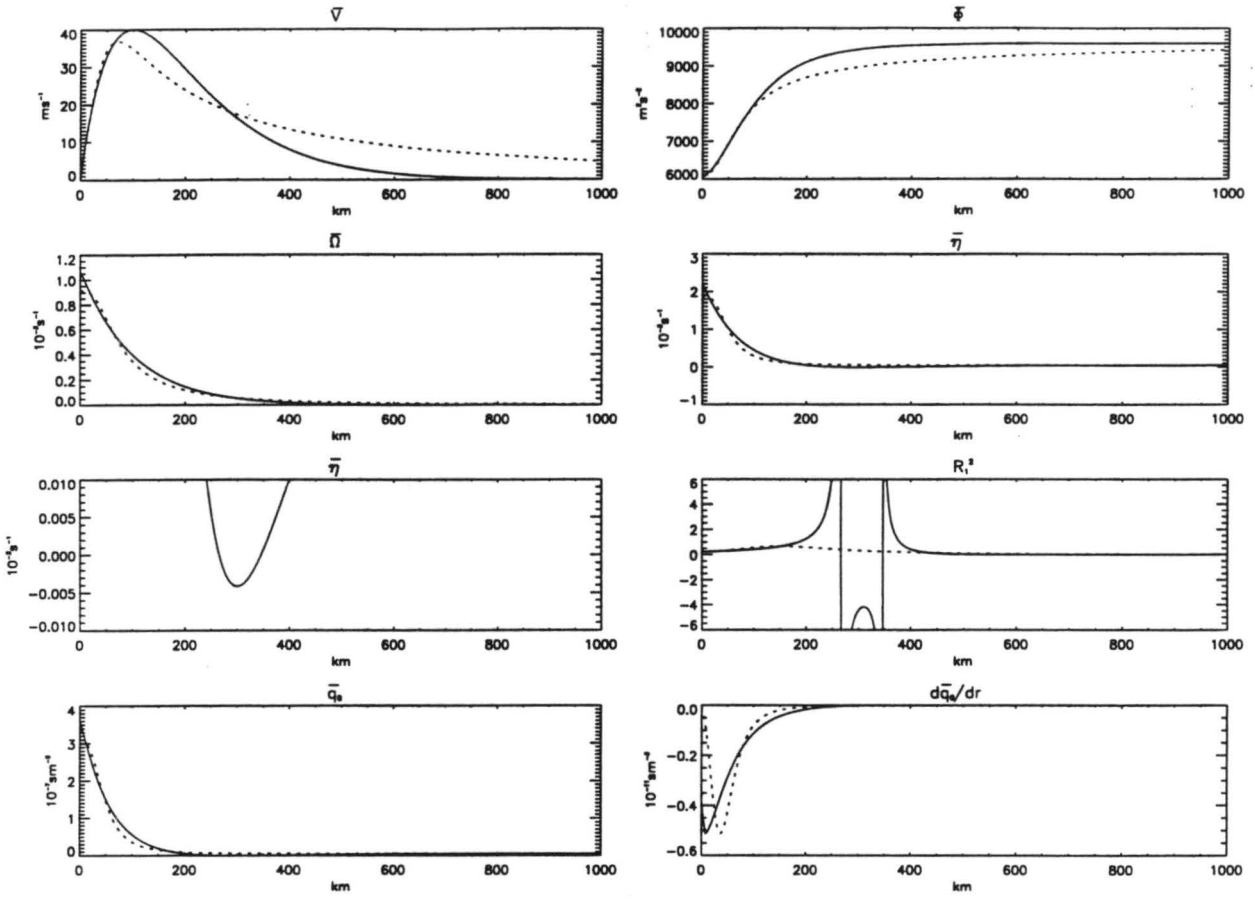

Figure 3.26: The Chan and Williams Vortex: $\bar{v}$ the tangential wind; $\bar{\Phi}$ the geopotential for a fluid with a resting depth of 1 km; $\bar{\Omega}$ the storm rotation rate; $\bar{\eta}$ the f-plane absolute vorticity; ${R_1}^2$ the local Rossby number for wavenumber 1; $\bar{q}_0$ the f-plane potential vorticity; $d\bar{q}_0/dr$ the radial derivative of $\bar{q}_0$. The dashed line is the benchmark vortex used in this chapter.

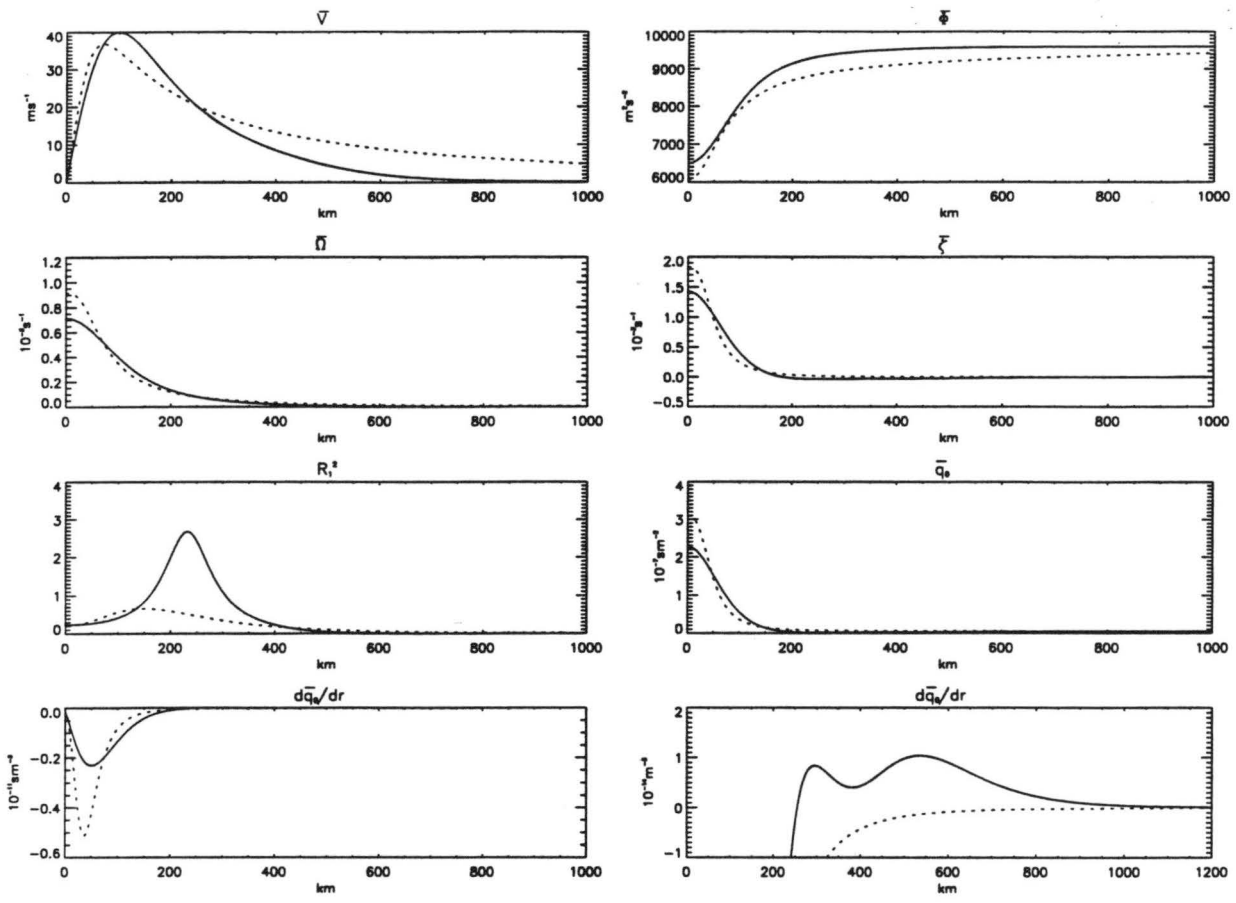

Figure 3.27: The SUD Vortex: $\bar{v}$ the tangential wind; $\bar{\Phi}$ the geopotential for a fluid with a resting depth of 1 km; $\bar{\Omega}$ the storm rotation rate; $\bar{\zeta}$ the f-plane relative vorticity; ${R_1}^2$ the local Rossby number for wavenumber 1; $\bar{q}_0$ the f-plane potential vorticity; $d\bar{q}_0/dr$ the radial derivative of $\bar{q}_0$. The dashed line is the benchmark vortex used in this chapter.

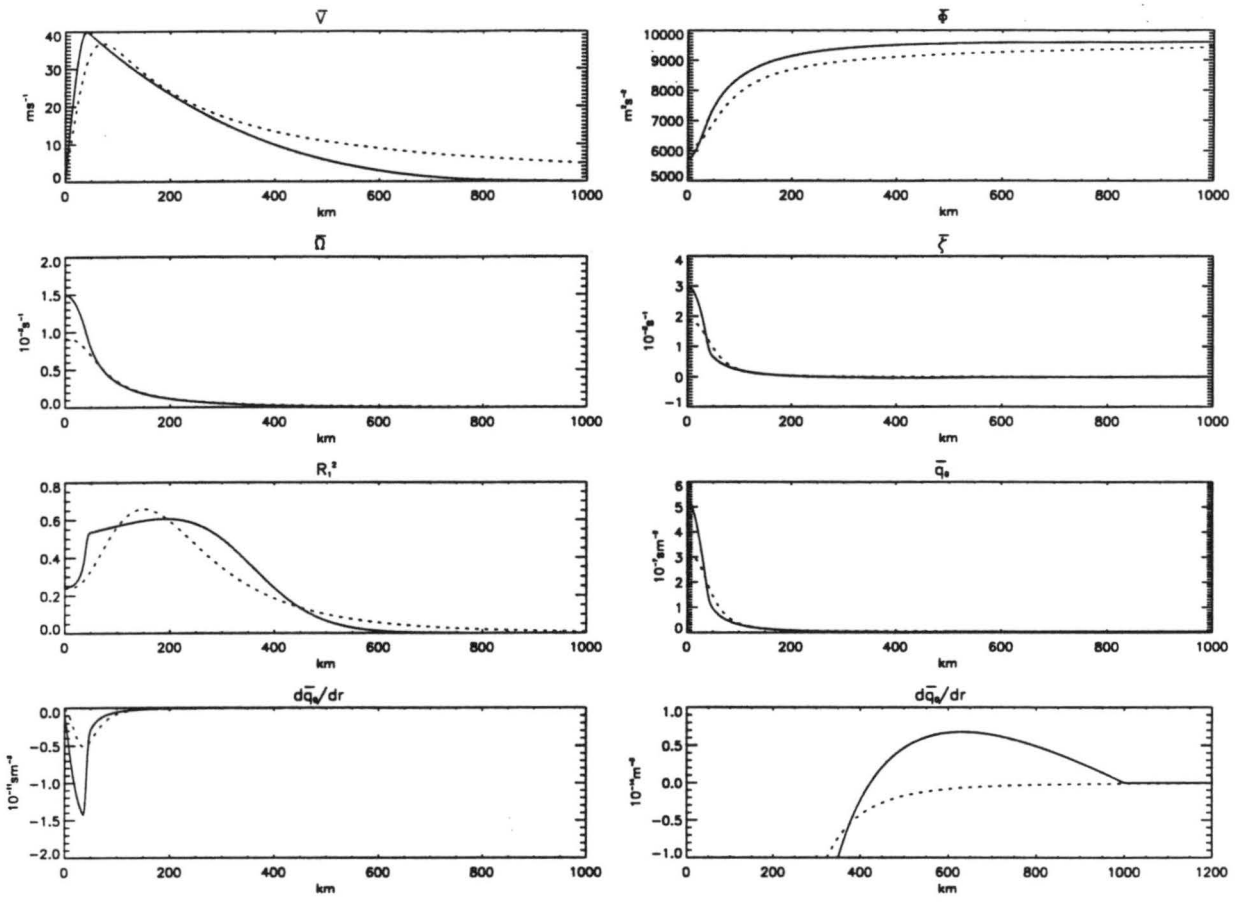

Figure 3.28: The Willoughby Vortex: $\bar{v}$ the tangential wind; $\bar{\Phi}$ the geopotential for a fluid with a resting depth of 1 km; $\bar{\Omega}$ the storm rotation rate; $\bar{\zeta}$ the f-plane relative vorticity; ${R_1}^2$ the local Rossby number for wavenumber 1; $\bar{q}_0$ the f-plane potential vorticity; $d\bar{q}_0/dr$ the radial derivative of $\bar{q}_0$. The dashed line is the benchmark vortex used in this chapter.

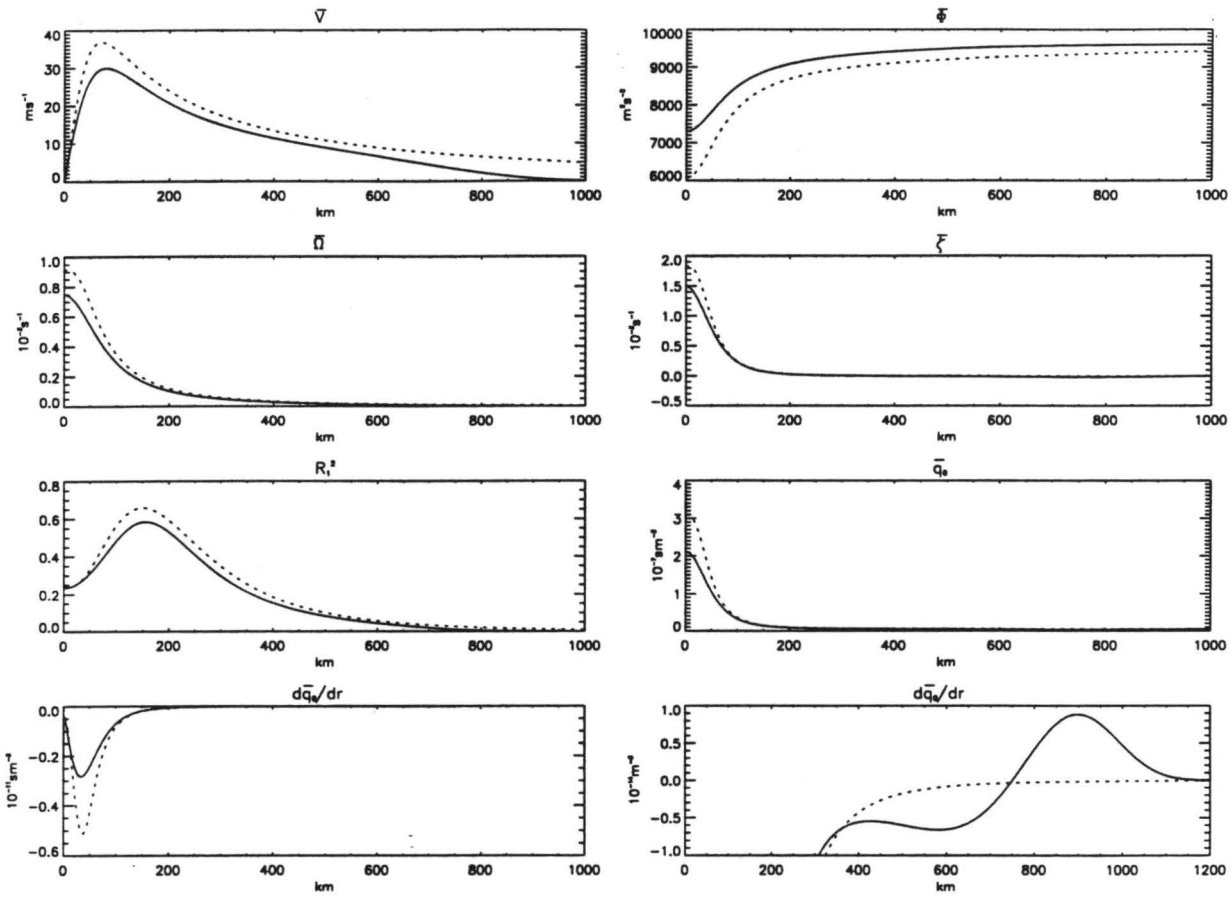

Figure 3.29: The DeMaria Vortex: $\bar{v}$ the tangential wind; $\bar{\Phi}$ the geopotential for a fluid with a resting depth of 1 km; $\bar{\Omega}$ the storm rotation rate; $\bar{\zeta}$ the f-plane relative vorticity; ${R_1}^2$ the local Rossby number for wavenumber 1; $\bar{q}_0$ the f-plane potential vorticity; $d\bar{q}_0/dr$ the radial derivative of $\bar{q}_0$. The dashed line is the benchmark vortex used in this chapter.

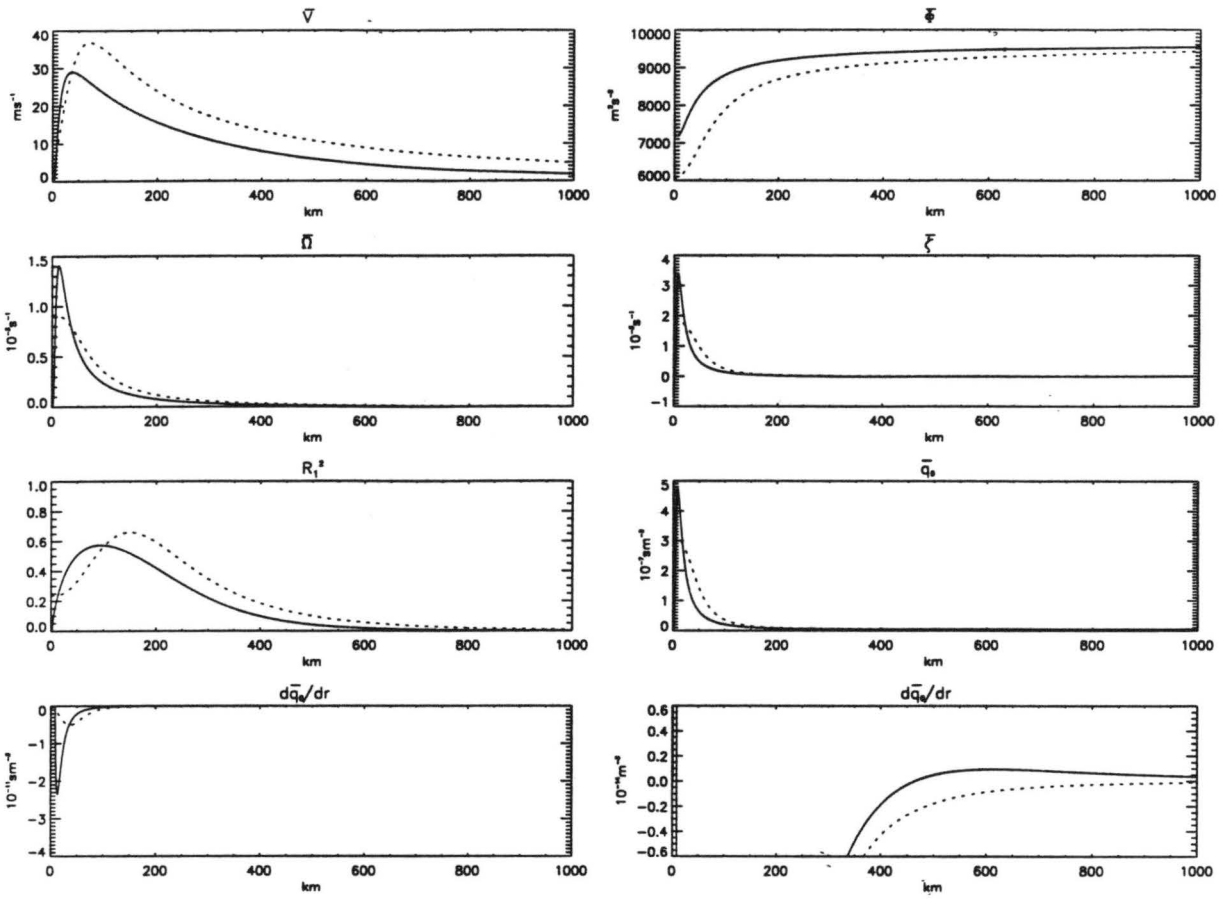

Figure 3.30: The Schloemer Vortex: $\bar{v}$ the tangential wind; $\bar{\Phi}$ the geopotential for a fluid with a resting depth of 1 km; $\bar{\Omega}$ the storm rotation rate; $\bar{\zeta}$ the f-plane relative vorticity; ${R_1}^2$ the local Rossby number for wavenumber 1; $\bar{q}_0$ the f-plane potential vorticity; $d\bar{q}_0/dr$ the radial derivative of $\bar{q}_0$. The dashed line is the benchmark vortex used in this chapter.

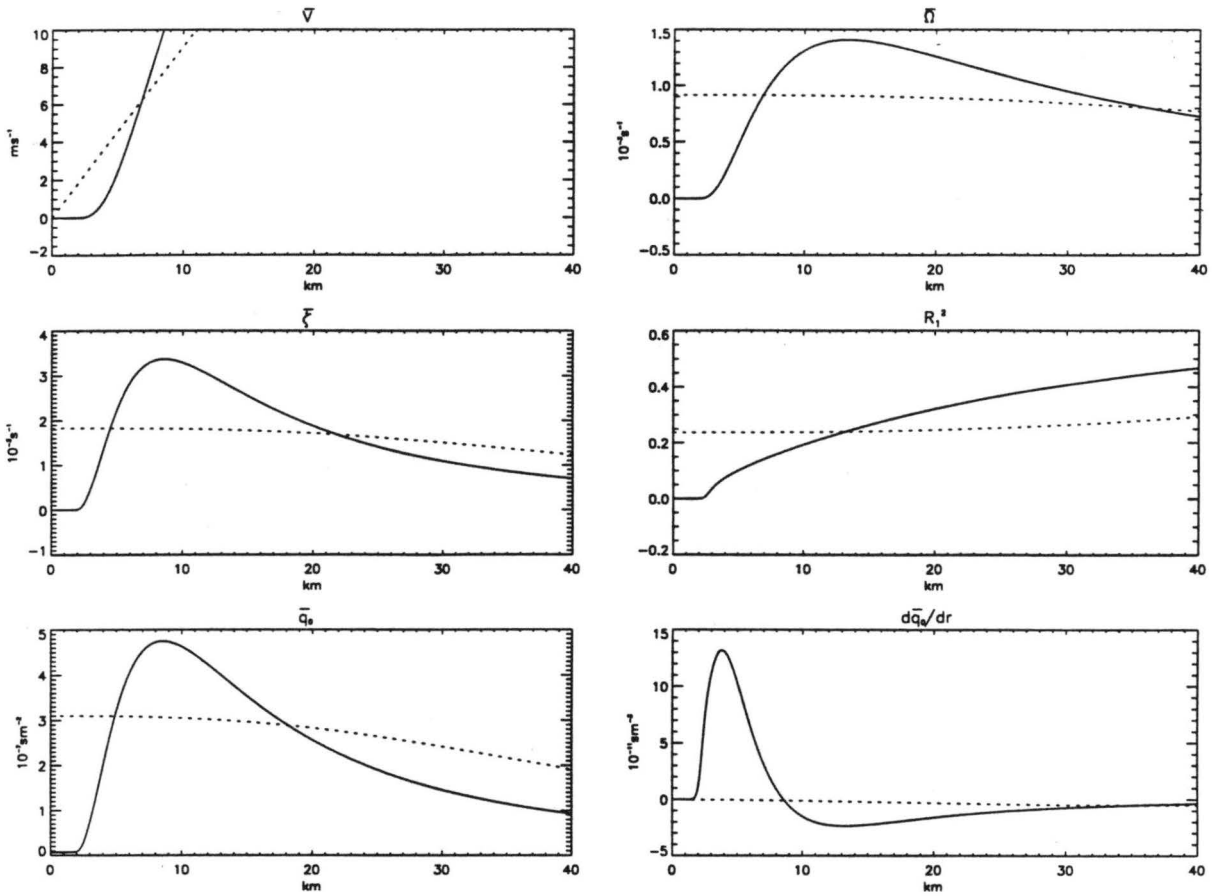

Figure 3.31: Inner Core of the Schloemer Vortex: $\bar{v}$ the tangential wind; $\bar{\Phi}$ the geopotential for a fluid with a resting depth of 1 km; $\bar{\Omega}$ the storm rotation rate; $\bar{\zeta}$ the f-plane relative vorticity; ${R_1}^2$ the local Rossby number for wavenumber 1; $\bar{q}_0$ the f-plane potential vorticity; $d\bar{q}_0/dr$ the radial derivative of $\bar{q}_0$. The dashed line is the benchmark vortex used in this chapter.

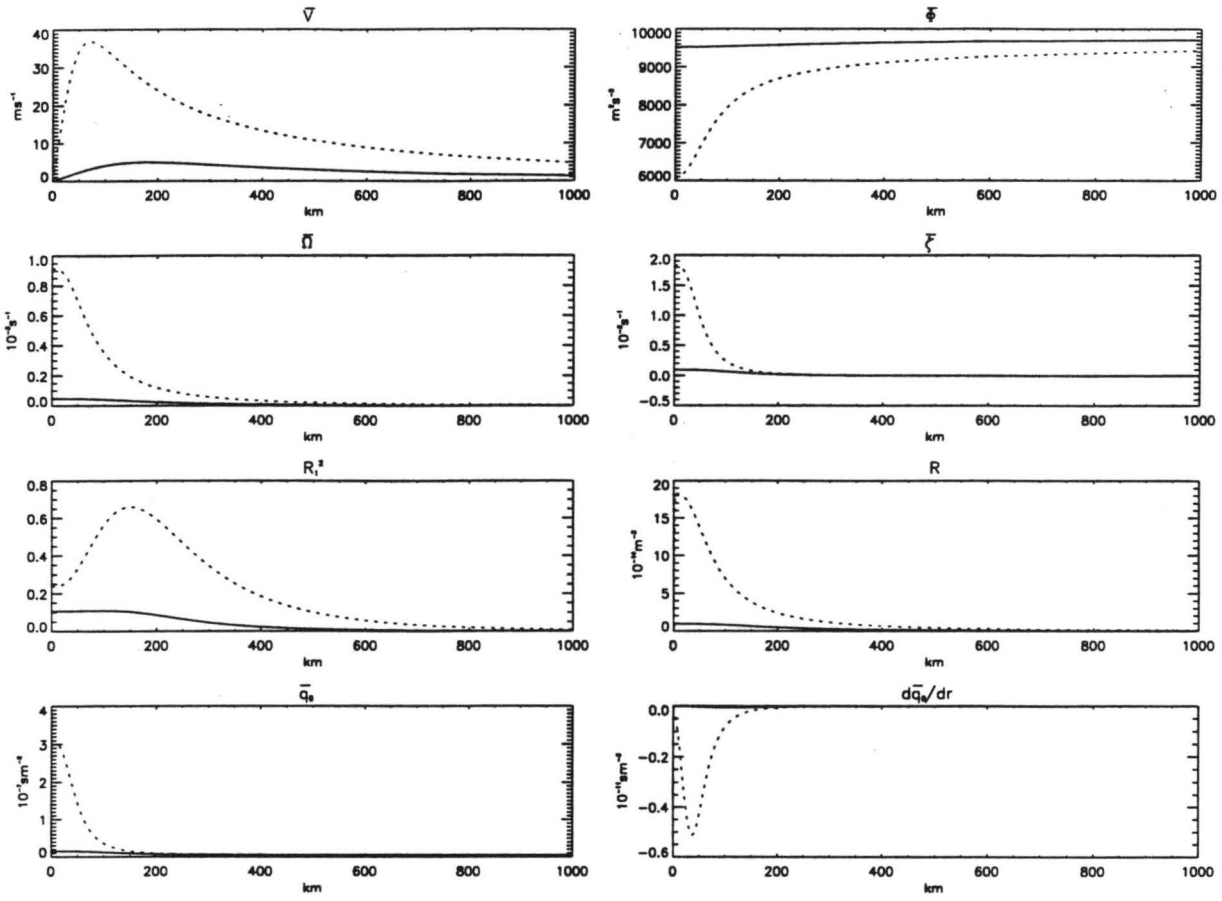

Figure 3.32: The tropical depression: $\bar{v}$ the tangential wind; $\bar{\Phi}$ the geopotential for a fluid with a resting depth of 1 km; $\bar{\Omega}$ the storm rotation rate; $\bar{\zeta}$ the f-plane relative vorticity; ${R_1}^2$ the local Rossby number for wavenumber 1; R the Rossby number; $\bar{q}_0$ the f-plane potential vorticity; $d\bar{q}_0/dr$ the radial derivative of $\bar{q}_0$. The dashed line is the benchmark vortex used in this chapter.

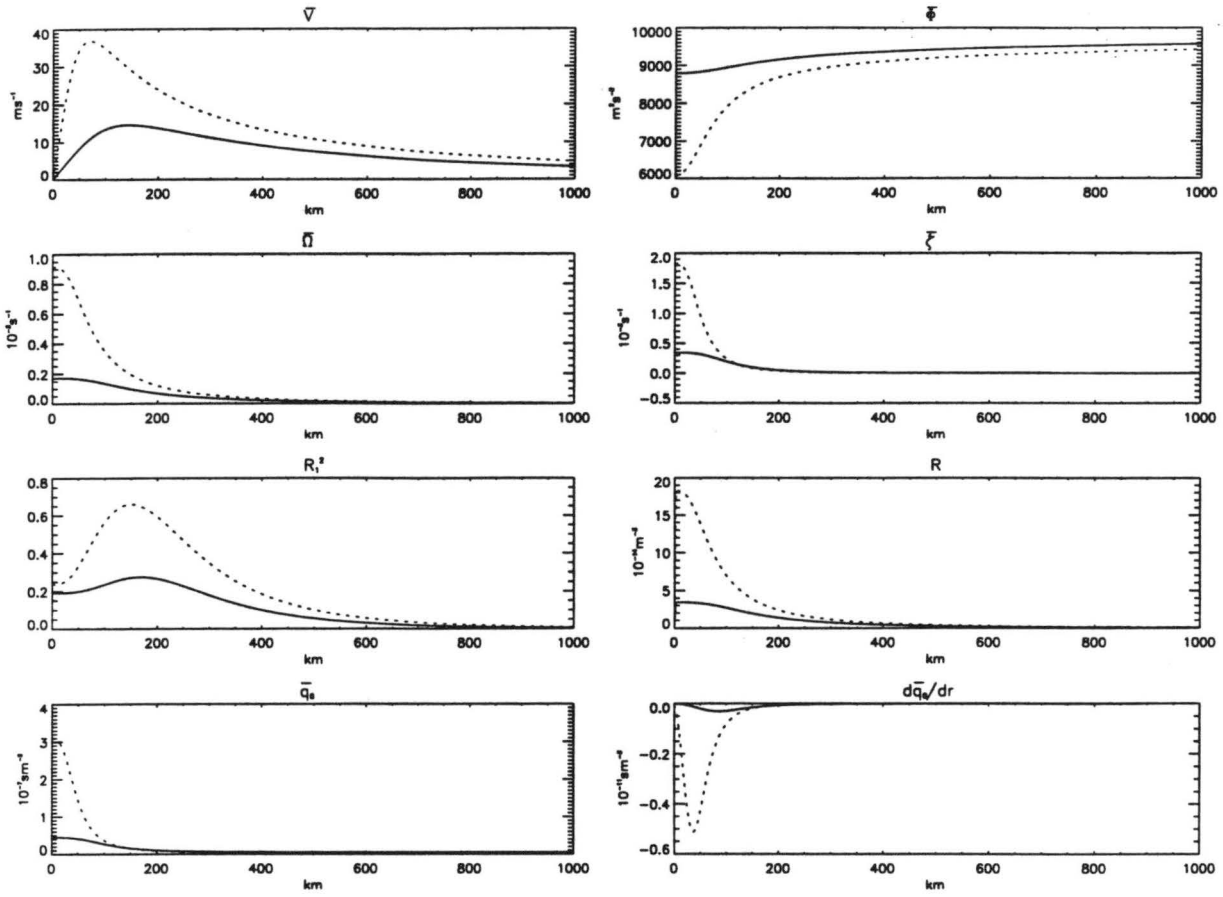

Figure 3.33: The tropical storm: $\bar{v}$ the tangential wind; $\bar{\Phi}$ the geopotential for a fluid with a resting depth of 1 km; $\bar{\Omega}$ the storm rotation rate; $\bar{\zeta}$ the f-plane relative vorticity; ${R_1}^2$ the local Rossby number for wavenumber 1; R the Rossby number; $\bar{q}_0$ the f-plane potential vorticity; $d\bar{q}_0/dr$ the radial derivative of $\bar{q}_0$. The dashed line is the benchmark vortex used in this chapter.

Chapter 4

IN SEARCH OF A TRANSLATING NORMAL MODE

4.1 Introduction

In a series of papers examining the linear motion of shallow water hurricane-like barotropic vortices, Willoughby (1988, 1990, 1992, 1995) interprets the vortex dipole forced by the mean-flow advection of planetary vorticity (the beta gyres) as a normal mode of the linear system. In simple terms a normal mode of a dynamical system is simply a free oscillation of that system [1]. In an analysis of linear vortex motion Willoughby (1995) states: "These modes can exist and maintain themselves independent of any forcing." This interpetation is perhaps driven by the peculiar property of constant acceleration of vortices that are placed into Willoughby's linear model, results which could not be duplicated in the linear β-AB model or the linear barotropic nondivergent model. The search for a normal mode of near-zero frequency has been a subject of some additional research in recent years. Peng and Williams (1991) and Weber and Smith (1993) were both unsuccessful in finding the desired normal mode. Willoughby (1995) addresses their failure, citing two possible reasons. The first is that their specific boundary conditions for a stationary vortex are not the same as for a moving vortex. The second concerned their numerical solution method. Both groups used shooting and relaxation algorithms to find eigenvalues of the barotropic vorticity equation. Willoughby claims such a method will

---

[1] In shear flows the concept of free oscillatory modes remains valid (e.g., Drazin and Reid 1981), but the non-normality of the associated linearized dynamical operator renders their description as "normal modes" probably more confusing than useful (Farrell and Ioannou 1993). Since this terminology persists in both textbooks and the literature we adhere to its usage with the understanding that it is the free oscillation aspect being referred to rather than the orthogonality in function space.

almost always converge on the pseudomode (a wavenumber one gyre resulting simply due to the mispositioning of the vortex grid when compared to the vortex center). Willoughby states the aforementioned studies found the normal modes of nontranslating vortices only.

This chapter takes a different approach to the problem of finding a possible normal mode. If the beta gyres are indeed representations of a near-zero frequency normal mode of the system, their amplitude, orientation, and the corresponding motion of the vortex should remain unchanged in the absence of forcing. In this section we will duplicate Willoughby's (1995) most recent experiments justifying the normal mode interpetation and will provide an alternative and more consistent interpretation of the phenomenon.

4.2 Results for the Linear Barotropic Nondivergent Model

4.2.1 The Experiment

The experiment to be run is detailed in Willoughby (1995). Because a normal mode should persist in the absence of forcing, the idea is to "turn off" the forcing after the beta gyres have "spun up". This is accomplished in both models by setting $\beta = 0$ after 240 hours. The vortex is then free to evolve on an f-plane. If the beta gyres do indeed force a normal mode of near-zero frequency, then the vortex should continue at its speed and direction obtained at 240 hours for all time thereafter. Careful analysis of the pertinent fields, as well as vortex track, should provide solid evidence for or against a normal mode in the barotropic nondivergent linear model.

4.2.2 Vortex Tracks

The experiment was run for two qualitatively different vortices, one the benchmark vortex of the previous chapter, and another for the completely cyclonic Willoughby profile. Recall that the benchmark vortex has a finite $\bar{v}$ throughout the model domain, while the Willoughby vortex has $\bar{v} = 0$ outside of 1000 km. Both vortices were allowed to evolve on the f-plane in the absence of β-forcing for times well beyond those run in Willoughby's experiments, 1920 hours for the benchmark vortex and 1320 hours for the Willoughby profile.

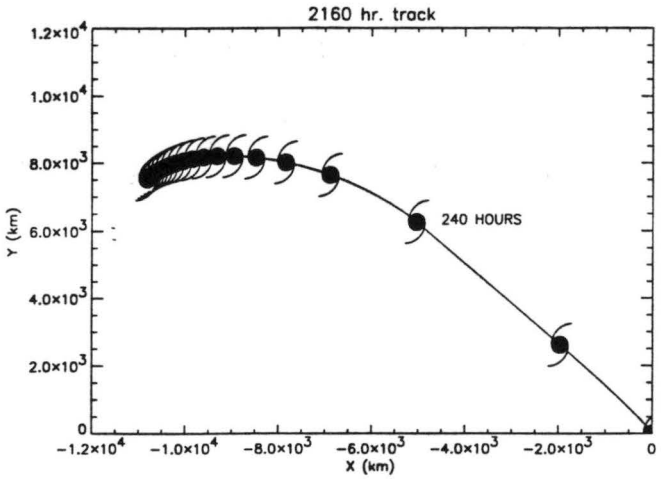

Figure 4.1: The track for the benchmark vortex in the linear barotropic nondivergent model. Beta forcing was discontinued at 240 hours. The cyclone symbols denote the vortex position at every 120 hours.

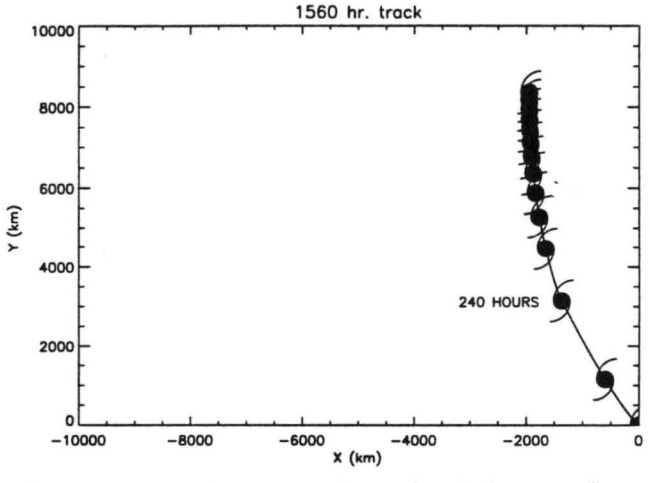

Figure 4.2: The track for the Willoughby vortex in the linear barotropic nondivergent model. Beta forcing was discontinued at 240 hours. The cyclone symbols denote the vortex position at every 120 hours.

As evidenced by Figs. 4.1 and 4.2, the vortices in question do not exhibit behavior consistent with that of a normal mode at near-zero frequency. For the benchmark vortex, the track takes a decidedly westward turn after the beta forcing is discontinued. The vortex eventually comes to rest. When the beta forcing is switched off in the Willoughby vortex, the vortex takes a northward turn and comes to rest at long times. To elucidate what is happening we now examine the perturbation streamfunction (ψ') and perturbation vorticity (ζ') fields.

4.2.3 Streamfunction and Vorticity Fields

As discussed in section 4.2.2, the tracks of the tested vortices do not exhibit behavior compatible with a near-zero frequency normal mode. Inspection of the wavenumber one ψ' and ζ' fields suggests these fields are not consistent with the hypothesis of a normal mode. Figures 4.3 and 4.4 both show a long lived ψ' asymmetry. Closer inspection, however, reveals this asymmetry is losing its amplitude in both cases. In the case of the benchmark vortex, the asymmetry also gets advected with the basic state flow. This is consistent with the track of the benchmark vortex shown in Fig. 4.1. On the other hand, the gyres found in the Willoughby vortex do not seem to be advected with the basic state flow, suggesting a fundamental difference in the behavior of the two vortices, best illustrated in the ζ' fields.

The wavenumber one ζ' fields (not shown in Willoughby's work) for the benchmark vortex (Fig. 4.5) clearly shows the asymmetries at 2160 hours are not the same as those generated by the beta effect (240 hours). There is now little doubt that once the beta forcing is discontinued, the asymmetries that were a result of that forcing begin to symmetrize. At 2160 hours they can hardly be recognized as beta gyres at all. We believe this behavior is inconsistent with a normal mode forced by beta.

The ζ' fields for the Willoughby vortex are shown in Fig. 4.6. At the 240 hour point, the beta gyres have pushed out rather far into the vortex, reaching a maximum at about 750 km. Refering to the basic state of the Willoughby vortex (Fig. 3.28), at 750 km $\bar{v} \simeq 0.5$ ms^{-1}. The result of such small mean tangential winds is that these gyres are oriented so the flow between them is almost northerly. As shown in the radial plots of $\hat{\zeta}'$

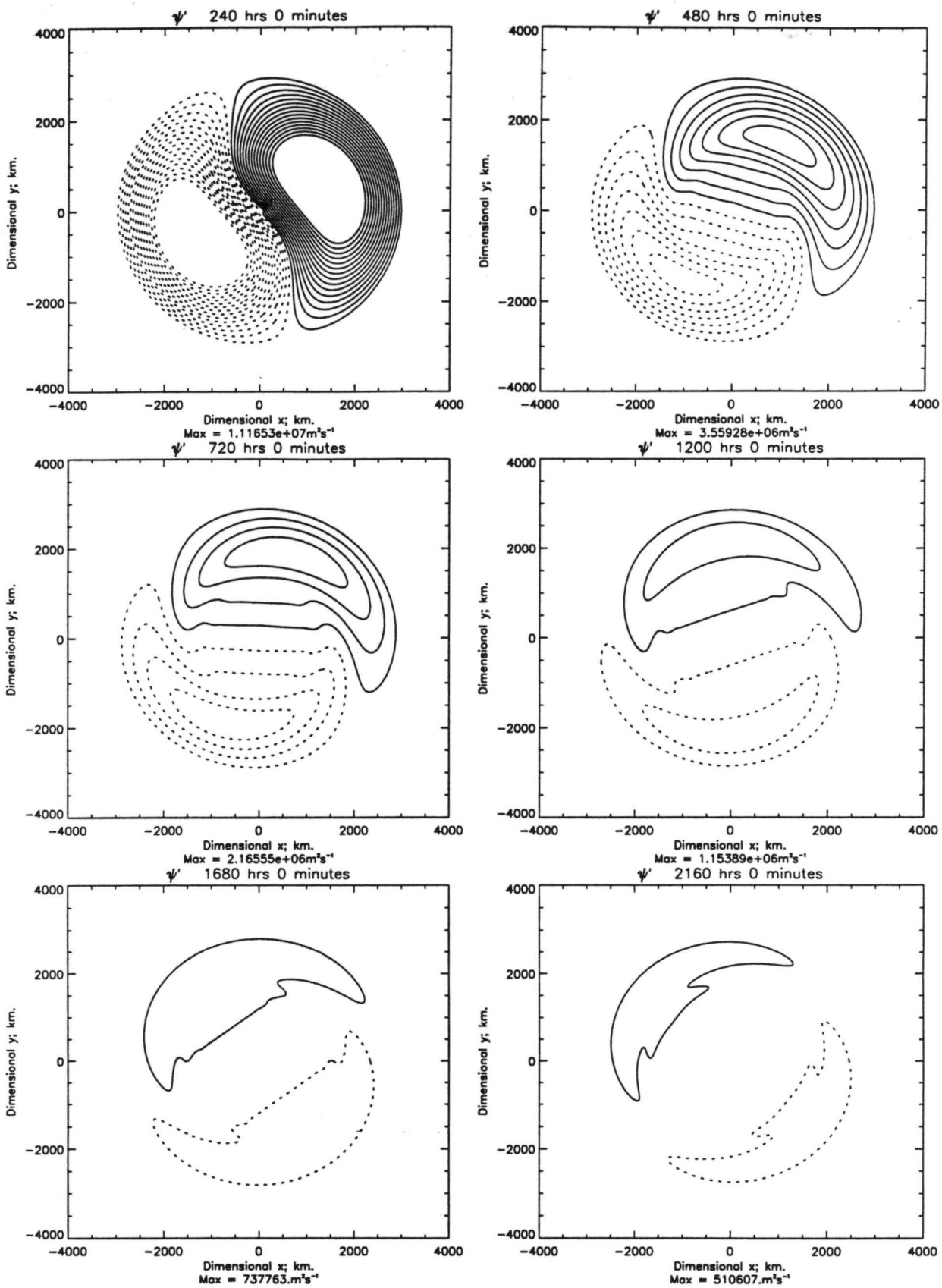

Figure 4.3: The wavenumber one ψ' fields for 240 hours through 2160 hours for the benchmark vortex. The beta forcing was discontinued at 240 hours. Contour interval: 5×10^5 m^2s^{-1}.

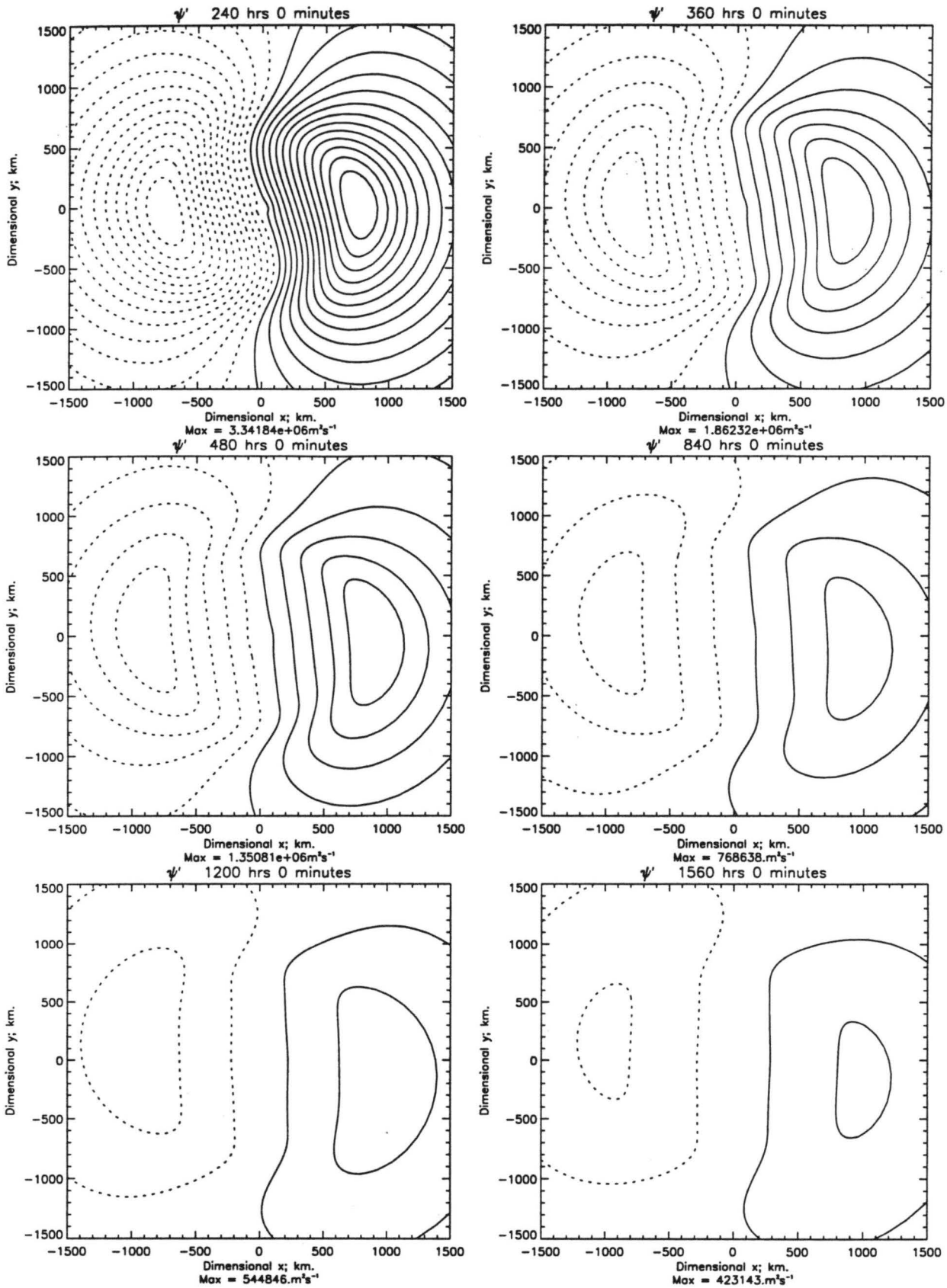

Figure 4.4: The wavenumber one ψ' fields for 240 hours through 1560 hours for the Willoughby vortex. The beta forcing was discontinued at 240 hours. Contour interval: 2.5×10^5 m^2s^{-1}.

(Fig. 4.7), the beta gyres are eroded most efficiently from the inner vortex side as that side possesses the most differential shear. This effect gives the appearence of an outward moving maximum. The part of the gyre in the least differential shear is the longest lived. More discussion on this topic is in section 4.4.

4.3 Results for the Linear β-AB Model

The linear β-AB model differs from the linear barotropic nondivergent model in that the linear β-AB model allows for divergence, being a shallow water model similar to what Willoughby used for his normal mode work. The experiments run in the β-AB model are formally identical to the ones in the previous chapter; specifically, the beta gyres were allowed to evolve for 240 hours at which point the beta forcing was discontinued.

4.3.1 Vortex Tracks

The tracks for the Schloemer and benchmark vortex are shown in Figs. 4.8 and 4.9. Both tracks are qualitatively similar to the benchmark vortex track in the linear barotropic nondivergent model. Neither vortex continues at the speed obtained by the 240 hour point and both take a decidedly westward turn after the beta forcing is discontinued.

4.3.2 Geopotential and PV Fields

As found in the linear barotropic nondivergent model, the geopotential fields (Fig. 4.10) and the potential vorticity fields (Fig. 4.11) produced by the beta effect for the benchmark vortex for wavenumber one do not persist unchanged as one would expect if they were indeed reflections of a zero frequency normal mode. Instead, the beta gyres symmetrize once the beta forcing is discontinued, consistent with the results in the linear barotropic nondivergent model. The Schloemer vortex shows qualitatively similar behavior (fields not shown).

4.4 Discussion

Three vortices have been run in two different linear models, the barotropic linear nondivergent and the β-AB, duplicating Willoughby's experiment of turning off the beta

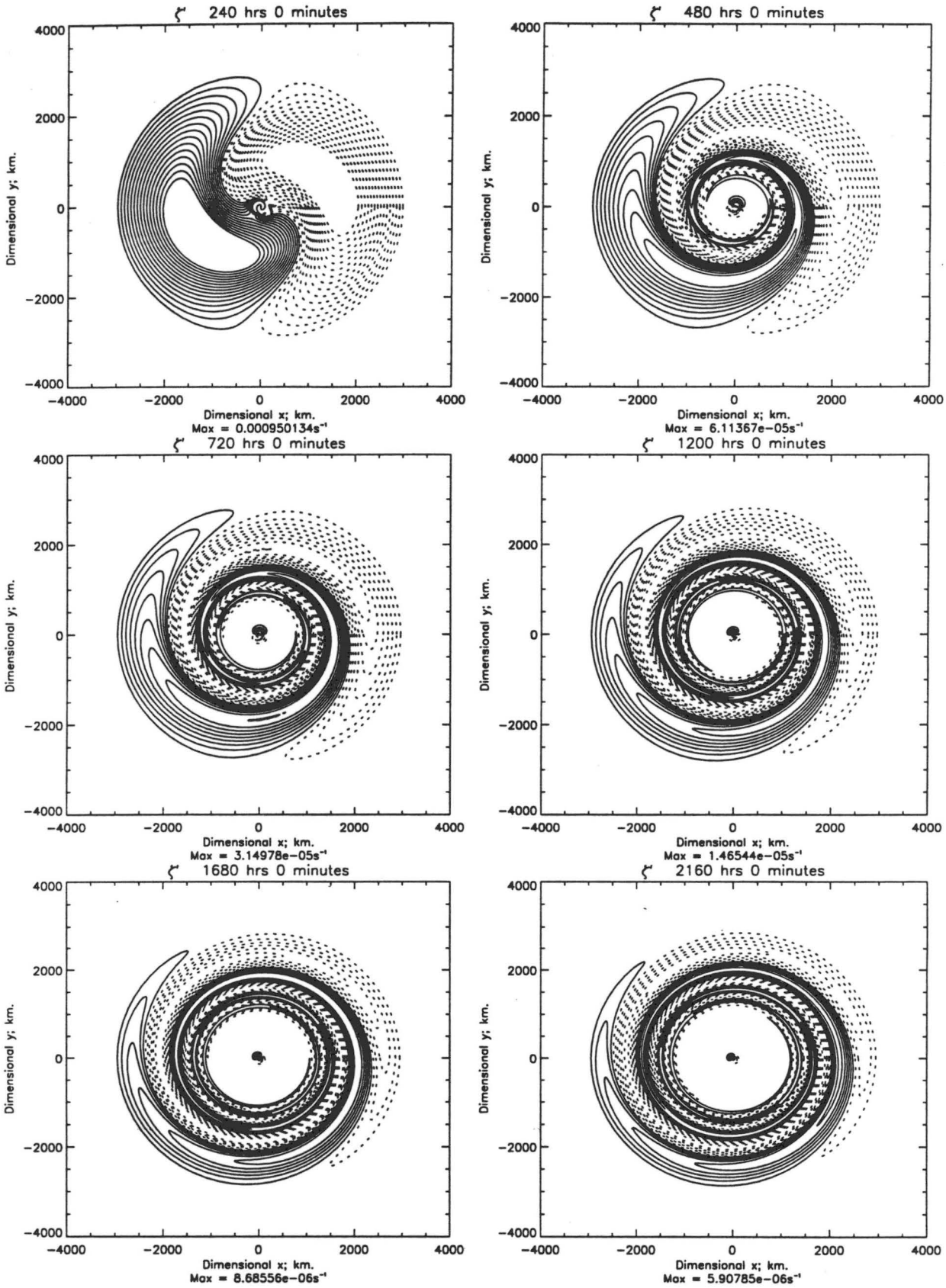

Figure 4.5: The wavenumber one ζ' fields for 240 hours through 2160 hours for the benchmark vortex. The beta forcing was discontinued at 240 hours. Contour interval: 1×10^{-6} s^{-1}. Values outside of $\pm 14.5 \times 10^{-6}$ s^{-1} are not contoured.

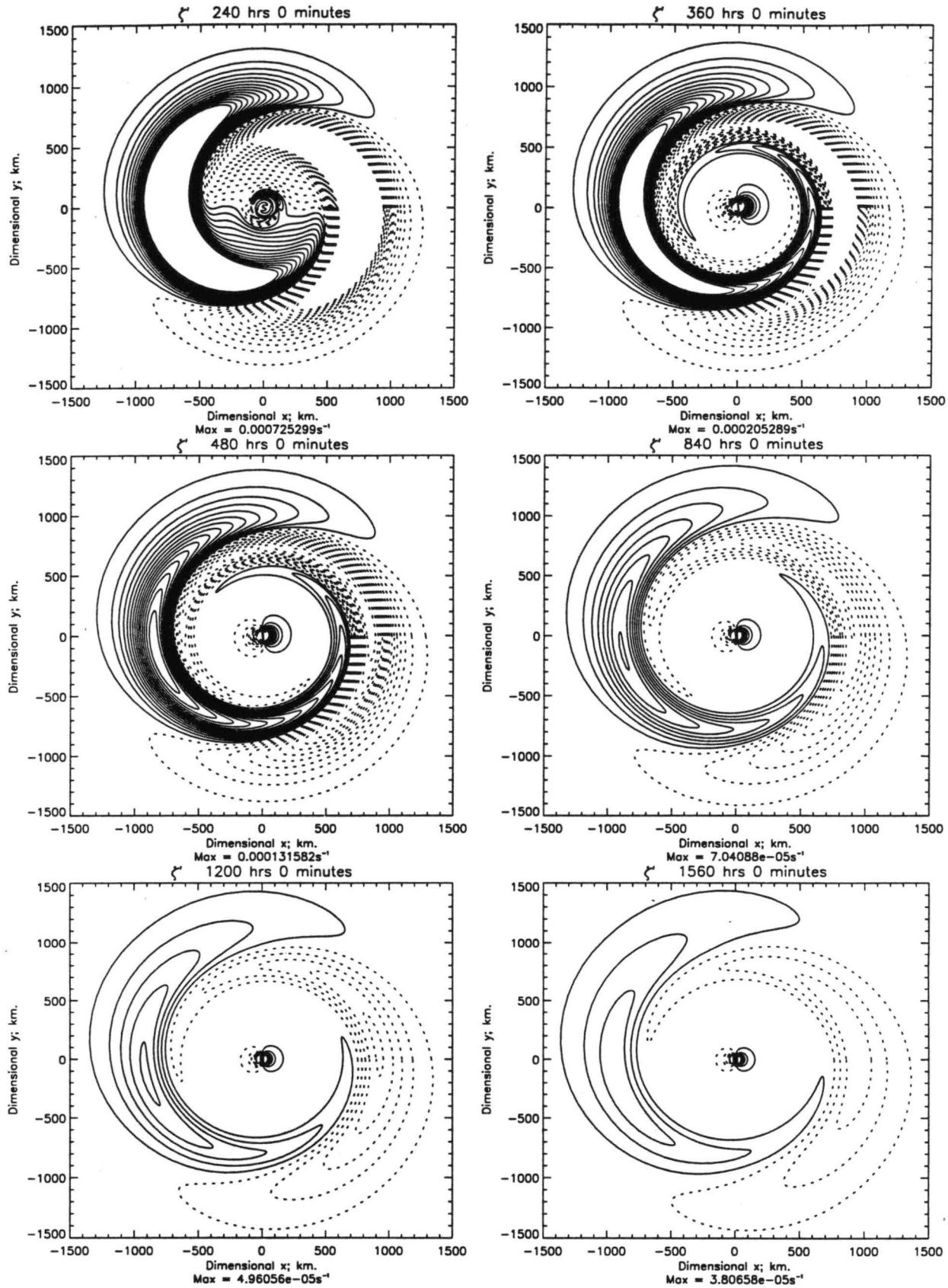

Figure 4.6: The wavenumber one ζ' fields for 240 hours through 1560 hours for the Willoughby vortex. The beta forcing was discontinued at 240 hours. Contour interval: 1×10^{-6} s^{-1}. Values outside of $\pm 14.5 \times 10^{-6}$ s^{-1} are not contoured.

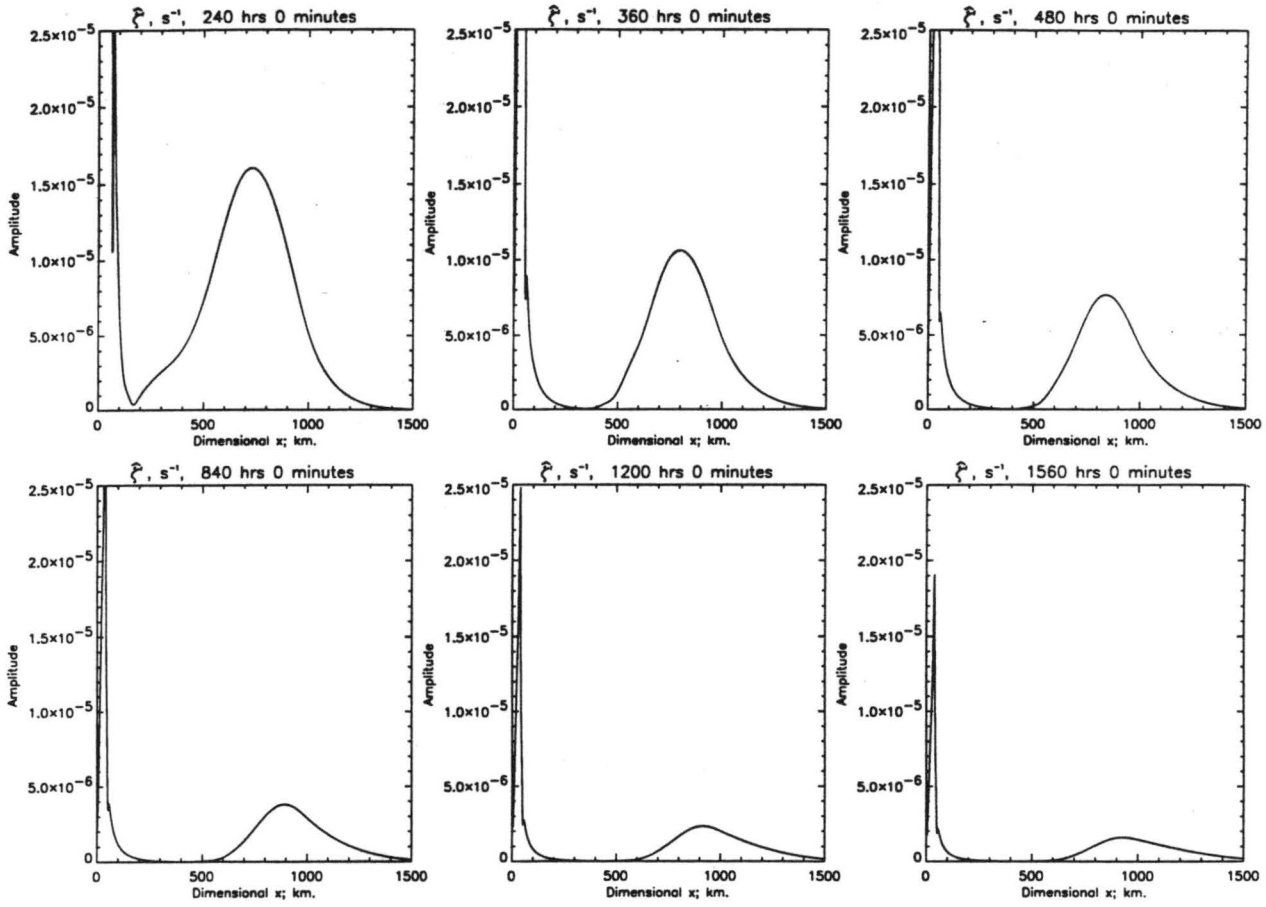

Figure 4.7: The radial plots of wavenumber one $|\hat{\zeta}|$, the Fourier azimuthal amplitude, for the Willoughby vortex.

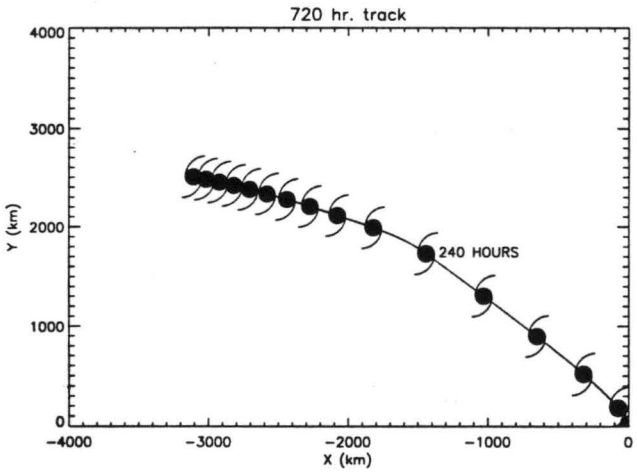

Figure 4.8: The track for the Schloemer vortex in the linear β-AB model. Beta forcing was discontinued at 240 hours. The cyclone symbols denote the vortex position at every 48 hours.

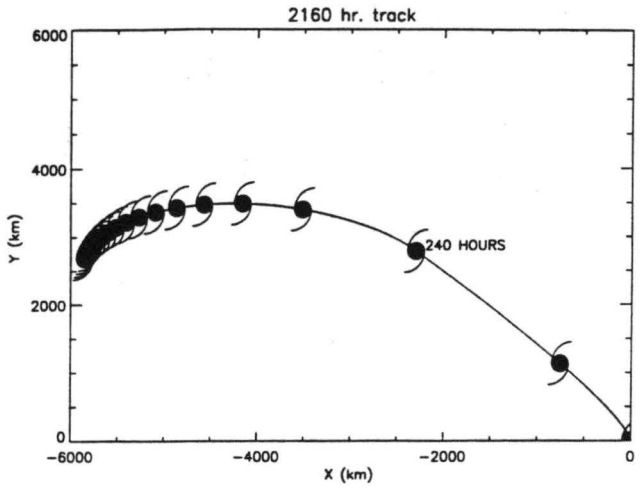

Figure 4.9: The track for the benchmark vortex in the linear β-AB model. Beta forcing was discontinued at 240 hours. The cyclone symbols denote the vortex position at every 120 hours.

forcing after 240 hours. If a normal mode of near-zero frequency was present in these formulations, the vortices should have continued in the same direction and at the same speed as that obtained at the end of 240 hours.

Close examination of vortex track and speeds as well as relevent fields in both models leads us to the conclusion that what is observed in these linear models is a symmetrization process rather than the behavior of a near-zero frequency normal mode. This interpetation is not inconsistent with the *results* presented in Willoughby (1995). For the same experiment as listed in this chapter, Willoughby's linear model shows qualitatively the similar behavior as both the the barotropic linear nondivergent and the β-AB for the Schloemer profile. In Willoughby (1995), the Schloemer vortex takes a turn to the west and slows down when the beta forcing is discontinued, and the wavenumber one gyres associated with the beta forcing also lose amplitude. This behavior is identical to the behavior of both benchmark vortex and the Schloemer profile in the barotropic linear nondivergent and linear β-AB models. Examination of the corresponding ζ' and q'_{ξ_0} fields reveals filamentation, a tell-tale mark of the symmetrization process. The vortex tracks are consistent with the behavior of vortices on an f-plane subject to outer-core asymmeteries as shown in Smith and Ulrich (1993) and Kallenbach and Montgomery (1995). These latter works

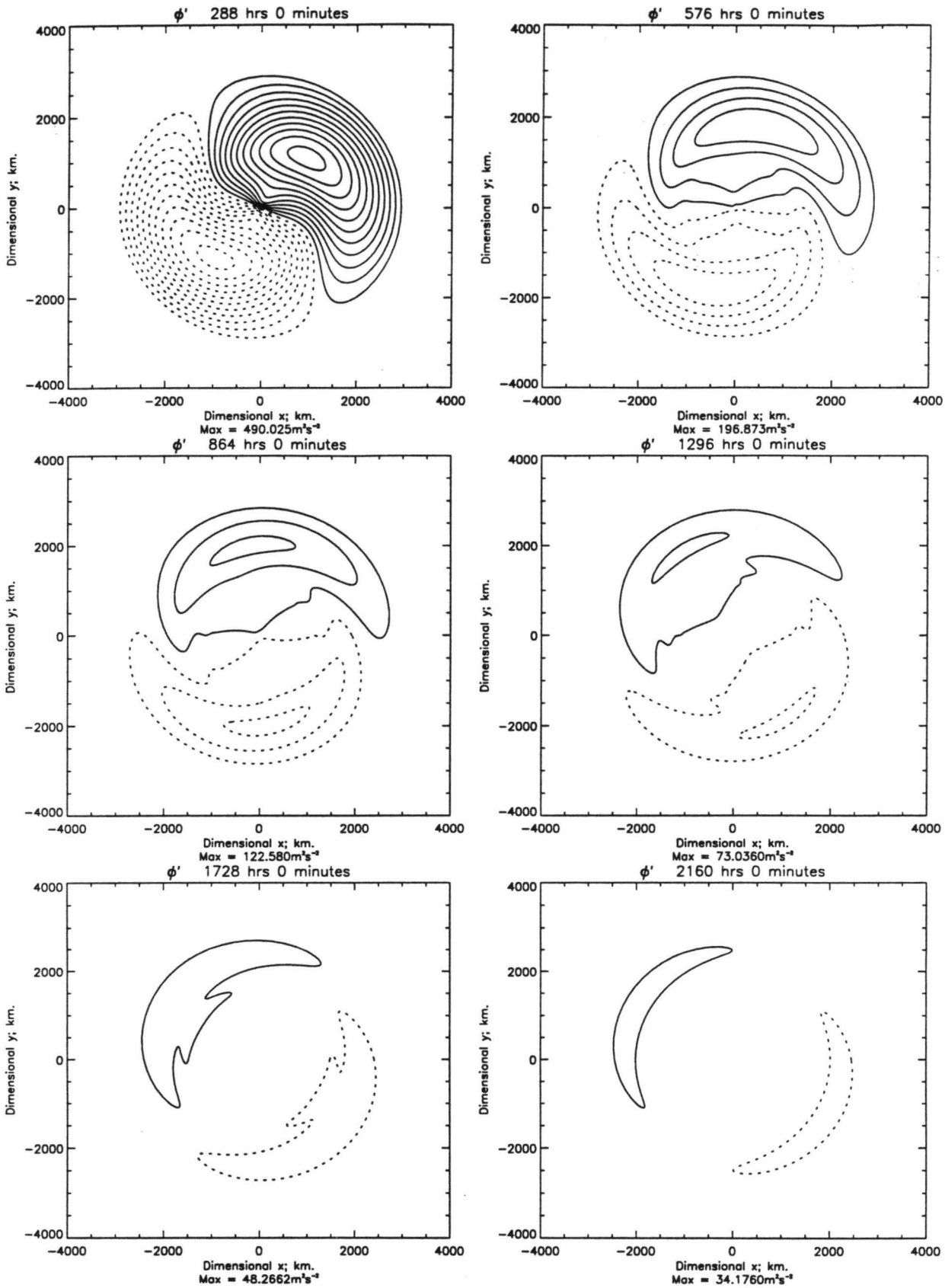

Figure 4.10: The wavenumber one ϕ' fields for the benchmark vortex from 288 hours through 2160 hours. The beta forcing was discontinued at 240 hours. Contour interval: 45 m^2s^{-2}.

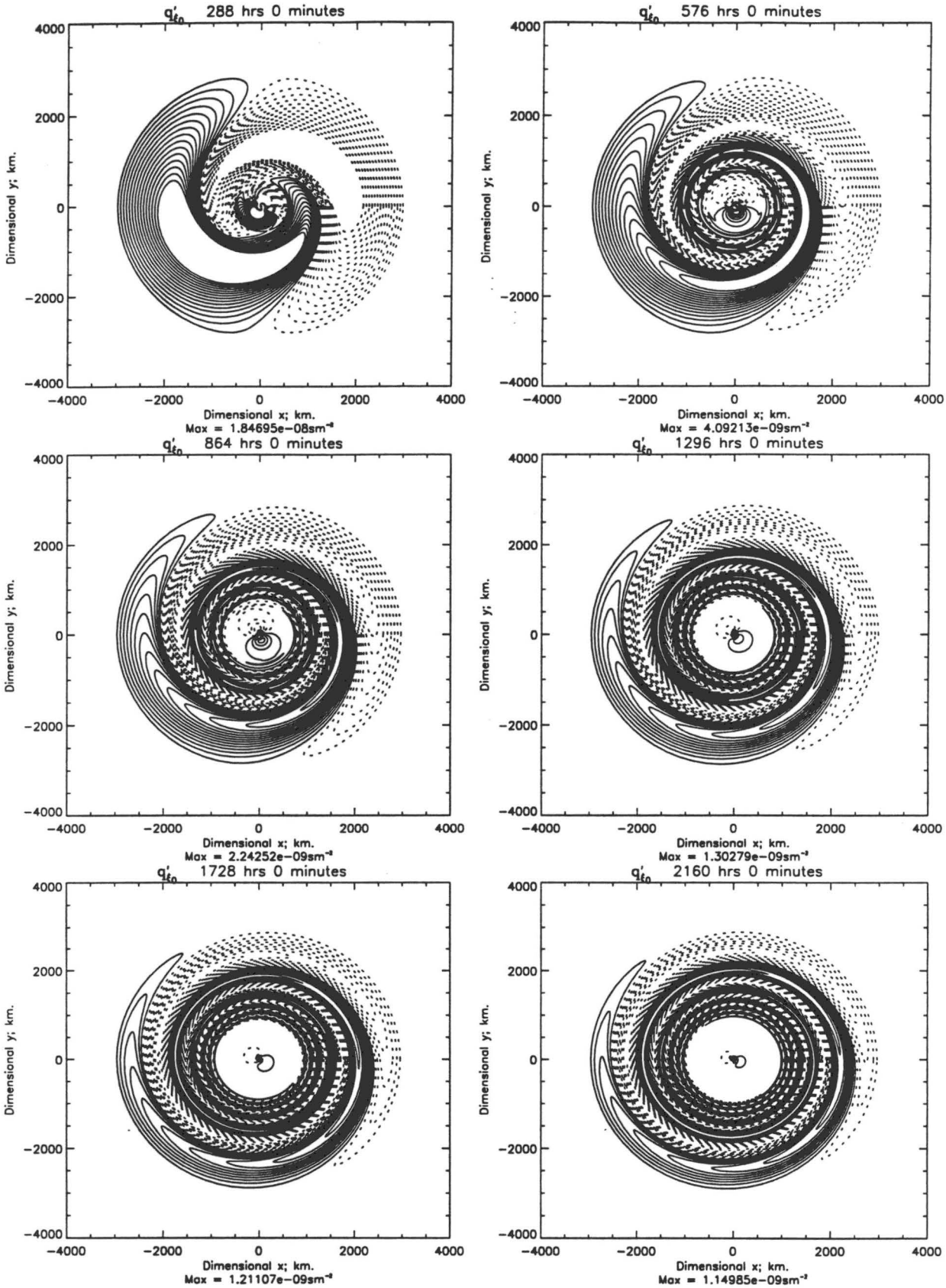

Figure 4.11: The wavenumber one q'_{ξ_0} fields for the benchmark vortex from 288 hours through 2160 hours . The beta forcing was discontinued at 240 hours. Contour interval: 1×10^{-10} sm^{-2}. Values outside of $\pm 14.5 \times 10^{-10}$ sm^{-2} are not contoured.

demonstrated that vortices on an f-plane turn toward the low-pressure asymmetry, just as we found in the experiment with the Schloemer and the benchmark vortex.

The behavior of the Willoughby vortex in the linear barotropic nondivergent model is consistent with the hypothesis of symmetrization when one considers the small basic state tangential wind near the beta gyres. The pertinent equation given in Smith and Montgomery (1995) relates the limiting energy-decay half-life of an asymmetry to the differential shear as

$$t_{half} = -\left[r\frac{d\bar{\Omega}}{dr}\right]^{-1}. \tag{4.1}$$

Plotted in Fig. 4.12 is t_{half} for the vortices discussed in this chapter. Refering to both Fig. 4.12 and Willoughby's (1995) results, if Willoughby were to initialize his model with his vortex and gyres centered "... at the edge of axisymmetric circulation", approximately 1000 km in his case, the corresponding gyres would be long-lived. The long-life of the gyres centered near 1000 km in the Willoughby vortex is likely not the reflection of a normal mode at a near-zero frequency but rather with the behavior of eq. (4.1) and how it relates to the basic state velocity profile. Even with their long half-life, the gyres presented in Willoughby (1995) appear to be undergoing the initial effects of the symmetrization process as evidenced by the decrease amplitude of the gyres. That the Willoughby vortex does not turn or slow down as much as the Schloemer profile should be expected by Fig. 4.12. The Schloemer vortex contains a higher differential shear, so the signs of symmetrization (track deviation to the west, loss of speed, loss of amplitude of the gyres) will be seen sooner and will be more pronounced in the Schloemer (or benchmark) vortex than in the Willoughby vortex.

4.5 Summary

While certainly not as exotic as a normal mode at zero frequency, detailed analysis of experiments performed both in this chapter and in Willoughby (1995) suggest that the beta gyres are not a normal mode in the traditional sense, but are simply asymmetries possessing long but not infinite lifetimes. While the Schloemer and Willoughby vortices

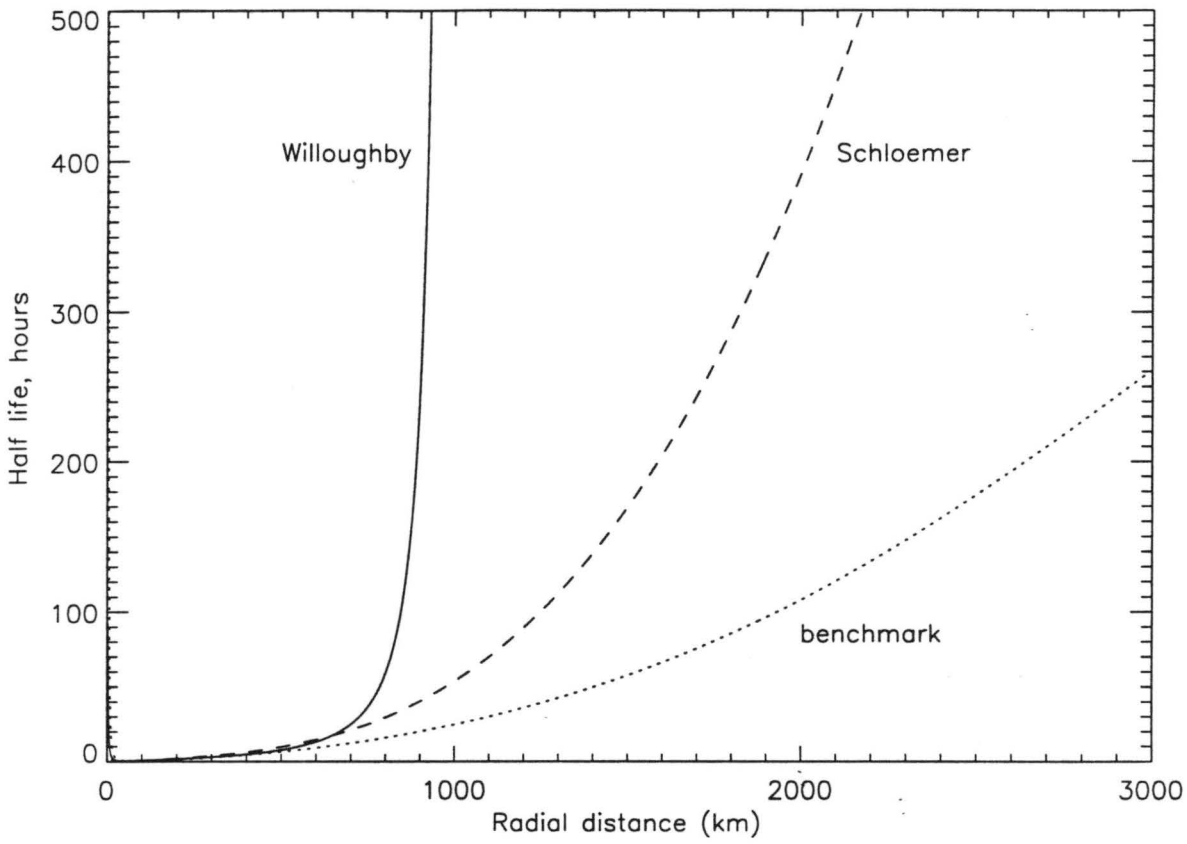

Figure 4.12: The limiting energy decay as a function of radial distance for the completely cyclonic Willoughby profile, the Schloemer profile, and the benchmark vortex.

appear to behave differently when viewed from the normal mode perspective, when considered as a symmetrization problem they in fact behave quite similarly. The experiments performed in this chapter, as well as those executed in Willoughby (1995), are more consistent with the symmetrization of outer core gyres than the forcing of a normal mode at near-zero frequency.

Chapter 5

CONCLUSION

Asymmetric balance theory has been extended to the β-plane in the context of shallow water linear dynamics. The linear β-AB forecast equation was shown to have an associated pseudo-momentum principle, a vertical vorticity equation, a PV equation, and an energy equation that are all analogous to the linearized PE.

For two seperate vortices the linear β-AB formulation has been shown to correctly capture the formation of the beta gyres and produces tracks consistent with previous research using fully nonlinear, barotropic nondivergent vortex models. Finite drift speeds were obtained in both cases, a result in opposition to Willougby's linear PE formulation (Willoughby 1990b, 1992).

In an investigation of the beta effect forcing a near-zero frequency normal mode, experiments were run in both the linear β-AB model and a linear barotropic nondivergent model in which the beta forcing was discontinued after 240 hours. Once the forcing was discontinued, the vortex speeds in both models steadily decreased and the associated beta gyres lost amplitude consistent with the axisymmetrization process. In contrast to the interpretation of a near-zero freqency normal mode, these findings suggest the beta gyres are simply asymmetries possessing long but not infinite lifetimes.

5.1 Suggested Future Work

The distortion term noted in Ch. 3 associated with the advection of planetary vorticity raises some unresolved issues. Possibly a higher-order scheme or a coordinate system moving with the storm would reduce the interpolation errors associated with grid repositioning and quantify whether the aforementioned distortion is a reflection of the β-AB formulation or of numerous grid moves and reinterpolations.

The weakly nonlinear terms in the environment and the fully nonlinear terms in the core are future enhancements. These terms will elucidate how the beta effect acts to modify the initial basic state vortex. The model could then be expanded to include various environmental factors such as shortwaves or horizontal shear.

Expanding the model into more than one layer is likely the only way to make full use AB's property of no formal restriction on the magnitude of divergence. It is here that AB could be used to understand the influence of outflow layer dynamics or how strong convection and its associated high divergence affect a hurricane's track.

Appendix A

FURTHER SIMPLIFICATION OF EQ. (2.34)

The rationale behind the additional simplification of eq. (2.34) is as follows. Neglected beta terms must be small compared to both the leading f-plane terms in the near-vortex region where $R \geq O(1)$ and the leading QG β-plane terms in the environment where $R << 1$ and $\beta r/f_0 \sim O(R)$. Beta terms not satisfying these requirements must be kept. Further simplifications and their associated *relative* errors in the near-vortex region and environment are summarized below:

$$\frac{1}{\bar{\xi}}\frac{D_{\mathrm{v}}}{Dt}\left(\frac{\phi'_\lambda}{r\bar{\eta}}\right) \simeq \frac{D_{\mathrm{v}}}{Dt}\left(\frac{\phi'_\lambda}{r\bar{\eta}\bar{\xi}}\right); ERRORS: \begin{cases} O(\frac{\beta r}{\bar{\xi}}) \text{ in core} \\ O(R) \text{ in environment} \end{cases} \tag{A.1}$$

$$\frac{1}{\bar{\eta}}\frac{D_{\mathrm{v}}}{Dt}\frac{\phi'_r}{\bar{\xi}} \simeq \frac{D_{\mathrm{v}}}{Dt}\left(\frac{\phi'_r}{\bar{\eta}\bar{\xi}}\right); ERRORS: \begin{cases} O(\frac{\beta r}{\bar{\eta}}) \text{ in core} \\ O(R) \text{ in environment} \end{cases} \tag{A.2}$$

$$\frac{d\bar{\Phi}}{dr}\left[-\frac{1}{\bar{\eta}}\frac{D_{\mathrm{v}}}{Dt}\left(\frac{\phi'_r}{\bar{\xi}}\right)\right] \simeq -\frac{d\bar{\Phi}}{dr}\frac{D_{\mathrm{v}}}{Dt}\left(\frac{\phi'_r}{\bar{\eta}\bar{\xi}}\right); ERRORS: \begin{cases} O(\frac{\beta r}{\bar{\eta}}) \text{ in core} \\ O(R) \text{ in environment} \end{cases} \tag{A.3}$$

On making these replacements, (2.34) becomes

$$\begin{aligned} &\frac{D_{\mathrm{v}}}{Dt}\phi' + \frac{\bar{\Phi}}{r}\frac{\partial}{\partial r}\left[\frac{-\phi'_\lambda}{\bar{\eta}} - r\frac{D_{\mathrm{v}}}{Dt}\left(\frac{\phi'_r}{\bar{\eta}\bar{\xi}}\right)\right] + \frac{\bar{\Phi}}{r}\frac{\partial}{\partial\lambda}\left[\frac{\phi'_r}{\bar{\xi}} - \frac{D_{\mathrm{v}}}{Dt}\left(\frac{\phi'_\lambda}{r\bar{\eta}\bar{\xi}}\right)\right] \\ &+\frac{d\bar{\Phi}}{dr}\left[-\frac{\phi'_\lambda}{r\bar{\eta}} - \frac{D_{\mathrm{v}}}{Dt}\left(\frac{\phi'_r}{\bar{\eta}\bar{\xi}}\right)\right] = -\frac{1}{r}\frac{\partial}{\partial r}\left(\frac{r\bar{\Phi}\bar{v}^2\beta\cos\lambda}{\bar{\eta}\bar{\xi}} - \frac{\beta^2\bar{v}^2r^2\bar{\Phi}\sin\lambda\cos\lambda}{\bar{\eta}\bar{\xi}^2}\right) \\ &+\frac{\bar{\Phi}}{r}\frac{\partial}{\partial\lambda}\left(\frac{r\bar{v}\beta\sin\lambda}{\bar{\xi}}\right). \end{aligned} \tag{A.4}$$

We further approximate

$$-\frac{\bar{\Phi}}{r}\frac{\partial}{\partial\lambda}\frac{D_{\mathrm{v}}}{Dt}\left(\frac{\phi'_\lambda}{r\bar{\eta}\bar{\xi}}\right) \simeq -\frac{\bar{\Phi}}{r}\frac{D_{\mathrm{v}}}{Dt}\left(\frac{\phi'_{\lambda\lambda}}{r\bar{\eta}\bar{\xi}}\right); ERRORS: \begin{cases} O(\frac{2r\beta}{\eta n}) \text{in core} \\ O(2R) \text{ in environment} \end{cases} \tag{A.5}$$

After further manipulation (A.4) may be written as

$$\frac{D_{\mathrm{v}}}{Dt}\phi' - \bar{\Phi}\frac{D_{\mathrm{v}}}{Dt}\left[\frac{1}{r}\frac{\partial}{\partial r}\left(\frac{r\phi'_r}{\bar{\eta}\bar{\xi}}\right) + \frac{1}{r^2\bar{\eta}\bar{\xi}}\phi'_{\lambda\lambda}\right] - \frac{1}{r}\frac{\partial}{\partial r}\left(\frac{\bar{\Phi}}{\bar{\eta}}\right)\phi'_\lambda - \frac{d\bar{\Phi}}{dr}\frac{1}{\bar{\eta}\bar{\xi}}\frac{D_{\mathrm{v}}}{Dt}\phi'_r$$
$$-\frac{\bar{\Phi}}{\bar{\xi}^2}\beta\cos\lambda\phi'_r = -\frac{1}{r}\frac{\partial}{\partial r}\left(\frac{r\bar{\Phi}\bar{v}^2\beta\cos\lambda}{\bar{\eta}\bar{\xi}} - \frac{\beta^2\bar{v}^2r^2\bar{\Phi}\sin\lambda\cos\lambda}{\bar{\eta}\bar{\xi}^2}\right)$$
$$+\frac{\bar{\Phi}}{r}\frac{\partial}{\partial\lambda}\left(\frac{r\bar{v}\beta\sin\lambda}{\bar{\xi}}\right). \qquad \text{(A.6)}$$

To further simplify the β–plane formulation it proves useful to make the dependence of $\bar{\eta}$, $\bar{\xi}$, and $\bar{q}$ on β explicit by defining:

$$\bar{\eta} = f + \frac{1}{r}\frac{d}{dr}(r\bar{v}) = f_0 + \frac{1}{r}\frac{d}{dr}(r\bar{v}) + r\beta\sin\lambda = \bar{\eta}_0(r) + r\beta\sin\lambda, \qquad \text{(A.7)}$$

$$\bar{q} = \frac{\bar{\eta}}{\bar{\Phi}} = \frac{f_0 + \frac{1}{r}\frac{d}{dr}(r\bar{v}) + r\beta\sin\lambda}{\bar{\Phi}} = \bar{q}_0(r) + \frac{r\beta\sin\lambda}{\bar{\Phi}}, \qquad \text{(A.8)}$$

$$\bar{\xi} = f + \frac{2\bar{v}}{r} = f_0 + \frac{2\bar{v}}{r} + r\beta\sin\lambda = \bar{\xi}_0(r) + r\beta\sin\lambda. \qquad \text{(A.9)}$$

In (A.7) – (A.9) the zero subscripts refer to the f–plane definition. Consistent with approximations already made, (A.6) simplifies to

$$\frac{D_{\mathrm{v}}}{Dt}\phi' - \bar{\Phi}\frac{D_{\mathrm{v}}}{Dt}\left[\frac{1}{r}\frac{\partial}{\partial r}\left(\frac{r\phi'_r}{\bar{\eta}_0\bar{\xi}_0}\right) + \frac{1}{r^2\bar{\eta}_0\bar{\xi}_0}\phi'_{\lambda\lambda}\right] + \frac{\bar{\Phi}}{\bar{\eta}_0\bar{\xi}_0}\left[\frac{\bar{\xi}_0}{\bar{\eta}_0}\frac{\bar{\Phi}}{r}\frac{d\bar{q}_0}{dr}\phi'_\lambda + \frac{\bar{\xi}_0}{\bar{\eta}_0}\bar{\Phi}\frac{\partial}{\partial r}\left(\frac{r}{\bar{\Phi}}\right)\frac{\phi'_\lambda\beta\sin\lambda}{r}\right]$$
$$-\frac{d\bar{\Phi}}{dr}\frac{1}{\bar{\eta}_0\bar{\xi}_0}\frac{D_{\mathrm{v}}}{Dt}\phi'_r - \frac{\bar{\Phi}}{\bar{\xi}^2}\phi'_r\beta\cos\lambda = -\frac{1}{r}\frac{\partial}{\partial r}\left(\frac{r\bar{\Phi}\bar{v}^2\beta\cos\lambda}{\bar{\eta}\bar{\xi}} - \frac{\beta^2\bar{v}^2r^2\bar{\Phi}\sin\lambda\cos\lambda}{\bar{\eta}\bar{\xi}^2}\right)$$
$$+\frac{\bar{\Phi}}{r}\frac{\partial}{\partial\lambda}\left(\frac{r\bar{v}\beta\sin\lambda}{\bar{\xi}}\right). \qquad \text{(A.10)}$$

Now, let the inverse local Rossby radius squared be denoted as $\bar{\gamma}_0^2 \equiv \bar{\eta}_0\bar{\xi}_0/\bar{\Phi}$. Multiplying (A.10) by $\bar{\gamma}_0^2$ and rearranging yields

$$\frac{D_{\mathrm{v}}}{Dt}\left[\frac{\bar{\gamma}_0^2}{r}\frac{\partial}{\partial r}\left(\frac{r\phi'_r}{\bar{\gamma}_0^2}\right) + \frac{\phi'_{\lambda\lambda}}{r^2} - \bar{\gamma}_0^2\phi'\right] - \frac{\bar{\xi}_0}{\bar{q}_0}\frac{d\bar{q}_0}{dr}\frac{\phi'_\lambda}{r} - \beta\sin\lambda\frac{\bar{\xi}_0}{\bar{\eta}_0}\bar{\Phi}\frac{\partial}{\partial r}\left(\frac{r}{\bar{\Phi}}\right)\frac{\phi'_\lambda}{r}$$
$$+\beta\cos\lambda\frac{\bar{\eta}_0\bar{\xi}_0}{\bar{\xi}^2}\phi'_r = \frac{\bar{\gamma}_0^2}{r}\frac{\partial}{\partial r}\left(\frac{r\bar{\Phi}\bar{v}^2\beta\cos\lambda}{\bar{\eta}\bar{\xi}} - \frac{\beta^2\bar{v}^2r^2\bar{\Phi}\sin\lambda\cos\lambda}{\bar{\eta}_0\bar{\xi}^2}\right)$$
$$-\frac{\bar{\eta}_0\bar{\xi}_0}{r}\frac{\partial}{\partial\lambda}\left(\frac{\bar{v}r\beta\sin\lambda}{\bar{\xi}}\right). \qquad \text{(A.11)}$$

We next invoke the standard β-plane approximation whereby β-terms that are not explicitly differentiated are approximated by their f-plane counterparts. The β-plane approximation introduces errors of $O(\beta r/f_0)$ relative to the leading QG β-plane terms in the environment. Consistent with this approximation the $\bar{\eta}$ and $\bar{\xi}$ terms on the right side of (A.11) are replaced by $\bar{\eta}_0$ and $\bar{\xi}_0$. The result is

$$\frac{D_V}{Dt}\left[\frac{\bar{\gamma}_0^2}{r}\frac{\partial}{\partial r}\left(\frac{r\phi'_r}{\bar{\gamma}_0^2}\right)+\frac{\phi'_{\lambda\lambda}}{r^2}-\bar{\gamma}_0^2\phi'\right]-\frac{\bar{\xi}_0}{\bar{q}_0}\frac{d\bar{q}_0}{dr}\frac{\phi'_\lambda}{r}-\beta\sin\lambda\frac{\bar{\xi}_0}{\bar{\eta}_0}\bar{\Phi}\frac{\partial}{\partial r}\left(\frac{r}{\bar{\Phi}}\right)\frac{\phi'_\lambda}{r}$$
$$+\frac{\bar{\eta}_0}{\bar{\xi}_0}\phi'_r\beta\cos\lambda=\frac{\bar{\gamma}_0^2}{r}\frac{\partial}{\partial r}\left(\frac{r\bar{v}^2\beta\cos\lambda}{\bar{\gamma}_0^2}-\frac{\beta^2\bar{v}^2r^2\bar{\Phi}\sin\lambda\cos\lambda}{\bar{\eta}_0\bar{\xi}_0{}^2}\right)-\bar{\eta}_0\bar{v}\beta\cos\lambda. \qquad \text{(A.12)}$$

When the first term in parentheses on the right-hand side of (A.12) is compared to the second term on the left-hand side of (A.12) the ratio scales as $O(\bar{v}^2\beta r/\bar{\xi}_0\phi'_\lambda)$. In the beta drift problem the perturbation geopotential $|\phi'| \sim O(\beta)$ (Reznik and Dewar 1994). Guided by the knowledge that the geopotential gradient across the storm center is proportional to the drift speed of the vortex, dimensional considerations based on the first term in (2.32) suggest that within the beta gyres $|\phi'| \sim \beta L^2 r\bar{\eta}_0(0)$, where L is the characteristic horizontal length scale determining the drift speed of the vortex (βL^2). As long as $(r^2/L^2)(\bar{\eta}_0(r)/\bar{\eta}_0(0))$ does not greatly exceed unity in the region of the beta gyres, $O(\bar{v}^2\beta r/\bar{\xi}_0\phi'_\lambda) \sim O({R_1}^2)$ and to be consistent with the approximations already made to derive (2.34) this first term in parentheses on the right-hand side of (A.12) can be neglected. Because the second term on the left-hand side of (A.12) scales as $O(\beta r/\bar{\xi}_0)$ compared to the first, it may also be neglected. The final result is eq. (2.35).

REFERENCES

Aberson, S. D., and M. DeMaria, 1994: Verification of a nested barotropic hurricane track forecast model (VICBAR). *Mon. Wea. Rev.*, **122**, 2804–2815.

Carr, L. E., III, and R. L. Elsberry, 1990: Observational evidence for predictions of tropical cyclone propagation relative to environmental steering. *J. Atmos. Sci.*, **47**, 542–546.

Chan, J.C., and W. M. Gray, 1984: Tropical cyclone movement and surrounding flow relationships. *Mon. Wea. Rev.*, **110**, 1354–1374.

Chan, J.C., and R. T. Williams, 1987: Analytical and numerical studies of the beta-effect in tropical cyclone motion. *J. Atmos. Sci.*, **44**, 1257–1265.

DeMaria, M., 1985: Tropical cyclone motion in a nondivergent barotropic model. *Mon. Wea. Rev.*, **113**, 1999–2110.

Drazin, P. G. and W. H. Reid, 1981: Hydrodynamic Stability. Cambridge University Press. 524 pp.

Elsberry, R. L., P. H. Dobbs, and D. W. Titley, 1993: Extraction of large-scale environmental flow components form the TCM-90 analyses: Implications for tropical motion studies. *Proc. 20th Conf. on Hurricanes and Tropical Meteorology*, San Antonio, TX, Amer. Meteor. Soc., 485-488.

Elsberry, R. L., and Abbey, A., 1991: Recent advances in understanding tropical cyclone motion. Tech. Rep. NPS-MR-91-003, Naval Postgraduate School, Monterey, CA 93943, 92 pp.

Evans, J. L., G. J. Holland,, and R. L. Elsberry, 1991: Interactions between a barotropic vortex and an idealized subtropical ridge. Part I: Vortex motion. *J. Atmos. Sci.*, **48**, 301–314.

Farrell, B. F., and P. J. Ioannou, 1993: Stochastic forcing of the linearized Navier-Stokes equations. *Phys. Fluids*, **5**, 2600–2609.

Fiorino, M., and R. L. Elsberry, 1989: Some aspects of vortex structure related to tropical cyclone motion. *J. Atmos. Sci.*, **46**, 975–990.

Franklin J. L., S. E. Feuer, J. Kaplan, and S. D. Aberson, 1996: Tropical cyclone motion and surrounding flow relationships: Searching for the Beta gyres in omeaga dropwindsonde datasets. *Mon. Wea. Rev.*, **124**, 64–84.

Flateau, M., 1992: The role of baroclinic processes in a tropical cyclone motion. *Colorado State University*, Atmospheric Science Paper No. 488.

George, J. E., and W. M. Gray, 1976: Tropical cyclone motion and surrounding parameters relationships. *J. Appl. Meteor.*, **15**, 1252–1264.

Holton, J. R., 1992: Dynamic Meteorology. Academic Press, Inc. 511 pp.

Kallenbach R. J. and M. T. Montgomery, 1995: Symmetrization, vortex Rossby waves, and hurricane motion in an asymmetric balance model. *Colorado State University*, Atmospheric Science Paper No. 588.

McWilliams J. C., and P.R. Gent, 1986: The evolution of sub-mesoscale, coherent vortices on the β-plane. *Geophys. Astrophys. Fluid Dyn.*, **35**, 235–255.

McWilliams J. C., P.R. Gent, and N. J. Norton, 1986: The evolution of balanced, low-mode vortices on the β-plane. *J. Phys. Oceanogr.*, **16**, 838–855.

Montgomery, M. T. and R.J. Kallenbach, 1995: A theory for vortex Rossby waves and its application to spiral bands and intensity changes in hurricanes. *Quart. J. Roy. Meteor. Soc.*, in press.

Myers, V.A., 1957: Maximum hurricane winds. *Bull. Amer. Meteor. Soc.*, **38**, 227–228.

Peng, M. S., and R. T. Williams, 1991: Stability of barotropic vortices. *Geophys. Astrophys. Fluid Dyn.*, **58**, 263–283.

Reznik, G. M., and W. K. Dewar, 1994: An analytical theory of distributed axisymmetric barotropic vortices on the β-plane. *J. Fluid Mech.*, **269**, 301-321.

Shapiro L. J., and K. V. Ooyama, 1990: Barotropic vortex evolution on a beta plane. *J. Atmos. Sci.*, **47**, 170–187.

Shapiro L. J., and M. T. Montgomery, 1993: A three–dimensional balance theory for rapidly rotating vortices. *J. Atmos. Sci.*, **50**, 3322–3335.

Smith, G. B., and M. T. Montgomery, 1995: Vortex axisymmetrization and its dependence on azimuthal wavenumber or asymmetric radial structure changes. *Quart. J. Roy. Meteor. Soc.*, **121**, 1615–1650.

Smith, R. K., and W. Ulrich, 1990: An analytical theory of tropical cyclone motion using a barotropic model. *J. Atmos. Sci.*, **47**, 1973–1986.

Smith, R. K., and W. Ulrich, 1993: Vortex motion in relation to the absolute vorticity gradient of the vortex environment. *Quart. J. Roy. Meteor. Soc.*, **119**, 207–215.

Smith, R. K., W. Ulrich, and G. Dietachmayer, 1990: A numerical study of tropical cyclone motion using a barotropic model. I: The role of vortex asymmetries. *Quart. J. Roy. Meteor. Soc.*, **116**, 337-362.

Sutyrin, G. G., and G. R. Flierl, 1994: Intense vortex motionon the beta plane: Development of the beta gyres. *J. Atmos. Sci.*, **51**, 773–790.

Weber, H. C., and R. K. Smith, 1993: The stability of barotropic vortices: Implications for tropical cyclone motion. *Geophys. Astrophys. Fluid Dyn.*, **70**, 1–30.

Willoughby, H. E., 1988: Linear motion of a shallow-water, barotropic vortex. *J. Atmos. Sci.*, **45**, 1906-1928.

Willoughby, H. E., 1990a: Gradient balance in tropical cyclones. *J. Atmos. Sci.*, **47**, 265–274.

Willoughby, H. E., 1990b: Linear normal modes of a shallow-water barotropic vortex. *J. Atmos. Sci.*, **47**, 2141–2148.

Willoughby, H. E., 1992: Linear motion of a shallow–water barotropic vortex as an initial–value problem. *J. Atmos. Sci.*, **49**, 2015–2031.

Willoughby, H. E., 1994: Nonlinear motion of a shallow water barotropic vortex. *J. Atmos. Sci.*, **51**, 3722–3744.

Willoughby, H. E., 1995: Normal-mode initialization of barotropic vortex motion models. *J. Atmos. Sci.*, **52**, 4501–4514.